SYNTHESIS, CHARACTERIZATION AND CATALYTIC PROPERTIES OF MOLYBDENUM CONTAINING MEDIUM PORE MOLECULAR SIEVES

A Thesis

Submitted to

THE UNIVERSITY OF PUNE

for the degree of

DOCTOR OF PHILOSOPHY

(IN CHEMISTRY)

BY

P.S. RAGHAVAN

CATALYSIS DIVISION

NATIONAL CHEMICAL LABORATORY

PUNE 411 008, INDIA

MARCH 1998

INVOCATION

The Almighty is perfect and complete, and because He is completely perfect, all emanations from Him, such as this phenomenal world, are perfectly equipped as complete wholes. Whatever is produced of the complete whole is also complete in itself. Because He is the complete whole, even though so many complete units emanate from Him, He remains the complete balance.

THIS WORK IS DEDICATED

TO

MY BELOVED PARENTS

ACKNOWLEDGEMENTS

I wish to express my deep sense of gratitude to my research guide, Dr.S. Sivasanker, for his valuable guidance, and encouragement throughout the course of the investigation. I would like to extend the same to his family members Mrs. Jaya Sivasanker, Mr.S. Arun and Ms.S. Anupamma for their moral support during the course of my stay at Pune.

I am deeply indebted to Dr.A.V. Ramaswamy and Dr.(Mrs.)V. Ramaswamy, for their constant help and encouragement during my research work.

My sincere thanks to Dr.B.S. Rao, Dr.H.S. Soni, Dr.N.E. Jacob, Dr.(Mrs.) A.J. Chandwadkar, Dr.R. Vetrivel, Dr.M.K. Dongare, Dr.S.G. Hegde, Dr.A.P. Singh, Mr.K. Ramakrishnan, Mr. Karunakaran, Ms.Violet Samuel, Dr.A. Sudalai and their families for their valuable support and considering me as one among their family members.

I would like to thank senior scientists Dr.A.N. Kotasthane, Dr.V.P. Shiralkar, Mrs.A.A. Belhekar, Ms.M. Agashe, Ms.Shoba Awate, Dr.K. Kamble, Dr.K.G. Waughmare, Dr.S.S. Thamankar, Dr.S.P. Mirajkar, Dr.M.J. Eapen, Dr.Rajiv Kumar, Dr.M.P. Kulkarani, Dr.C. Gopinathan, Dr.(Mrs.) Gopinathan, Dr.Shaikh, Mr.Kavedia, Dr.A.P. Budkar, Dr.Sahapure, Dr.Awasarkar, Dr.Chumble, Dr.Sonsole, Dr.Pardhay, Mr.P.K. Purushotham, for their constant encouragement.

At this juncture I remember the help extended by all my seniors Dr.R. Ravishankar, Dr.Puyam Singh, Dr.A. Keshavaraja, Dr.D. Bhattacharya, Dr.R. Bandopadyay, Dr.T. Selvam, Dr.M. Sasidharan, Dr.A. Bahumik, Dr.N.K. Mal, Dr.S.B. Kumar, Dr.S. Koner, Dr.Tapan Kumar Das, Dr.Tapas Sen, Dr.N. Venkatathri, Dr.M. Jayaram, Dr.K.Sakthivel, Dr.R. Robert and all my friends Mr.Selvaraj, Mr.A.K. Sinha, Ms.K. Choudhary, Mr.D.P. Sabde, Mr.R. Deka, Dr.M.P. Vinod, Mr.Suresh Waughmode, Ms.Sindu, Mr.Suhas, Ms.Bhavana, Ms.Ranjeet, Mr.Rajaram Bal, Mr.Priyo, Mr.Siddesh Shevde, Mr.Patric Benziher, Mr.D. Ebenizer, Mrs.Sushma Kale, Mr.Balaji, Ms.Ajitha, Ms.Shylaja, Mr.A. Ramani, Mr.B.S. Balaji, Mr.Ramanathan, Mr.Patil, Mr.Datta Ponde, Mr.C.V. Madusoodanan, Mr.C. Mannakatti, Mr.Milind Jadav, Mr.Saikh, Mr.Mani, Mr.Ethiraj, Mr.Shivashankar, Dr.S. Kannan, Dr.S. Velu, for their academical as well as entertaining discussions.

I thank scientists from SIL, Dr.Date, Dr.Sainkar, Dr.Badrinarayanan, Dr.Shinde, Dr.Bakre, Dr.V. Puranik for their help in analyzing the samples and Mrs.Jyothi who helped in drafting figures, Mr.Prabhune who helped me in to bind the chapters in the form of thesis.

I would like to express my gratitude to the NCL Tamil Mandram members, Dr.Jagannathan, Dr.G.R.V. Krishnan, Dr.S. Krishanan, Mr.V. Balaji, Dr.S. Devotta, Dr.Ponrathnam, Dr.S. Ganapathy, Dr.S.K. Sabapathy, Mr.Natarajan, Dr.Balakrishnan, Dr.Naidu, and their family members and all tamil friends for their love and affection towards me.

I cannot express in words and also it should not be, the love and affection extended by my parents, sister, brother and my wife in order to come up in life up to this stage. The same is extended to my grandfather Shri.S. Chakrapani, who has guided me from the early stage of my life.

I thank the director Dr.Paul Ratnasamy for his kind permission to sumit my work in the form of thesis. I take this instant to pay my gratitude towards CSIR, for extending financial assistance by awarding fellowship.

P.S. Raghavan

(P.S. RAGHAVAN)

CERTIFICATE

Certified that the work incorporated in the thesis entitled "Synthesis, Characterization and Catalytic properties of Molybdenum Containing Medium Pore Molecular Sieves", submitted by Mr.P.S. RAGHAVAN for the degree of Doctor of Philosophy was carried out by the candidate under my supervision at the National Chemical Laboratory, Pune, India. Such material as has been obtained from other sources has been duly acknowledged.

Dr.S. SIVASANKER
5/3/98
Research Guide.

CONTENTS

Page No.

Chapter I

INTRODUCTION

1. INTRODUCTION

1.1 Zeolites

Zeolites are crystalline, microporous, aluminosilicates with 3-dimensional frameworks made up of SiO_4^{4-} and AlO_4^{5-} tetrahedra. They are found in nature or synthetically prepared by hydrothermally reacting aluminate and silicate anions in highly alkaline media. More than forty different naturally occurring zeolites have been identified and over 150 types of synthetic zeolites have been prepared so far.

The general empirical formula of zeolites is $(\mathbf{M^{n+}})_{x/n}(\mathbf{AlO_2})_x(\mathbf{SiO_2})_y.\mathbf{mH_2O}$, where 'M' is a cation, 'm' is the number of moles of water of crystallization and (x+y) gives the number of AlO_4 and SiO_4 tetrahedra in the unit cell.

1.2 Zeolite Structure

The primary building block of the zeolite structure is a tetrahedron of four oxygen atoms surrounding a central silicon atom $-(SiO_4)^{4-}$ (Fig. 1.1a). These silicon tetrahedra are connected through their corners of shared oxygen atoms to form a wide range of small secondary building units (Fig. 1.1b). These are interconnected to form a wide range of polyhedra (Fig. 1.1c), which in turn connect to form the infinitely extended frameworks of the various specific zeolite crystal structures (Fig. 1.1d).

1.3 Classification of Zeolites

Classification of zeolites has been made on the basis of their

i) morphology *[1]*

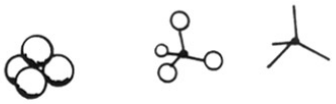

(a) Primary units [• - Si^{4+}, Al^{3+}, etc.; o - O^{2-}]

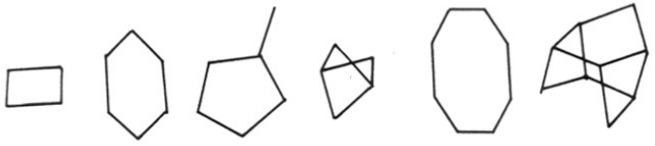

(b) Secondary units

(c) Tertiary units or building units

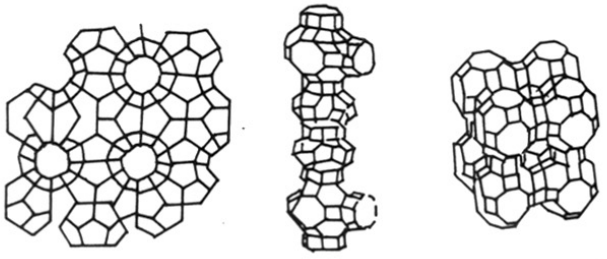

(d) Zeolite structures (Melanoplogite, Paulingite and RHO, respectively).

Fig. 1.1 : Monomers (a) polymerize to low-molecular weight rings and chains (b) and in turn combine to form polyhedral units (c) or sheet structures. These (d) attach to growing crystal surfaces or final zeolites [D.E.W. Vaughan, *Chemical Engineering Progress*, February (1988) 25.]

ii) crystal structure *[2]*

iii) chemical composition *[3]*, and

iv) pore diameter *[4]*

Based on the morphology, zeolites are classified as fibrous, lamellar or those having framework structures. In the fibrous group, tetrahedra are linked in one crystallographic direction while in lamellar their structural linkages are in one plane with platy cleavage.

The classification according to the crystal structure is based on the work by Meier *[2]*. It consists of 10 groups. Depending on the differences in the secondary building units, the ten groups of zeolites are : Analcime, Natrolite, Chabazite, Philipsite, Heulandite, Mordenite, Faujasite, Laumontite, Pentasil and Clathrate. Classifications made on the basis of chemical composition and pore diameter are presented in Table 1.1.

1.4 Shape Selectivity in Zeolites

The name "Shape-Selective Catalysis" was coined by P.B. Weisz and V.J. Frilette *[5]*, in order to describe the catalytic properties of small pore molecular sieves. Latter the terminology was used to describe catalysis by medium pore zeolites such as ZSM-5 *[6]*, ZSM-11 *[7]*, ZSM-48 *[8]*, etc. The pore size and shape of the zeolite may influence the selectivity of a reaction in four ways.

1.4.1 Reactant shape selectivity (RSS)

When the operative pore size of the zeolite is such that it admits only certain smaller molecules present in the reactant and excludes the larger molecules (Fig. 1.2a), then, only the

TABLE - 1.1

Classification of zeolite molecular sieves based on chemical composition and pore structure.

Classification	Sub Classification	Si/Al ratio	Example
Chemical composition	Low Silica	1 - 1.5	A, X, Sodalite
	Intermediate	2 - 5	Erionite, Mordenite
	High Silica	10 - thousands	ZSM-5, ZSM-11, Beta
	Silicalites	thousands - ∞	Silicalite-1, Silicalite-2
Pore diameter	Small port	8 membered ring	Zeolite A, ZK-5, ZK-4
	Medium port	10 membered ring	ZSM-5, ZSM-11
	Large port	12 membered ring	Linde X,Y, Omega

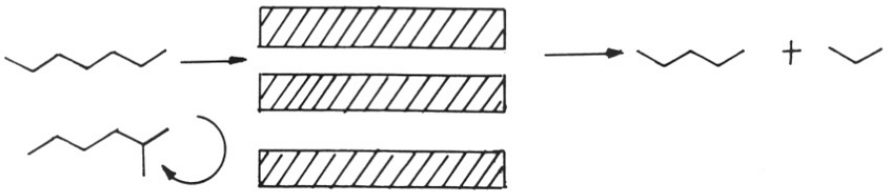

Fig. 1.2a : Reactant Shape Selectivity.

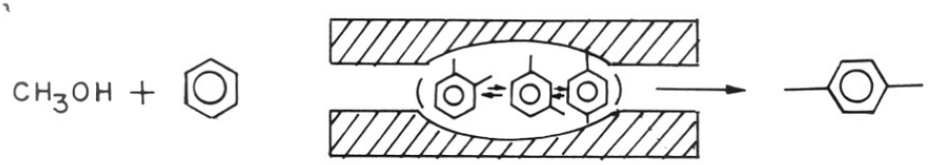

Fig. 1.2b : Product Shape Selectivity.

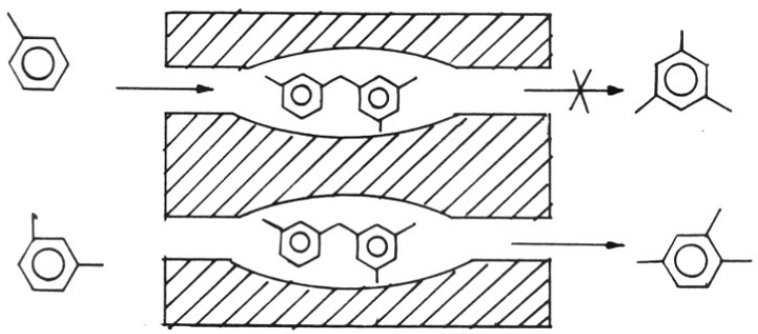

Fig. 1.2c : Restricted Transition State Selectivity.

smaller molecules react effectively. This preferential transformation of the smaller molecules is called Reactant Shape Selectivity.

1.4.2. Product shape selectivity (PSS)

This type of selectivity operates when some of the compounds formed within the pores are too bulky to diffuse out as products. The bulky product molecules will either decompose to smaller molecules or they will block the catalyst pores resulting in the deactivation of the catalyst. The products formed in this case are due to restricted diffusivity of the products during the course of the reaction *[9]* (Fig. 1.2b) and thus, creating a selectivity towards the product of certain dimensions.

1.4.3 Restricted transition state selectivity (RTSS)

This occurs when certain reactions involve transition states that require more space than is available in the zeolite pore. Diffusion of reactants and products in this situation is not hindered and only those products can form which involve transition states that can fit into the available space (Fig. 1.2c).

1.4.4 Molecular traffic control (MTC)

A new type of shape selectivity in zeolites containing intersecting channels of different diameters has been proposed by Derouane and Gabelica *[10]*. In the case of zeolites, with more than one type of intersecting channels, the reactants enter preferentially through one set of channels and the products diffuse out through the other, thus minimizing counter diffusion.

1.5 Synthesis and Structure of Medium Pore Zeolites

Eventhough, a large number of medium pore zeolites such as ZSM-5, ZSM-11, ZSM-48, ZSM-22, EU-1 are known, ZSM-5 has been used extensively in industries. In fact, it is also one of the most studied zeolites. This thesis deals with molybdenum silicalites with structures similar to ZSM-5 and ZSM-11. ZSM-5 belongs to the MFI structure type, while ZSM-11 belongs to the MEL structure type. The syntheses and structures of the two zeolites are discussed below.

The synthesis of ZSM-5 using tetrapropylammonium cation as the template was reported by Argauer and Landolt in the year 1972 *[6]*. ZSM-11 can be synthesized using tetrabutylammonium cation as the template *[7]*. Zeolites are generally prepared using the sources of silica and alumina, templates and the required amount of water. These ingredients are blended together in the requisite amounts to form a homogeneous gel or slurry, which is then aged under desired conditions, followed by hydrothermal treatment between 90 - 180°C. After complete crystallization of the desired product, the reaction is arrested by quenching the reaction vessel to room temperature.

Kokotailo *et al.*, reported the structure of ZSM-5 in the year 1978 *[11]*. Then, Flanigen *et al.*, synthesized a highly siliceous (Al^{3+} free) isomorph and named it "Silicalite" *[12]*. The building blocks of ZSM-5 are formed from pentasil units (Fig.1.3a & 1.3b) linked through edges to form chains and these chains are connected to form sheets (Fig. 1.3c); the sheets link to form a three dimensional framework. ZSM-5 consists of two intersecting channels formed by rings of 10 oxygen atoms *[13]* (Fig. 1.4a). These two channels have slightly different pore dimensions. One runs parallel to the a-axis of the unit cell which is

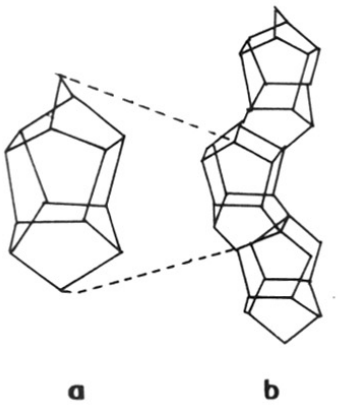

Fig. 1.3
Building chain units
(a) Secondary building unit
(b) Chain units made up of SBU found in ZSM-5 and ZSM-11.

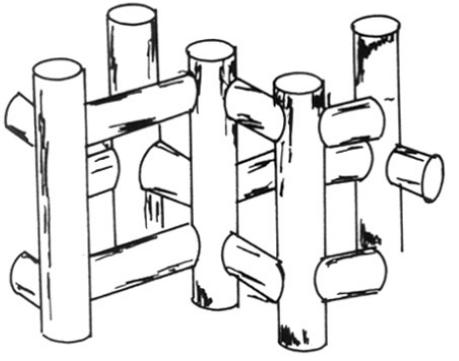

Fig. 1.3c
"Hollow tube" representation of ZSM-5

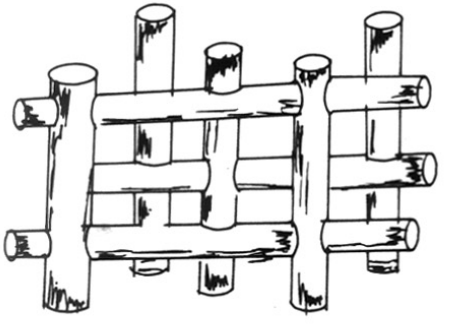

Fig. 1.3d
"Hollow tube" representation of ZSM-11

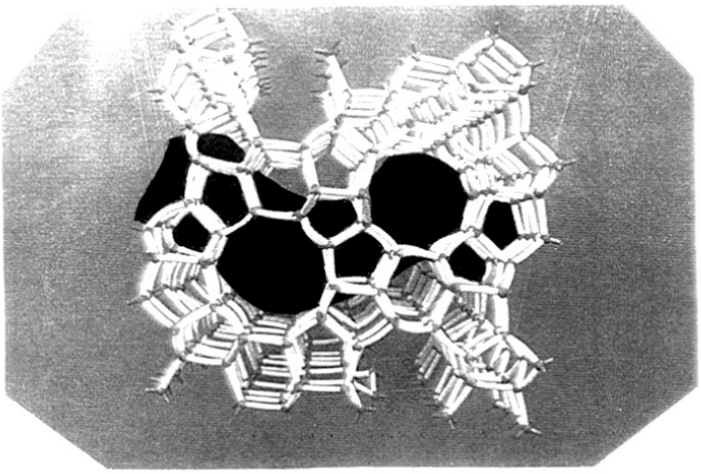

Fig. 1.4a : Structure of ZSM-5 (sinusoidal channel)

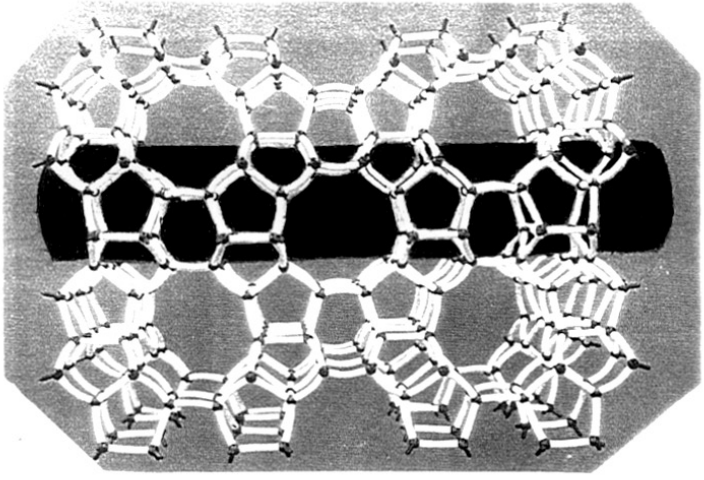

Fig. 1.4b : Structure of ZSM-11 (straight channel)
[P.A. Jacobs and J.A. Martens (Eds.), *Stud. Surf. Sci. Catal.*, 33 (1987) 175.]

sinusoidal and nearly of circular dimension (5.4 X 5.6 Å). The other runs parallel to the b-axis and has a straight but elliptical opening with dimensions 5.1 X 5.5 Å. In general, the medium pore pentasils, unlike other zeolites have pores of uniform dimension and have no large super cages, believed to be responsible for deactivation by coking in acid catalyzed reactions. The 'less-deactivating' characteristic of ZSM-5 is one of the important factors for its applications in industrial catalysis. ZSM-11 is a medium pore pentasil zeolite. It contains two straight elliptical channels, intersecting at right angles to each other. Both the channels are of dimension 5.1 X 5.5 Å *[14]* (Fig. 1.4b). The two zeolites can be easily differentiated through X-ray diffraction profiles which will be discussed in detail in the forth coming chapters.

1.6 Characterization of Zeolite Molecular Sieves

Characterization of the zeolites can be divided into three main groups:

1. Characterization of bulk properties,
2. Determination of structure and surface properties, and
3. Characterization of internal structure or pore structure.

1.6.1 Bulk characteristics

a) Scanning electron microscopy (SEM)

Scanning electron microscopy is a direct technique through which one can visualize the morphology and crystallinity of the sample. Qualitative analysis of particulate distribution, sizes and shapes can be studied using SEM. The subject has been reviewed by Hilliard *[15]*. The relationship between catalytic activity and

particle size and the morphological changes brought about by promoters in zeolite samples can be visualized.

b) X-Ray diffraction (XRD)

This is the first and foremost technique applied to characterize any crystalline sample. Each and every sample exhibits a characteristic finger print pattern. It is possible to determine the structure class to which the sample belongs from the above pattern. The powder XRD pattern provides information on the degree of crystallinity as well as the phase purity of the sample. A decrease in the cell volume indicates dealumination, due to removal of the larger Al atoms. An increase in cell volume substantiates the incorporation of any guest ions (having larger ionic radii than Si^{4+} ion) in the framework of Al free samples (e.g., Ti containing isomorph *[16]*). Single crystal XRD can reveal the complete structure of the crystalline sample *[17]*.

c) Chemical analysis

The catalyst composition at the end of the preparation can be different from the expected value. Also, the reproducibility of chemical composition is a very common problem faced in zeolite synthesis, and hence, compositional analysis after each batch of preparation of the catalyst is essential. Chemical analysis can be carried out by atomic absorption spectroscopy of the solution, prepared by dissolving the dry sample of known weight in a minimum quantity of aqueous HF (38%), followed by dilution to the required concentration. The X-Ray Fluorescence spectroscopy (XRF) and Energy Dispersive X-Ray photometry (EDX) analysis are also often used to analyze the solid samples directly.

d) Thermal analysis (TG/DTA/DSC)

The thermal analysis of the samples gives valuable information such as the number of defect sites (by weight loss due to water of hydration), template loss, temperature of structurel collapse, etc. Generally, the calcination temperature of a catalyst is optimized after carrying out thermal studies of the catalyst. The amount of organic components such as the template molecules present in the samples can be estimated by TGA. Reactions involving mass change such as decomposition and combustion can be detected by TGA/DTA methods. Solid-solid, solid-gas or liquid-gas transitions can be determined by DSC or DTA analysis.

1.6.2 Determination of structure and surface properties

a) FT-Infra red spectroscopy (FTIR)

Infra-red spectroscopy can give structural information of the zeolites, especially the acid characteristics and isomorphous substitution. *[18,19]*. The pentasil zeolites can be easily identified by a characteristic band at 550 cm^{-1} *[20]*. The bond vibration in zeolites can be classified into two types:

(i) internal vibrations of TO_4 units called structure insensitive vibrations and

(ii) vibrations due to external linkages of TO_4 units called structure sensitive vibrations *[18]*.

Internal vibrations

Asymmetric stretching 1250 - 950 cm^{-1}

Symmetric stretching	720 - 650 cm^{-1}
T-O bending vibration	420 - 500 cm^{-1}
External linkage vibrations	
Double ring vibration	650 - 500 cm^{-1}
Pore opening vibration	300 - 420 cm^{-1}
Symmetric stretching	750 - 820 cm^{-1}
Asymetreic stretching	1050 - 1150 cm^{-1}

b) *UV-Visible spectroscopy (UV-Vis)*

UV-Visible spectroscopy is a simple and highly useful molecular spectroscopic technique to study the catalyst. Even though it is possible to investigate the bulk properties like the d-d transitions of the transition elements (Ti, Zn, Sn, Mo, etc.,), the possibility of determining oxidation states, type of ligands, and coordination number, makes the technique suitable to evaluate the structure of the catalyst. The changes in oxidation state involve variations in electronic configuration which in turn influence the spectra. The nature of the ligand influences the electronic transitions. The presence of inclusion complexes such as $Cu(II)(NH_3)_4$ inside the channels/cage of zeolites X and Y were proved by comparing the DRS of free complex with that of Cu(II)X and Cu(II)Y *[21]*. The DRS at different wavelength regions provide information about the environment of the metal ions (e.g. Ti, Sn, V etc.) in metallosilicate molecular sieves. *[22-24]*. The approximate position of absorption bands in the UV-Visible region of some metal ions in different coordinations are presented in Table 1.2.

TABLE - 1.2

Absorption of some metal ion with different coordinations in UV-Visible region.

Metal	Coordination type	Asorbance (nm)	References
Ti	tetrahedral	212	*[28a]*
Ti	octahedral	240	*[28a]*
V	tetrahedral	233-250	*[28b]*
V	octahedral	333-500	*[28b]*
Mo	tetrahedral	220	*[28c]*
Mo	octahedral	300	*[28c]*
Mo	bridging	260-280	*[28c]*
Sn	squarepyramidal	221-225	*[23]*
Sn	octahedral	255-260	*[23]*

c) *X-Ray photoelectron spectroscopy (XPS)*

Among the techniques applied for analysis of a sample, XPS finds an important role, not only yielding information regarding lattice ions, but also the counter cations and the occluded elements. In the case of zeolites, information on the variation of Si/Al ratio, the changes in the nature of counter cation, the ion exchange level, the occlusion of extraframework phases, and acidic/basic strength can be obtained. XPS analysis can reveal relative surface enrichment of metal ions present in zeolites. The steps involved in the quantitative analysis of these surfaces are well documented by Bouwman and Biloen *[25]*. The influence of support on the chemistry of metal atoms or ions on its surface were clearly illustrated using XPS by Biloen and Pott *et al. [26]*. In the case of zeolites, quantitative studies have suggested varying degrees of deviation of the surface composition from that of bulk. *[27]*.

1.6.3 Characterization of the internal structure or pore structure

Adsorption of nitrogen at liquid nitrogen temperature (77K), gives valuable information about the sample. The adsorption isotherms (volume of nitrogen adsorbed *vs.* relative pressure) is unique for microporous materials (zeolites) *[29]*. The analysis of the data with a suitable model gives following information:

(i) total surface area of the solid (BET method).

(ii) total external surface area/mesopore area (t-plot method).

(iii) micropore volume (t-plot or α_s plot methods).

(iv) The pore size distribution (by analysis of the desorption isotherm).

The adsorption and desorption of nitrogen do not follow the same path, resulting in a hysterisis loop *[30]*. Among other things, the hysterisis loop is also characteristic of the pore shape.

1.7 Isomorphous Substitution in Zeolites

The isomorphous replacement of ions is one of the important properties shown by zeolites and is of several types *[31,32]* such as,

i) isomorphous replacement of intracrystalline salts or molecular water by other salts or guest molecules,

ii) cation exchange,

iii) replacement of Si or Al in tetrahedral sites in the ionic framework by elements such as Al, Si, Ga, Ge, Be, B, Fe, Cr, etc., and

iv) replacement of framework oxygen.

The most important isomorphous replacement is type (iii). Replacements of Al ions by transition metals alter the catalytic properties of the resulting isomorphs, generally called metallosilicates. The basic building units of zeolites consist of TO_4 tetrahedra, where T denotes a metal ion located in the tetrahedral position of a framework. According to Pauling criterion (ρ) *[33]*, the central metal ions adopt a tetrahedral coordination as in TO_4, if the ratio ρ is in the range of $0.414 > \rho > 0.225$, where $\rho = r_c / r_a$ (r_c is the radius of the cation T, and r_o is the radius of oxygen anion). For other values of ρ the coordination numbers are different. The critical values of the parameter ρ (ρ_{crit}) for selected cations are listed in Table 1.3 *[34]*.

TABLE - 1.3

Critical values (ρ_{crit}) and preferred coordination numbers for chosen ions*.

Critical values (ρ_{crit})	Coordination number	Cations with the expected coordination number
$0.225 > \rho_{crit} > 0.147$	3	B^{3+}
$0.414 > \rho_{crit} > 0.225$	4	Al^{3+}, As^{5+}, Be^{2+}, Cr^{6+}, Ge^{4+}, Mn^{2+}, P^{5+}, Se^{6+}, Si^{4+}.
$0.732 > \rho_{crit} > 0.414$	6	As^{3+}, Bi^{5+}, Co^{2+}, Cr^{3+}, Cr^{2+}, Fe^{2+}, Fe^{3+}, Ga^{3+}, Hf^{4+}, In^{3+}, Mn^{2+}, Mn^{4+}, Sb^{5+}, Sn^{4+}, Ta^{5+}, Ti^{3+}, Ti^{4+}, V^{4+}, V^{5+}, Zn^{2+}, Zr^{4+}, Mo^{6+}.
$\rho_{Crit} > 0.732$	8	Bi^{3+}, Ce^{2+}, Ce^{3+}, Eu^{3+}, Nd^{3+}, Pb^{2+}, Sn^{2+}, Tl^{3+}.

* B. Sulikowsko, *Heter. Chem. Rev.*, 3 (1996) 203.

The most important metallosilicate to be used commercially is the titaniumsilicate, TS-1. Vanadium containing analogues were also found to be active in selective oxidation reactions *[35]*. Extensive work on characterization and catalytic applications of vanado silicates have been carried out by Sen *et al.* and others *[24,28b]*. The isomorphous substitution of elements such as B, Be, Ge, Ga, Cr, Ti, V, Sn, Zr, P, etc., for silicon and aluminium in the zeolitic framework has been studied *[36-42]*.

1.8 Catalysis by Medium Pore Zeolites

Olefins undergo a variety of acid catalyzed reactions including double-bond isomerization, oligomerization, cracking, cyclization and aromatization. Due to the restricted pore size in medium pore zeolites, the above reactions produce products. Other reactions reported over zeolites are cracking and hydrocracking *[43]*, hydration *[44]*, hydroisomerization of light paraffins *[45]*, and transalkylation *[46]*.

HZSM-5 and its metal supported analogues have been used in many industrially important reactions like xylene isomerization, alkylation, skeletal isomerization of n-butene, aromatization, etc. In Fluid Catalytic Cracking process, ZSM-5 is used as an additive in order to produce high octane gasoline and light alkenes. More than 50 commercial units world wide are using ZSM-5 additives in FCC operations *[47]*. Production of propene, isobutene and n-butene are favored in the above process *[48]*.

The Mobil-Badger process *[49]* uses HZSM-5 to produce ethyl benzene, from ethylene and benzene. The acidic Ga-HZSM-5 is used to produce benzene, toluene and xylene (BTX) from C_3 and C_4 compounds in the cyclar *[50]* and aroforming process *[51]*.

1.9 A Short Review on Molybdenum Containing Catalysts

The characterization and catalytic activity of supported Mo on alumina (oxide form) are well documented in the literature. A variety of techniques have been adopted to fix the Mo on the support. For example, a coprecipitation method of depositing MoO_3 on alumina was adopted by Giordano *et al. [52]* who studied the relationship between structure and catalytic activity. An equilibrium adsorption method has been devised to overcome the shortcomings of the conventional impregnation technique *[53]*. The supports were contacted with relatively large volumes of aqueous solutions containing the transition metal anions, followed by filtration. The loading was controlled by varying the pH of the solution using aqueous NH_3.

Extensive characterization of MoO_3-NaY zeolite was carried out by Cid *et al.*. *[54]*. They have impregnated Mo using ammonium heptamolybdate as the Mo source with Mo loading ranging from 1 to 15 wt.%. A well dispersed Mo-ZSM-5 was prepared using $Mo(\pi\text{-}C_3H_5)_4$ as the Mo source by Valyon *et al. [55]*. They have compared the activity of the above catalyst with Mo/ZSM-5 prepared by a conventional impregnation method and concluded that Mo-ZSM-5 prepared by impregnation generates acidic sites on the surface, while that prepared by the present technique showed homogeneous distribution of Mo within the crystals. Aqueous ion-exchange of $Mo_2(en)_4^{4+}$ was reported by Word *et al.*, *[56]* and the exchange of MoO_2^{2+} complex in Na-Y was reported by Moorehead *[57]*.

TABLE - 1.4

Molybdenum containing catalysts used in industries*.

Process	Catalyst	Year
Hydrodesulfurization (HDS)	Co,Mo sulfides	1950
Naphthalene oxidation to phthalic anhydride	V, Mo Oxides	1950
Pyrolysis of naphtha	Co-Mo/Al_2O_3	1950
Ammoxidation of propylene (ACN)	Bi, Mo Oxides	1960
Propylene oxidation to acrolein/acrylic acid	Bi, Mo, Oxides	1960
Propylene Metathesis	Mo, W, etc.	1960
Propylene oxidation to propylene oxide	Mo	1960
Isomerization/Metathesis (SHOP)	Ni, Mo	1970
Methylacrylate via t-butanol oxidation	Mo Oxides	1980
Improved coal liquifaction	Co, Mo sulfides	1980
Oxidation of 1-butene to maleic anhydride	MoO_3-V_2O_5	1990

* D. Sanfilippo, *Catalysis today,* 34 (1997) 261.

In general, impregnation methods result mostly in surface loading, since, the large oxoanionic or neutral complexes will not penetrate into the zeolite pores. This drawback was overcome by Fierro *et al., [58]* by vaporizing Mo from the surface of the zeolite crystals and further solid-state exchange of $MoO_2(OH)_2$ within the pores of the Na-Y zeolite. Electron accepting/donating nature of Mo sites in MoO_3-NaY zeolite were determined by Khulbe *et al., [59]* in all samples prepared using ammonium heptamolybdate as the Mo source.

Ione *et al.* have incorporated a series of elements during the hydrothermal synthesis of ZSM-5 *[31]*. The Si/Mo ratio of final sample synthesized by them was very high *[31]*. Incorporation of Mo in the framework of large pore zeolites during hydrothermal synthesis were attempted by some authors *[60,61]* but details of characterization, stability, nature of the Mo species and their catalytic activity are not well documented.

1.10 Objective of the Present Investigation

Eventhough, appreciable work has been carried out on supported Mo catalysts, the literature on the incorporation of Mo in the zeolite framework is scarce. It was, therefore, realized that a study of Mo containing MFI and MEL molecular sieves will be useful in understanding the incorporation of large metal ions in zeolite frameworks. The replacement of the T atoms in the zeolitic framework with metal ions like Ti^{4+}, V^{5+}, and Sn^{4+} modifies the catalytic properties of the resulting metallosilicates appreciably. It was also expected that the incorporation of Mo in the framework of medium pore zeolites should result in Mo silicalites possessing better activities than the impregnated analogue (prepared by conventional wet impregnation method). Throughout the thesis, wherever necessary, the characterization and

catalytic properties of the Mo-incorporated samples have been compared with those of a Mo-impregnated sample and with corresponding parent analogues (silicalite-1, silicalite-2). This thesis is a study of the synthesis, characterization and catalytic properties of Mo containing MEL and MFI zeolites.

The general synthesis procedure adopted in the synthesis of Mo-MEL (MoS-2) samples is presented in Chapter II. The influence of various parameters, viz., temperature, and the concentration of Mo, the organic template content, and water content in the synthesis gel, on the crystallization of the sample are investigated. The conditions for the synthesis have been optimized to get a good crystalline sample. The synthesis of Mo-silicalite-1 (MoS-1) and procedure for the preparation of impregnated analogue are also reported in detail.

Chapter III reports the physicochemical characterization of Mo-silicalite-2 (MoS-2) samples with different Si/Mo ratios. The details of the sampling techniques adopted and the instruments used during investigation by SEM, XRD, FTIR, UV-Visible, TG/DTA, and sorption of probe molecules are presented. The nature of the Mo species in MoS-2, its coordination and redox properties are discussed on the basis of the results obtained in the above studies.

The results of the characterization of Mo-silicalite-1 are discussed in chapter IV. The oxidation states of the Mo species present in Mo-MFI and their acidic nature are investigated. The crystallinity, thermal stability and morphology of the Mo-silicalite-1 are discussed in detail.

Chapter V reports the catalytic properties of the Mo containing molecular sieves with MFI and MEL topology. The catalytic oxidation of thioethers to the corresponding sulfoxides without producing sulfones over MoS-1 is discussed. Oxidation of ethanol has been used to

investigate the nature of active sites in the Mo catalysts. The activities of Mo-silicalites are compared with that of supported MoO_3 catalysts. The activities of MoS-1 samples with different Si/Mo ratios and the influence of process parameters are presented. The oxidation of ethanol over MoS-2 is also reported and the activity is compared with that of MoS-1.

The Mo-silicalites prepared by hydrothermal methods were found to be active in the direct conversion of methane to aromatics, especially benzene, under non-oxidative conditions. The aromatization of methane has been carried out over Mo and Al containing molecular sieves with MFI and MEL topology has been carried out. The physico-chemical characteristics of the above samples were studied. The reaction has been carried out over Mo/Al isomorphs and the influence of Mo and Al content on the activity has been investigated. The activities of Mo/Al-MFI and Mo/Al-MEL have been compared.

1.11 References

1. W.L. Bragg, "The Atomic Structure of Minerals", Cornell University Press, NY, (1937).

2. W.M. Meier, "Molecular Sieves", Soc. Chem. Ind., London, (1968) 10.

3. E.M. Flanigen, "Proc. 5th Int. Confer. Zeo." (Rees, L.V.C. Eds.) Naples, Italy, (1980) 760.

4. R.M. Barrer, "Molecular Sieves", Soc. Chem. Ind., London, (1968); L.B. Sand, Econ. Geol., (1967) 191.

5. P.B. Weisz and V.J. Frilette, *J. Phys. Chem.* 64 (1960) 382.

6. R.J. Argauer and G.R. Landolt, *US Pat* 3702886, 1972.

7. P. Chu, *US Pat* 3709979, I973.

8. P. Chu, *US Pat* 4397827, 1983; L.D. Rollmann and E.W. Valyocsik, *US Pat* 4423021, 1983.

9. P.B. Weisz, *Stud. Surf. Sci. Catal.*, 7A (1981) 3.

10. E.G. Derouane and Z. Gabelica, *J. Catal.*, 65 (1980) 486.

11. G.T. Kokotailo, S.L. Lawton, D.H. Olson and W.M. Meier, *Nature*, 272 (1978) 437.

12. E.M. Flanigen, J.M. Bennet, R.W. Grose, J.P. Cohen, R.L. Patton, R.M. Kirchnev and J.V. Smith, *Nature*, 272 (1978) 840.

13. S.L. Meisel, J.P. McCullough, C.H. Lechthaler and P.B. Weisz, *Chemtech*, 6 (1976) 86.

14. G.T. Kokotailo, P. Chu, S.L. Lawton and W.M. Meier, *Nature*, 275 (1978) 119.

15. J. Hilliard, *J. Microsc.* 97 (1972) 45.

16. M. Taramasso, G. Perego, and B. Notari, *US Pat.*,4410801 (1983).

17. J.J. Pluth, J.V. Smith and J.M. Bennett, *Acta. Crystallogr.* C42 (1986) 283.

18. E.M. Flanigen, H Khatami and H.A. Szymanski, *Molecular Sieve Zeolite-1*, ACS series, 101 (1971) 210.

19. E.M. Flanigen, "Zeolite Chemistry and Catalysis (Ed.J.A. Rab), *ACS Monograph.*", 171 (1976) 80.

20. P.A. Jacobs, H.K. Beyer and J. Valyon, *Zeolites*, 1 (1981) 161.

21. W. DeWilde, R.A. Schoonheydt and J.G. Uytherboven, ACS Symp. Ser., 40 (1977) 132.

22. M.R. Boccuti, K.M. Rao, A. Zecchier, G. Leofanti and G. Pefrini, *Stud. Surf. Sci. Catal.*, 48 (1989) 133.

23. N.K. Mal, Ph.D., thesis submitted to "University of Pune", India, Jan. 1997.

24. T. Sen, Ph.D., thesis submitted to "University of Pune", India, June 1997.

25. R. Bouwman and P. Biloen, *Surface Sci.*, 41 (1974) 348.

26. P. Biloen and G.T. Pott, *J. Catal.*, 30 (1973) 169.

27. J. Tempere, d. Delagosse and J. Contour, *J. Phys. Chem. Lett.*, 33 (1975) 95.

28. a) J.S. Reddy, R.Kumar and P. Ratnasamy, *Appl. Catal.*, 58 (1990) L1.

    b) P.R.H.P. Rao, A.V. Ramaswamy and P. Ratnasamy, *J. Catal.*, 137 (1992) 225.

    c) Helge Jeziorowski and Helmut Knozinger, *J. Phys. Chem.*, 83 (1979) 1166.

29. S. Lowell and J.E. Shields in "Powder surface area and porosity", (B. Scarlett, Eds.), Chapman and Hall, (1984) .

30. J.M. Thomas and W.J. Thomas in "Introduction to the principles of Heterogeneous Catalysis", Academy Press, (1967) 197.

31. K.G. Ione, L.A. Vostrikora and V.M. Mastikhin, *J. Mol. Catal.*, 31 (1985) 355.

32. R.M. Barrer, "Proc. Int. Zeo. Conf., 6th, Reno-USA", (Eds.D. Oldon and A. Bisio), (1983) 870.

33. L. Pauling, "The Nature of the Chemical Bond", Cornell Univ. Press, Ithaca, (1960).

34. B. Sulikowski, *Heter. Chem. Rev.*, 3 (1996) 203.

35. A.V. Ramaswamy, S. Sivasanker and P. Ratnasamy, *Microporous Mater.*,2 (1994) 451.

36. R.M. Barrer, "Hydrothermal Chemistry of Zeolites", Academic Press, London, (1982) 251.

37. M. Taramasso, G. Perego and B. Notari, Proc. Int. Conf. Zeo. 5th, Napoli Heyden, London (1989) 40.

38. N.A. Kutz, Proc. Symp. Ind., 2nd, Univ. Coop. Chem. Progm., Texas, (1989) 121.

39. R.M. Dessau and G.T. Kherr, *Zeolites*, 4 (1984) 315.

40. Z. Gabelica, G. Debras and T.B. Nagy, "Catalysis in Energy Science", Elsevier, 21 (1984) 113.

41. C.T.W. Chu and C.D. Chang, *J. Phys. Chem.* 89 (1985) 1569.

42. V.M. Rmanikov, L.S. Chumachenko, V.M. Mastikhin, and K.G. Ione, *J. Catal.*, 94

(1985) 508.

43. N.Y. Chen, J. Mazink, A.B. Schwartz and P.B. Weisz, *Oil Gas J.* 66 (47) (1968) 154.

44. C.D. Chang and N.J. Morgan, *US pat* 4214307, 1980.

45. W.O. Haag and R.M. Lago, *US Pat* 43374296, 1983.

46. H.G. Karge, J. Ladebeck, Z. Sarbak and K. Hatada, *Zeolites*, 2 (1982) 94.)

47. A.A. Avida, *Akzo Catalytsis Symposium*, 1991.

48. K.Y. Yung, P.O'Connor, N.M.vant Klooster and S.J. Yanik, *Akzo Catalysis Symposium*, South Africa, 1995.

49. F.W. Dwyer, P.J. Lewis and F.H. Schneider, *Process Technology Chem. Eng.*, 83 (1976) 90.

50. P.C. Doolan and P.R. Pujado, *Hydrocarbon Processing,* 68 (1989) 72.

51. L. Mank, A. Minkkien and R. Shaddich, H.T.I. Quarterly, (1992) 69.

52. N. Giordano, J.C.J. Bart, A. Vaghi , A. Castellen and G. Martinotti, *J. Catal.*, 36 (1975) 81.

53. L. Wang and WK. Hall, *J. Catal.*, 77 (1982) 232.

54. R. Cid, F.J. Gil Llambias, J.L.G. Fierro, A.L. Agudo and J. Villasenor, *J. Catal.*, 80 (1984) 478.

55. J. Valyon and A. Meszares-kis, *Stud. Surf. Sci. Catal.*, 49B (1989) 1015.

56. M.B. Word and J.H. Lunsford, in Proceedings of 6th Int. Zeo. Confer. 1983 (D.H. Olson and A. Bisio Eds.), Butterworths, 1984.

57. E.L. Moorehead, *US Pat.* 4,297,243 (1981).

58. J.L.G. Fierro, J.C. Conesa and A.L. Agudo, *J. Catal.*, 108 (1987) 334.

59. K.C. Khulbe, R.S. Mann and C.D. Ajaka, *Zeolites*, 13 (1993) 572.

60. W. Pang, L. Yu, X. *Shiyou, Shiyou Jiagong*, 5 (2) (1989) 355.

61. L. Yu, W. Pang, *Jilin Daxue Liran Kexue Xuebao*, 3 (1989) 77.

Chapter II

SYNTHESIS OF Mo-SILICALITES

2 SYNTHESIS OF Mo-SILICALITES

2.1 Synthesis of Mo-silicalite with MEL Topology (MoS-2)

The hydrothermal synthesis of the Mo-silicalite samples were carried out using teflon lined stainless-steel autoclaves (150 mL) under static conditions (Fig.2.1). Prior to synthesis the autoclaves were cleaned with boiling NaOH for half an hour and rinsed with deionized water. This process dissolved out zeolite impurities present if any, thus minimizing seeding effects. The raw materials used in the syntheses were tetraethylorthosilicate (TEOS, Aldrich, 99%), tetrabutylammonium hydroxide (TBAOH, Aldrich, 40% aqueous solution), tetrapropylammonium hydroxide (TPAOH, Aldrich, 20% aqueous solution), and sodium molybdate (LOBA Chemie, Bombay).

The general synthesis of the Mo-silicalites involved (i) mixing of silica source (TEOS) and templates (TBAOH/TPAOH) thoroughly, (ii) the addition of the Mo source dissolved in calculated amount of water to form a transparent gel, and (iii) the hydrothermal crystallization under autogeneous pressure in static conditions for several hours (24 -72 h). The product was then separated by centrifugation, washed well with deionized water and dried to get the as-synthesized Mo-silicalite.

Based on a large number of trials, the most suitable composition of the gel (in terms of molar ratios) for the synthesis of Mo-silicalite-2 (MoS-2) was found to be: Si/Mo = 100, $TBAOH/SiO_2$ = 0.3, H_2O/SiO_2 = 23. In a typical synthesis, 29.9 g of TEOS was added to 28 g of TBAOH (40% aqueous solution) under vigorous stirring. After 15 min., 0.35 g of sodium molybdate dissolved in 60 g of water was added in drops. The mixture was left

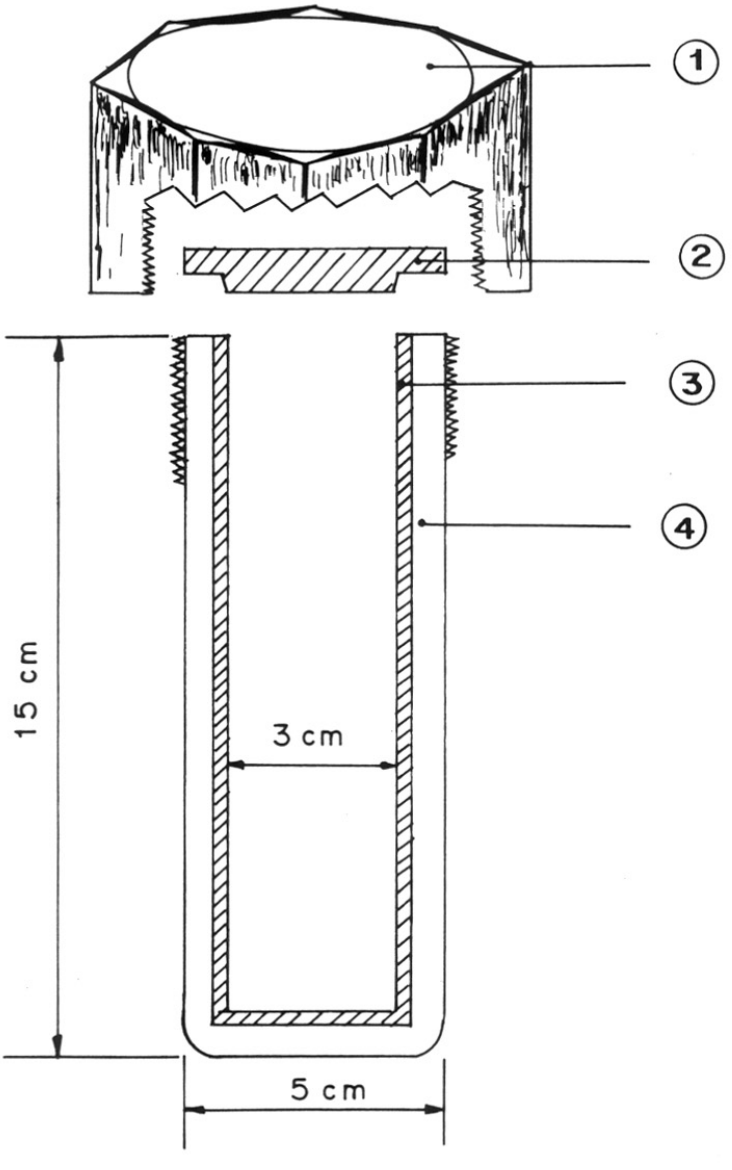

Fig. 2.1 : Stainless steel autoclave used in the synthesis of Mo-silicalites
1) stainless steel cap, 2) teflon cap, 3) teflon lining
4) autoclave body (ss)

undisturbed for 10 minutes (pH = 11.6). The contents were then transferred to an autoclave, heated to 453 K and kept under autogeneous pressure at this temperature for 2 days. The as-synthesized Mo-silicalite-2 (MoS-2) was separated by centrifuging, washed well and dried at 383 K for 12 h. The sample was calcined at 783 K for 8 h in a flow of dry air. The temperature of the furnace was increased at the rate of 10 K/min., holding for 1 h after every 100 K increase.

2.1.1 Influence of Mo content in the synthesis gel

The effect of Mo content on the crystallization of the sample was studied for Si/Mo (input) gel ratios in the range, 35 to 200. The crystallinity of the samples at different intervals can be evaluated by water vapor sorption, nitrogen sorption at a fixed p/p_o value or from intensities of the peaks in the XRD pattern *[1]*. In this study the XRD method was used. The sample with the highest intensity (synthesized in this study) was taken as the 100% crystalline sample [XRD crystallinity (%) = I_t/I_o X 100; where I_o is the intensity in counts of the 100% crystalline sample and I_t is the intensity of the sample at time 't' in hours]. An important observation in our studies was the enhancement of the rate of crystallization by the Mo salt. This enhancement is attributable to the MoO_4^{2-} species present in the gel. Kumar *et al.* have already observed that the rates of crystallization of many zeolites were enhanced by the presence of some cations *[2]*. In the present case, the MoO_4^{2-} species act both as the promoter and as the Mo source. Silicalite-2 (blank) was found to crystallize completely at 72 h, while, the crystallization of MoS-2 was found to be complete at about 45 h. The crystallinity of the samples after different crystallization times are presented in Fig. 2.2. The typical composition of the initial gel mixture is given in Table 2.1

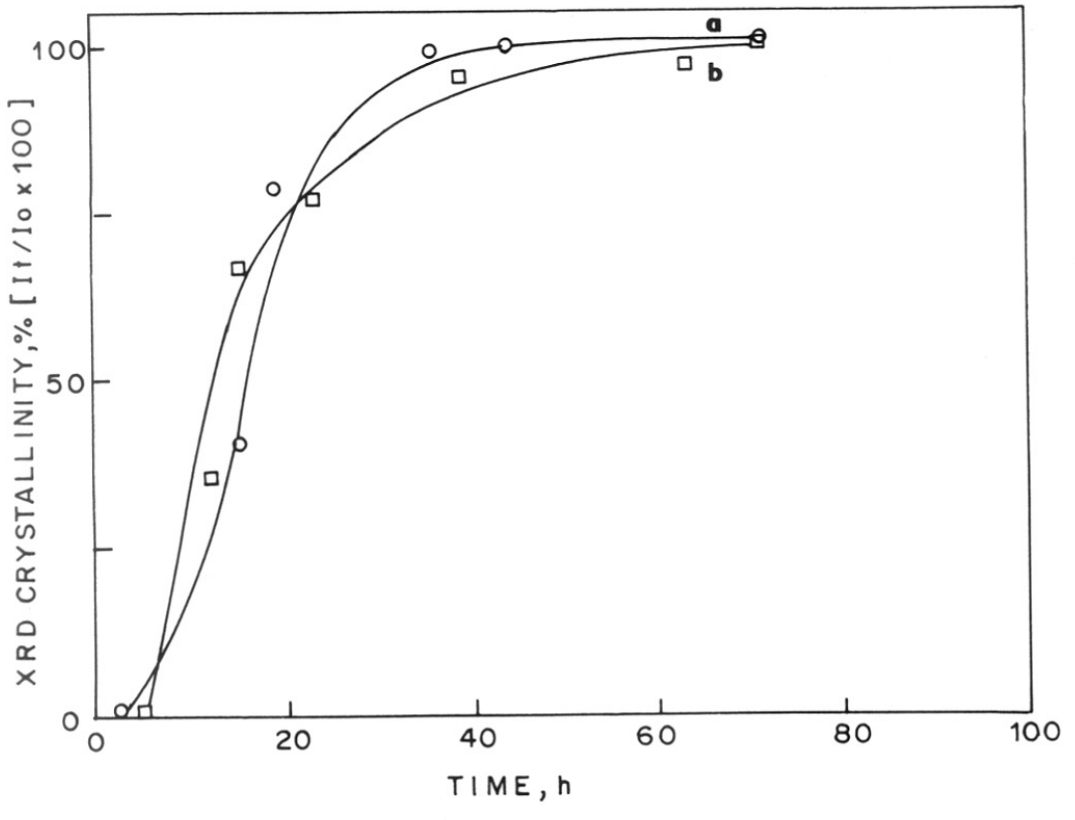

Fig. 2.2 : Enhancement in the rate of crystallization on the addition of Mo to the synthesis gel (a) MoS-2 (b) silicalite-2.

(I_t = intensity of the XRD peak at $2\theta = 23.1°$ at time t, and
I_o = intensity of the XRD peak at $2\theta = 23.1°$ of the most crystalline sample obtained in the study).

TABLE - 2.1

Composition of initial gel mixture (typical) in terms of oxide mole ratios.

SiO_2 :	TBAOH :	MoO_3 :	H_2O
1	0.3	0.01	23

The intercept at the time axis is the induction period (Fig. 2.2). The induction period was followed by crystallization. A steep increase in the crystallinity was observed within 10 h, followed by a decrease in the rate of crystallization. A good crystalline material was obtained after 40 h. The X-ray diffraction patterns of the samples collected at different time interval are given in Fig. 2.3. A gradual increase in the intensity (crystallinity) of the sample can be observed. The effect of Si/Mo ratio on the crystallinity of the sample at different time intervals are presented in Fig. 2.4. The typical composition of the initial gel mixtures (used in this study) are given in Table 2.2

TABLE - 2.2

Influence of Mo content on the crystallization of MoS-2: composition (moles) of the synthesis gel mixture.

SiO_2 :	TBAOH :	MoO_3 :	H_2O
1	0.3	0.029	23
1	0.3	0.01	23
1	0.3	0.005	23

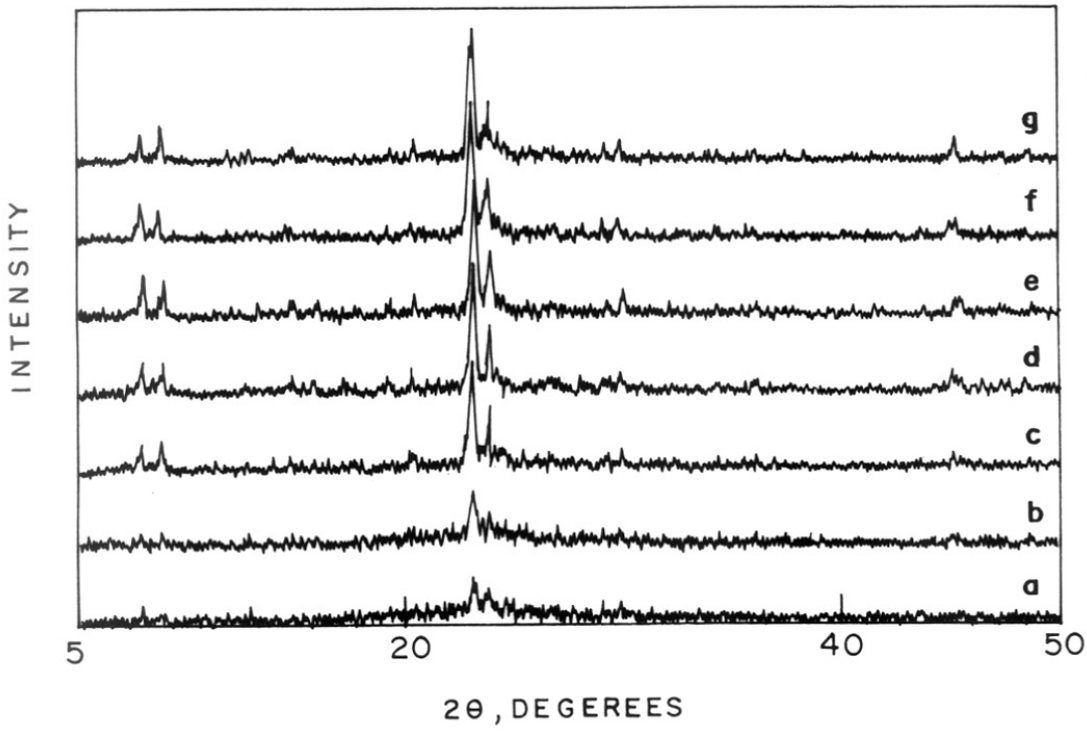

Fig. 2.3 : The XRD profiles of MoS-1 at different time intervals.
(a) 13h; (b) 16h; (c) 20h; (d) 23h; (e) 37h; (f) 45h; (g) 72h.

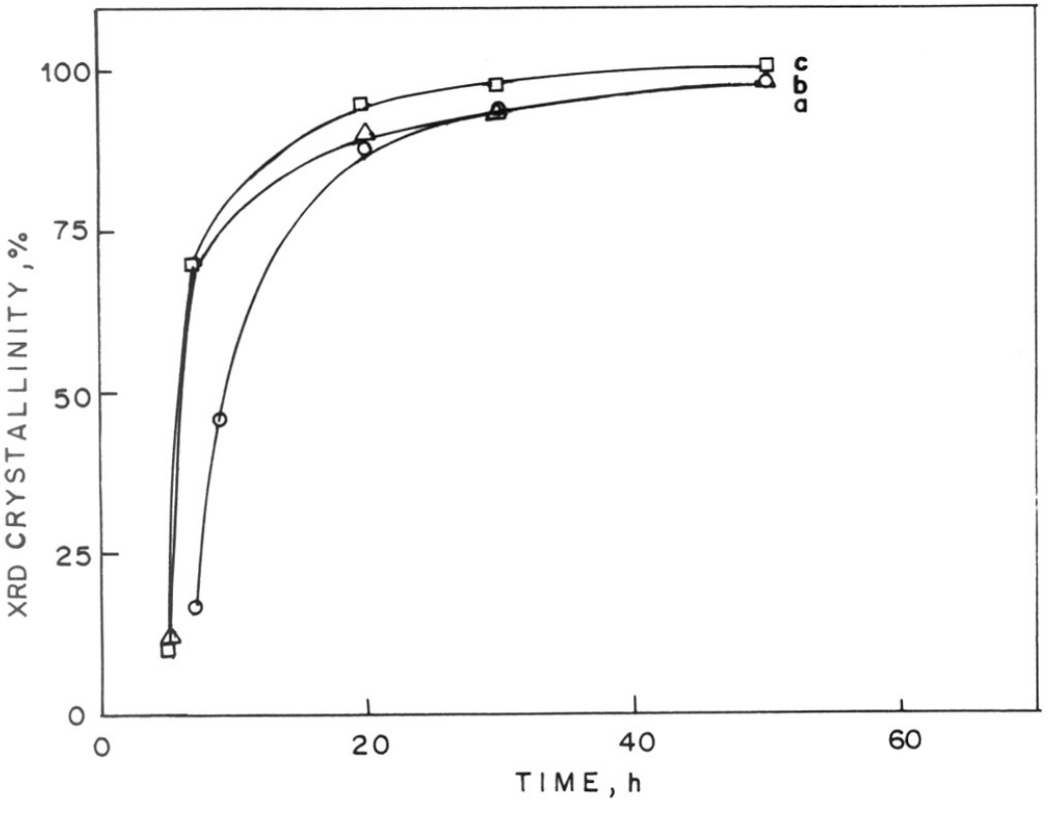

Fig. 2.4 : Influence of Mo content on the crystallization of MoS-2. (a) Si/Mo = 35; (b) Si/Mo = 100; and (c) Si/Mo = 200.

Even though the MoO_4^{2-} accelerates the rate of crystallization, it is seen from Fig. 2.4, that a high Mo concentration (Si/Mo) retards the same, and reduces the crystallinity of the sample. However, even at this concentration, the rate of crystallization is faster than for pure silicalite (Fig. 2.2).

2.1.2 Influence of temperature

The influence of temperature on the rate of crystallization was studied between 433 and 473 K. The induction period was found to be inversely proportional to temperature. The rates of crystallization at different temperatures with respect to time are shown in Fig. 2.5. The crystallization rates at 453 and 473 K were similar. But at the lower temperature of 433 K, the rate of crystallization was slower and the sample was also less crystalline. The typical composition of the initial gel mixture used in the above studies is given in Table 2.3

TABLE - 2. 3

Influence of temperature on the crystallization of MoS-2: Composition (moles) of the synthesis gel mixture.

SiO_2 :	TBAOH :	MoO_3 :	H_2O
1	0.3	0.01	23

2.1.3 Influence of water content in the synthesis gel

Water always plays an important role in the hydrothermal synthesis of molecular sieves. The influence of water content on the crystallization of MoS-2 was studied by changing the amount of water in the synthesis gel (Fig. 2.6). For convenience, the water

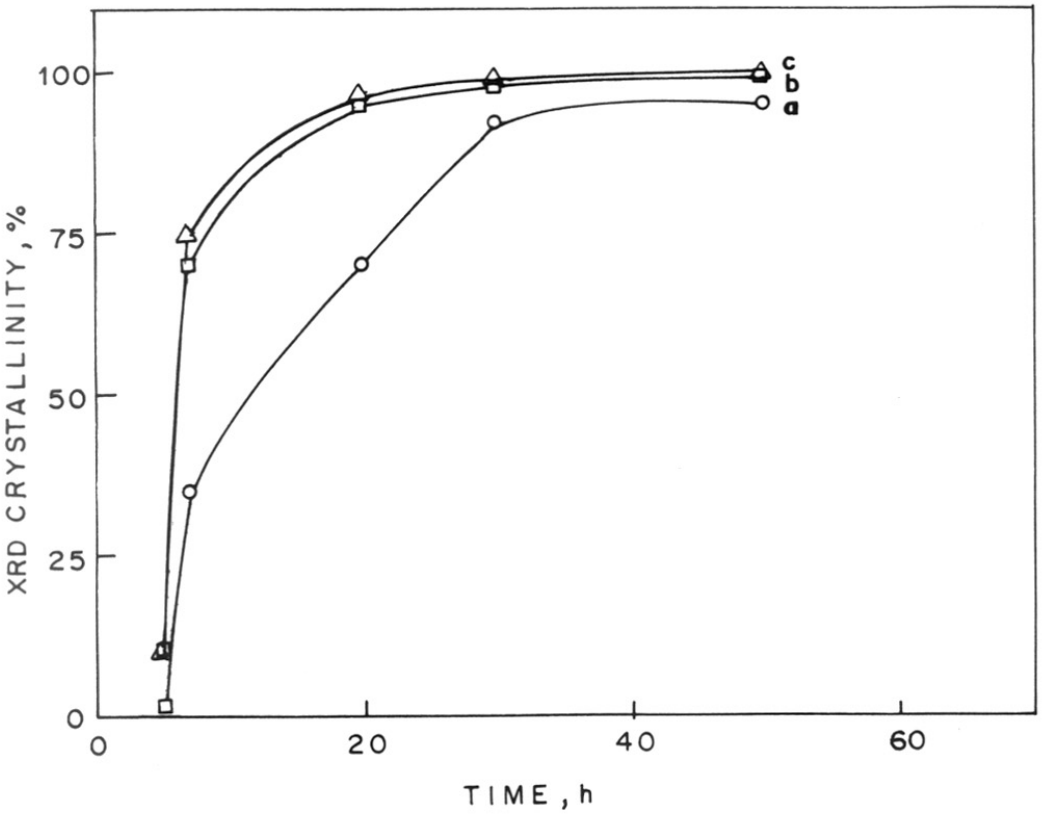

Fig. 2.5 : Influence of temperature on the crystallization of MoS-2.
(a) 433 K; (b) 453 K; (c) 473 K.

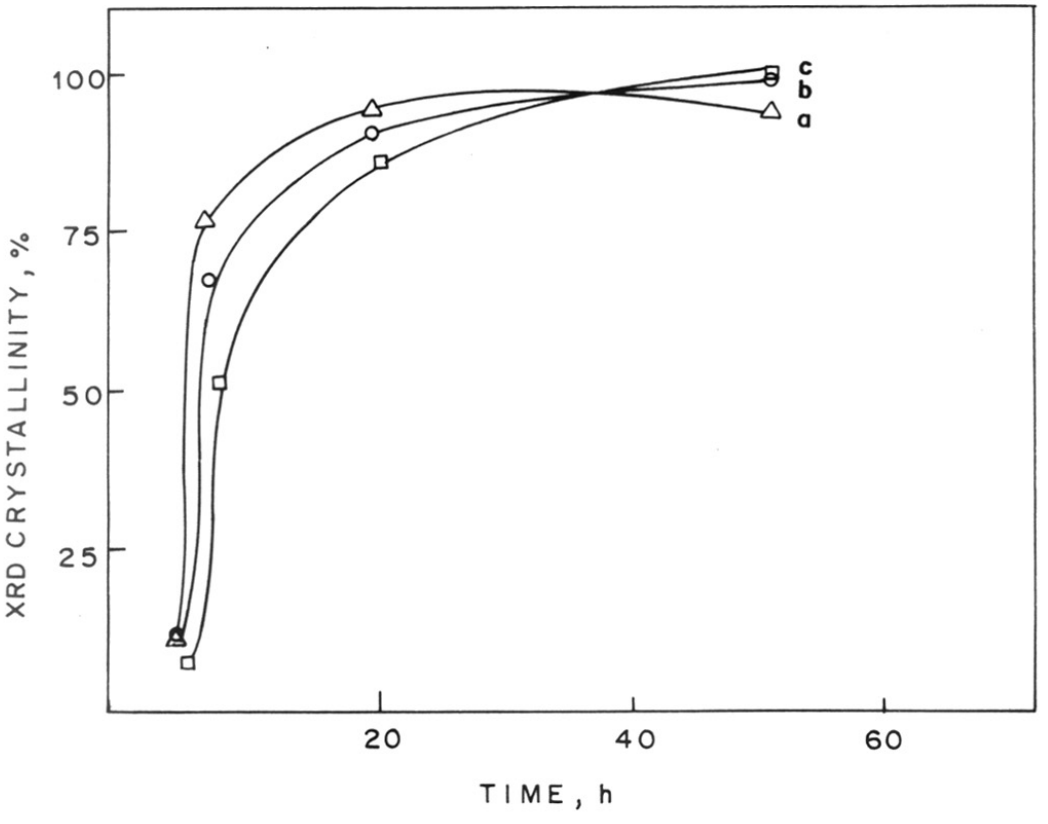

Fig. 2.6 : Influence of water content in the synthesis gel on crystallization. (a) $H_2O/SiO_2 = 15.4$; (b) $H_2O/SiO_2 = 23$; (c) $H_2O/SiO_2 = 30.8$.

content has been expressed as H_2O/SiO_2 ratio. The typical compositions of the gels with different water contents are presented in Table 2.4. An increase in the crystallization rate was observed with a decrease in the water content in the initial gel mixture. Similar observations have already been made by earlier workers *[3]*. Further decrease in water content did not produce any crystalline solid, even after 72 h. Redissolution of the sample was observed when the water content was low, due to the increase in pH (pH = 13.1), thus reducing the crystallinity of the sample.

TABLE - 2.4

Influence of water content in the initial gel mixture: Composition (moles) of the synthesis gel mixture.

SiO_2 :	TBAOH :	MoO_3 :	H_2O
1	0.3	0.01	15.4
1	0.3	0.01	23.0
1	0.3	0.01	30.8

2.1.4 Influence of organic base (template concentration)

Figure 2.7 shows the effect of organic base concentration on the crystallization rate of the sample. The crystallization of the sample was not complete (~50%) even after 72 h when the template concentration was decreased in the initial gel mixture ($TBAOH/SiO_2$ = 0.21). The typical composition of the initial gel mixtures with different template concentrations are presented in Table 2.5.

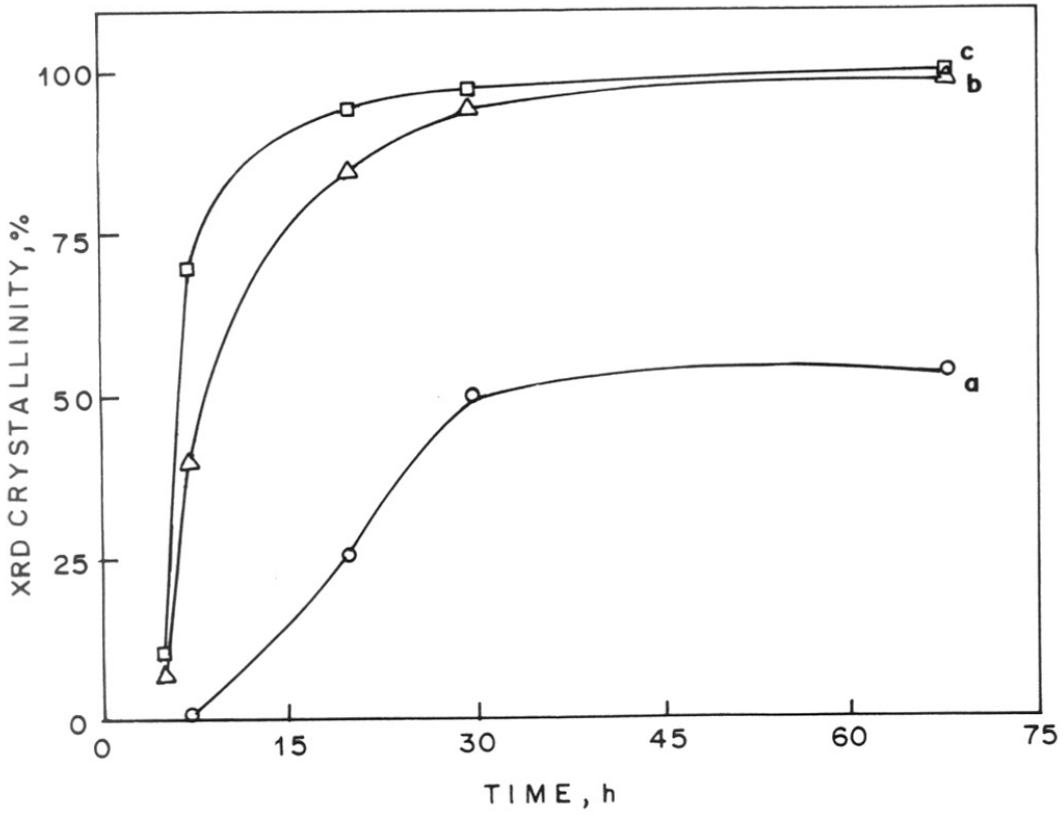

Fig. 2.7 : Influence of template content in the synthesis gel on crystallization.
(a) TBAOH/SiO_2 = 0.21 (b) TBAOH/SiO_2 = 0.3 (c) TBAOH/SiO_2 = 0.56.

The template (TBAOH) being a strong base, the pH of the initial gel mixtures were found to be high (11.5). Earlier workers *[4]* have concluded that an increase in pH after complete crystallization indicates the formation of a stable and crystalline material. While an insignificant change or a decrease in pH as a function of time indicates a less stable phase or amorphous material. The change in the value of pH at different template concentrations are shown in Fig. 2.8. There was an insignificant change in pH in the case of $TBAOH/SiO_2$ = 0.21, resulting in the formation of a less crystalline material. The $TBAOH/SiO_2$ ratio of 0.3 was found to be ideal, as it resulted in the most crystalline material. Besides, the increase in pH (11.6 - 12.9) during crystallization was the highest among the 3 cases.

TABLE - 2.5

Influence of template content on the crystallization of MoS-2: Composition (moles) of the synthesis gel mixture.

SiO_2 :	TBAOH :	MoO_3 :	H_2O
1	0.21	0.01	23
1	0.30	0.01	23
1	0.56	0.01	23

2.1.5 Influence of aging time

The aging time plays an important role in the crystallization of MoS-2. A longer aging time of the gel (~30 min.) results in amorphous material containing a physical mixture of silica and molybdena. An optimum aging time of around 10 minutes was found to be

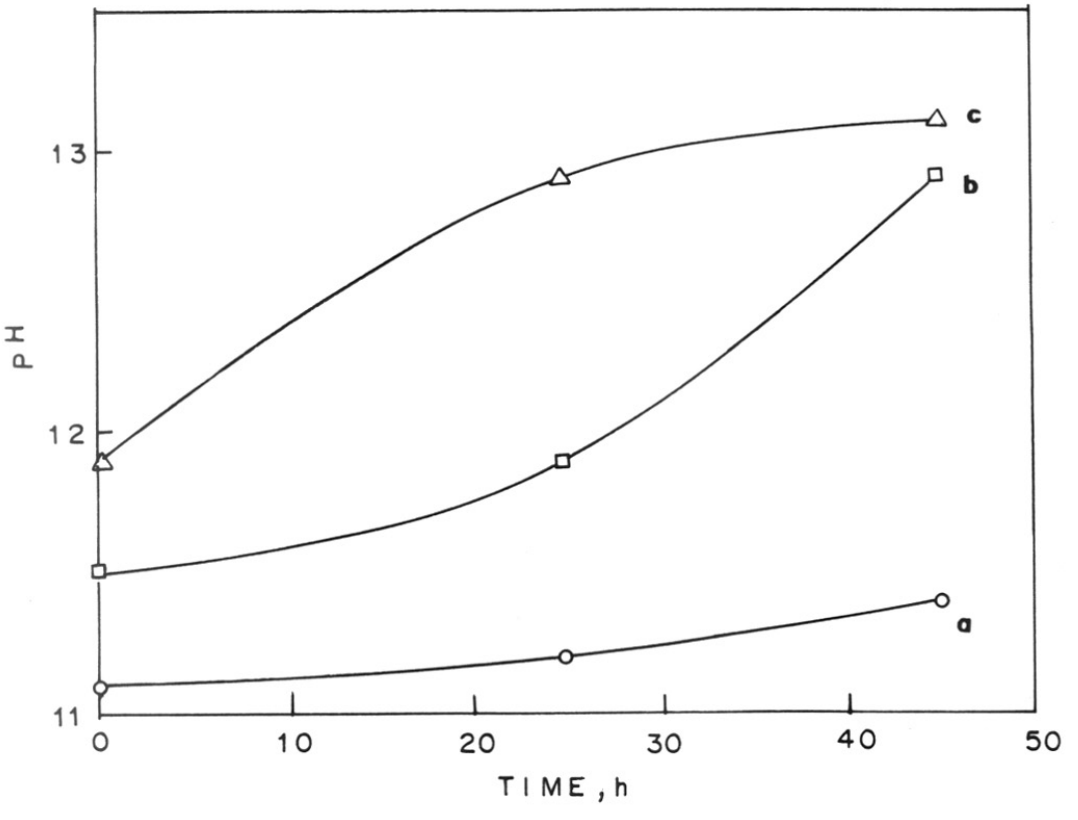

Fig. 2.8 : Change in pH during the crystallization of MoS-2.
(a) TBAOH/SiO_2 = 0.21 (b) TBAOH/SiO_2 = 0.3 (c) TBAOH/SiO_2 = 0.56.

suitable. This observation was found to be similar for synthesis gels with different Mo concentrations.

2.2 Synthesis of Silicalite-2

Tetrabutylammonium hydroxide (TBAOH, 28 g, Aldrich, 40% aqueous solution) was mixed with tetraethyl orthosilicate (TEOS, 29.9 g, Aldrich) under vigorous stirring. After 15 minutes, 60 g of deionized water was added, mixed and the contents kept undisturbed for 30 minutes. The contents were transferred into an autoclave and treated hydrothermally under autogeneous pressure at 453 K for 72 h to get as-synthesized silicalite-2.

2.3 Synthesis of Mo-silicalite with MFI Topology (MoS-1)

In a typical synthesis, 29.76 g tetraethylorthosilicate (TEOS; Aldrich) was slowly added to 47.36 g tetrapropylammonium hydroxide (TPAOH; Aldrich; 20% solution) under vigorous stirring. After 15 min., 0.74 g of ammonium heptamolybdate in 25.1 g of water was added dropwise to the above mixture with continuous stirring. The mixture was aged for 30 min. The final clear solution was transferred to a stainless steel autoclave with teflon lining and kept in a static air oven maintained at 443 K for 24 h. The crystalline material was separated by centrifuging and washed well with distilled water. The as-synthesized material was calcined at 783 K for 8 h. The calcined material was characterized by various techniques. The MoS-1 with different Si/Mo ratios were prepared by varying the Mo content in the initial gel mixture. Unlike, MoS-2, the crystallinity of MoS-1 was not affected by a longer aging time.

The composition of a typical gel mixture used in the synthesis of MoS-1 expressed in terms of mole ratios is presented in Table 2.6.

TABLE - 2.6

The typical gel composition used for the synthesis of MoS-1

SiO_2	:	Template (TPAOH)	:	MoO_3	:	H_2O
1		0.326		0.028		24.33

2.3.1 Influence of Mo content in the synthesis gel

The influence of Mo content on the crystallization of MoS-1 was studied for Si/Mo (input) gel ratios in the range 35 to 200.

TABLE - 2. 7

Gel compositions (mole) used in the synthesis of MoS-1: Studies on the influence of Mo content.

SiO_2	:	Template (TPAOH)	:	MoO_3	:	H_2O
1		0.326		0.028		24.33
1		0.326		0.010		24.33
1		0.326		0.005		24.33

Plots of XRD crystallinity Vs time in hours are shown in Fig. 2.9. It is important to note that the presence of Mo cationic species accelerates the rate of crystallization in this case also. The parent molecular sieve silicalite-1 was found to crystallize completely at ~22 h while the MoS-1 was found to crystallize within 10 h (Fig.2.9). But, the presence of a large amount of Mo (Si/Mo = 35) retards the rate of crystallization to a small extent (Fig. 2.10). The samples with Si/Mo = 100 and 200 were found to follow similar crystallization kinetics. The compositions of the initial gel mixtures are given in Table 2.7

2.3.2 Influence of temperature on the crystallization of MoS-1

The kinetics of crystallization of Mo-silicalite with MFI structure followed nearly the same trend as that of the Mo-MEL sample. But, the rate of crystallization was found to be rapid in the case of MoS-1. The influence of temperature on the crystallization of MoS-1 is shown in Fig. 2.11. As the temperature was increased, the induction period decreased and the rate of crystallization was enhanced. The composition of the gel mixture used in the above studies is given in Table 2.6.

2.3.3 Influence of organic template in the synthesis gel

The effect of the organic base on the crystallization rate of the samples is shown in Fig. 2.12. Unlike MoS-2, a decrease in the concentration of the template increases the rate of crystallization. The increase in the pH in all the three cases was found to be nearly the same (pH_{final} - $pH_{initial}$ = 0.74), indicating the formation of a stable crystalline phase *[4]*. But, the crystallite size was found to be small for the gel with a higher template content (0.2 μm). It increased to 0.5 μm to 1 μm, when the template concentration was decreased. The

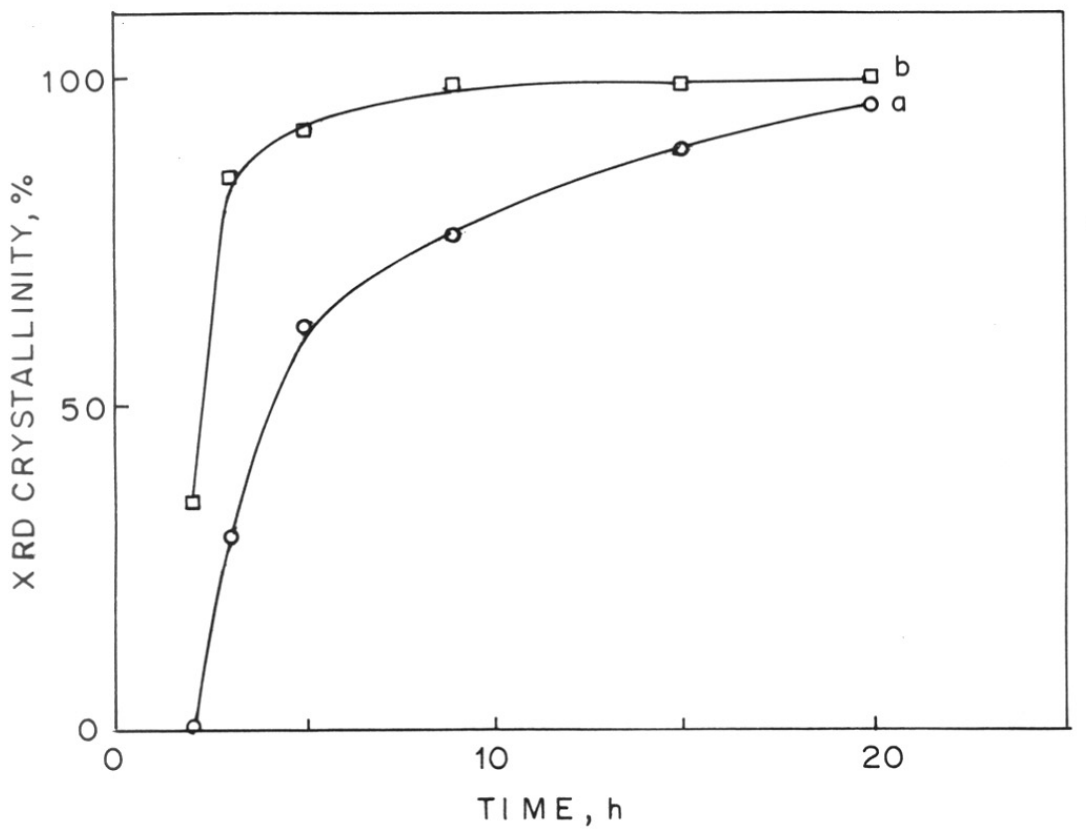

Fig. 2.9 : Synthesis of MoS-1: Enhancement in rate of crystallization on the addition of Mo to the synthesis gel (a) silicalite-1 (b) MoS-1 [100].

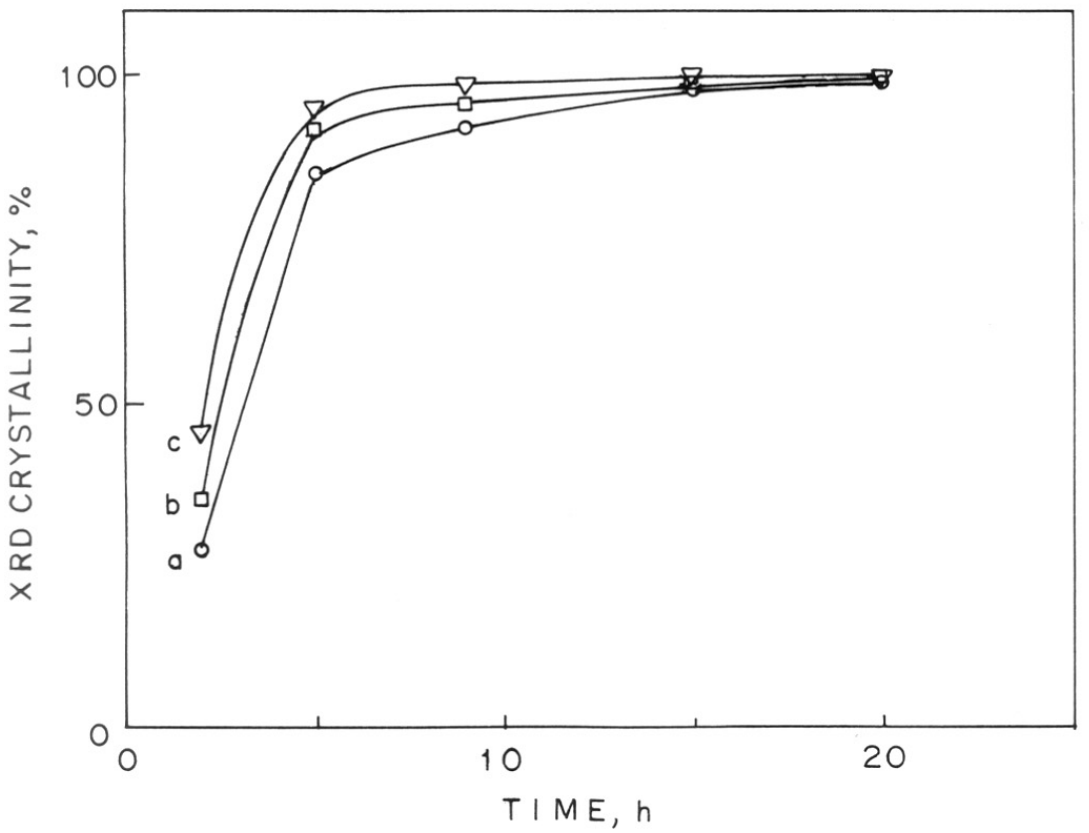

Fig. 2.10 : Influence of Mo content on the crystallization of MoS-1.
(a) Si/Mo = 35; (b) Si/Mo = 100; (c) Si/Mo = 200.

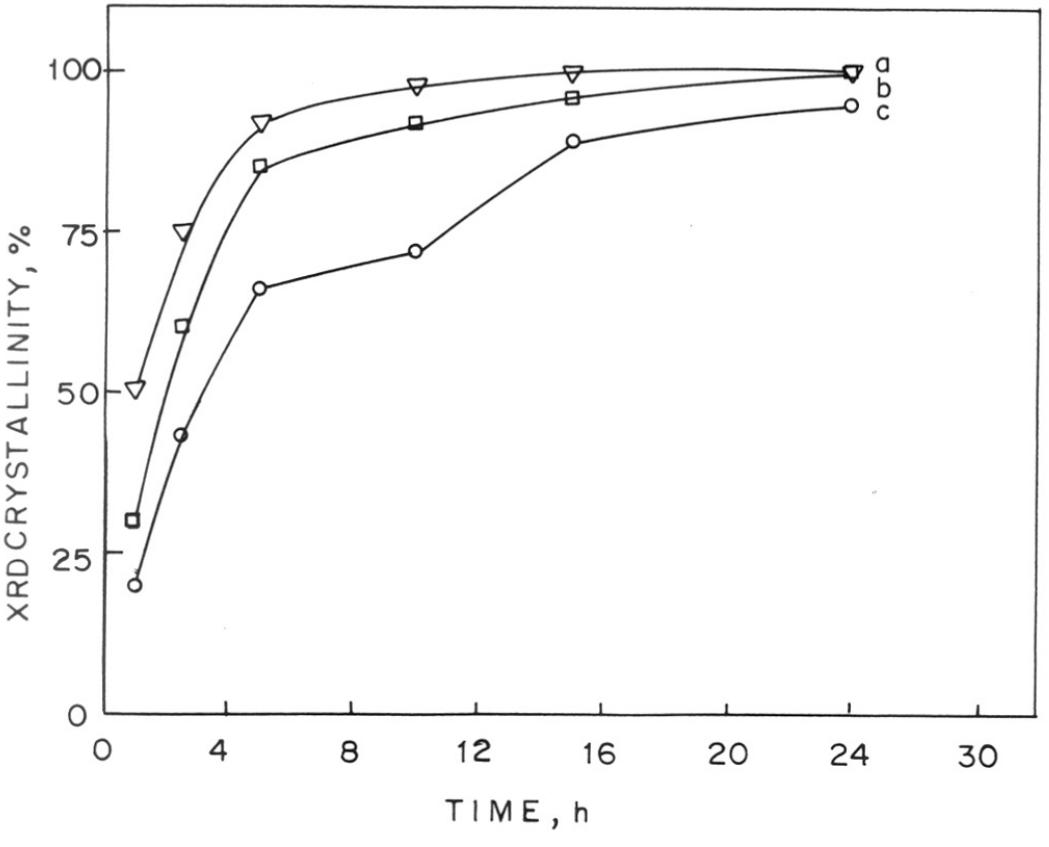

Fig. 2.11 : Influence of temperature on the crystallization of MoS-1. (a) 463 K; (b) 443 K; (c) 423 K.

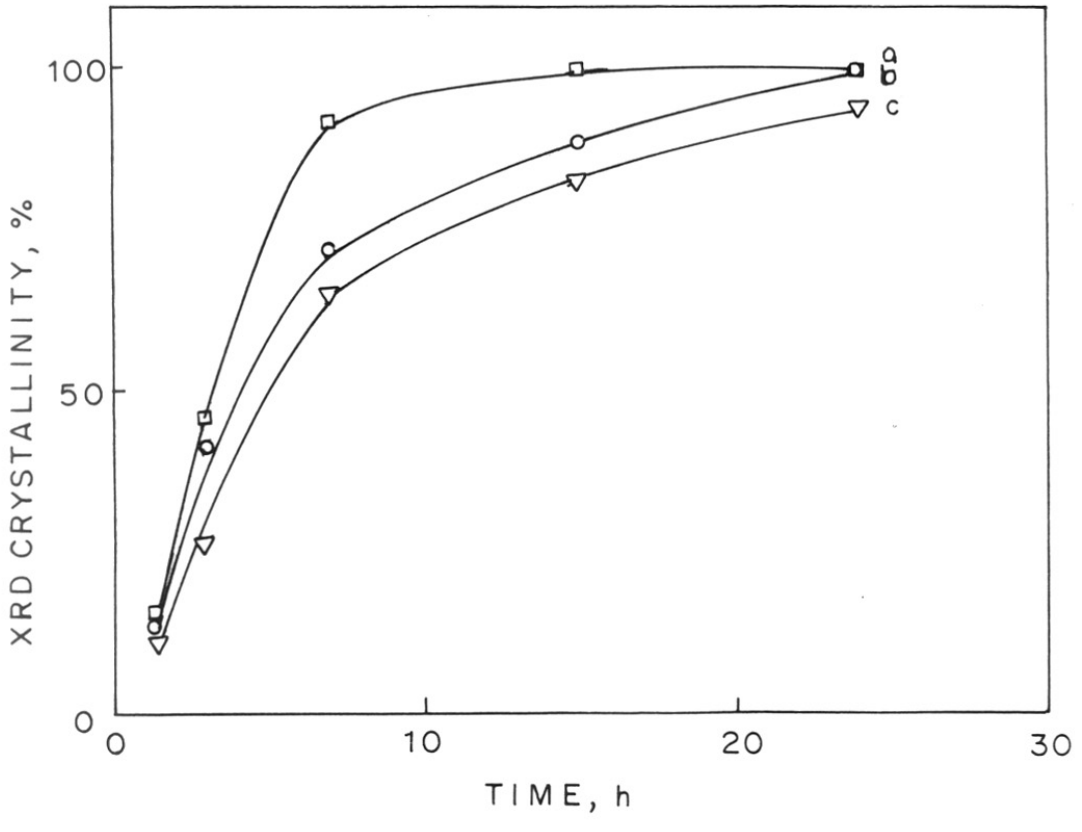

Fig. 2.12 : Influence of organic template on the crystallization of MoS-1
(a) TPAOH/SiO_2 = 0.199; (b) TPAOH/SiO_2 =0.326; (c) TPAOH/SiO_2 = 0.652.

crystallinity of the sample was found to be less for samples with higher template content (~96 %). This is attributed to a very high final pH (pH_{final} = 13.04), whence, redissolution of the crystalline samples occurs. A TPAOH/SiO_2 ratio of ~0.3 was found to be suitable. The typical compositions of the synthesis gel with different template concentrations are presented in Table 2.8.

TABLE - 2. 8

Gel compositions (mole) used in the synthesis of MoS-1 : Studies on the influence of template content.

SiO_2	: Template (TPAOH)	: MoO_3	: H_2O
1	0.652	0.01	24.33
1	0.326	0.01	24.33
1	0.199	0.01	24.33

2.4 Synthesis of Silicalite-1

Tetrapropylammonium hydroxide (TPAOH, 47.5 g, Aldrich, 20% aqueous solution) was mixed with tetraethyl orthosilicate (TEOS, 29.9 g, Aldrich) under vigorous stirring. After 15 minutes, 25.1 g of deionized water was added to the mixture and stirring was continued for 30 minutes. The contents were autoclaved and treated hydrothermally at 443 K for 24 h to get the as-synthesized silicalite-1.

2.5 Preparation of Mo-Impregnated Silicalite-1 (Mo-Imp.)

The impregnated Mo-silicalite (Mo-imp; Si/Mo = 55) sample was prepared by adding an aqueous solution of ammonium heptamolybdate (0.05 g in 1.5 mL of water) to 1 g of silicalite-1 and evaporating the mixture under vacuum at 343 K with continuous rotation of the flask. The sample was dried at 383 K for 8 h, calcined in air at 653 K for 3 h and at 823 K for 4 h.

2.6 Studies on the Effect of Temperature on the Crystallization Kinetics of MoS-1 and MoS-2 Molecular Sieves

The formation of the nuclei during the induction period is an energetically activated process and since nucleation is the rate determining step during the induction period, the apparent activation energy (E_a) for the process of nucleation can be conveniently calculated from the temperature dependence of the rate of nucleation.

TABLE - 2. 9

Results of Arrhenius plots.

Sl.No.	Sample	E_n (KJ/mol)	E_c (KJ/mol)
1.	MoS-1	6.25	2.0
2.	MoS-2	7.50	4.4

The rate of nucleation is inversely proportional to the induction period. The temperature dependence of the rate of nucleation can be expressed by the Arrhenius equation *[5]*, and the apparent activation energy for nucleation, E_n can be calculated from the expression, $d\ln(1/n)/d(1/T) = -E_n/R$, where 'n' is the induction period, i.e., the point on the crystallization curve at which conversion to the crystalline phase just occurs.

Similarly, E_c, the apparent activation energy for crystal growth was calculated from the temperature dependence of the rate of crystallization and was obtained from the point in the crystallization curve where 50% crystallization was complete. The rate equation can be represented as, $d\ln(1/\theta)/d(1/T) = -E_c/R$, where θ represents the time in hours for 50% crystallization. The corresponding curves for the MoS-1 samples are given in Fig. 2.13 and that of MoS-2 are given in the Fig. 2.14. The apparent activation energies were calculated from the slopes of the curves and are given in the Table 2.9.

2.7 Conclusions

1. Highly crystalline Mo-silicalite-2 (MoS-2) can be synthesized using a gel of composition: $SiO_2/MoO_3 = 100$, $TBAOH/SiO_2 = 0.3$, $H_2O/SiO_2 = 23$.
2. The aging time has a significant impact on the crystallization of MoS-2. A longer aging time leads to an amorphous silica-molybdenum oxide mixture.
3. The most crystalline samples are obtained when the organic base content is in the narrow range of $TBAOH/SiO_2 = 0.3 - 0.4$.

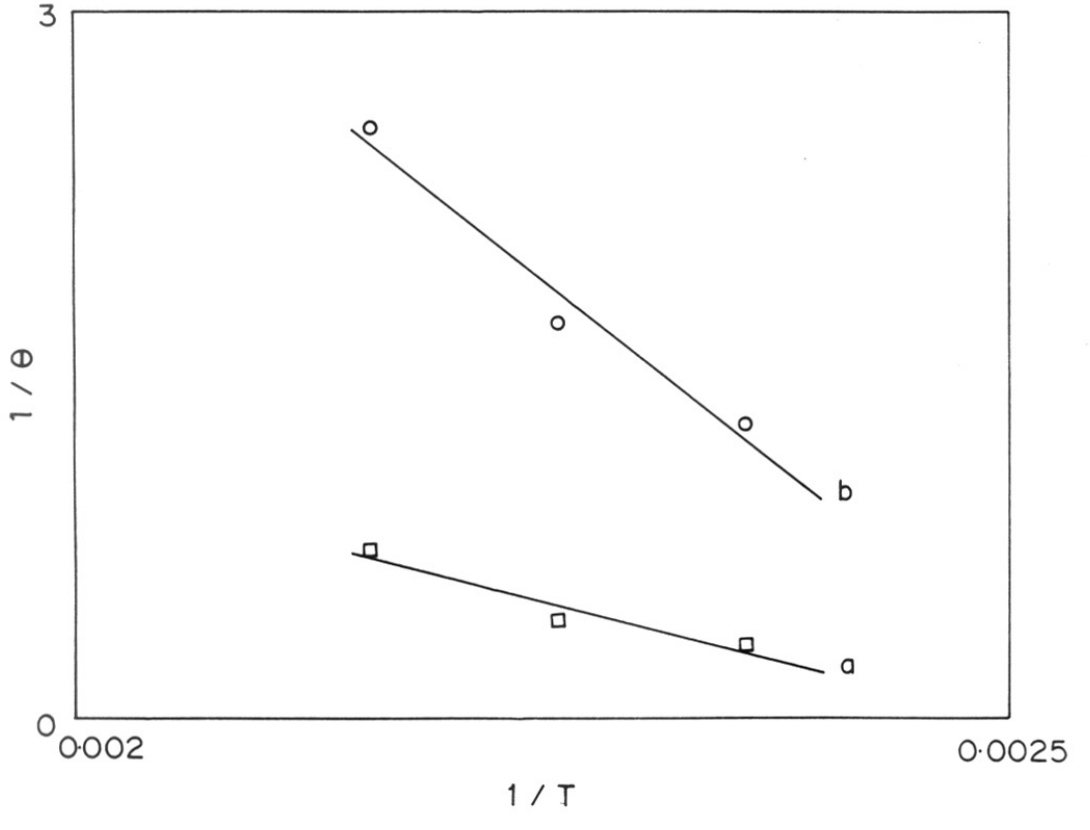

Fig. 2.13 : Arrhenius plots for MoS-1 (a) induction period; (b) at 50% completion of crystalline phase.

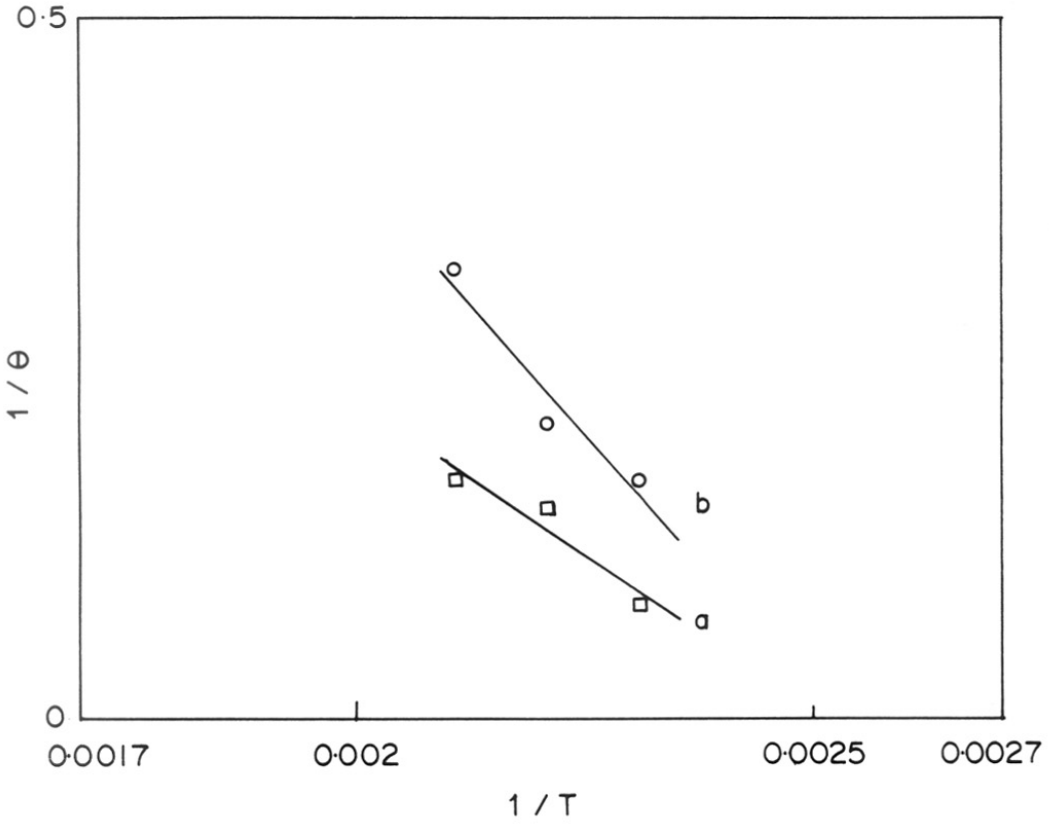

Fig. 2.14 : Arrhenius plots for MoS-2 (a) induction period; (b) at 50% completion of crystalline phase.

4. Even though, the addition of MoO_4^{2-} enhances the rate of crystallization (compared to silicalite-2), excess addition reduces both the crystallinity and the rate of crystallization of the sample.

5. Mo-silicalite-1 (MoS-1) can be synthesized in a broad range of SiO_2/MoO_3 and $TPAOH/SiO_2$ ratios. Unlike MoS-2, the aging time does not affect the crystallinity of the sample. Based on the studies, the gel compositions most suited for the synthesis of MoS-1 were, SiO_2/MoO_3 = 35-200; $TPAOH/SiO_2$ = 0.326; H_2O/SiO_2 = 24.3.

2.8 References

1. K.J. Chao, T.C. Tasi, M.S. Chen, and I. Wang, J. Chem. Commun, Faraday. Trans., 77 (1981) 547.
2. R. Kumar, A. Bhaumik, R.K. Ahedi and S. Ganapathy, *Nature*, 381 (1996) 298.
3. J.S. Reddy and R. Kumar, Zeolites 12 (1992) 95.
4. J.L. Casci and B.M. lowe, Zeolites, 3(1983)186.
5. A. Cultaz, and L.B. Sand, *Adv. Chem. Ser.*, 121 (1973) 140.
6. M.J. Avrami, *Chem. Phys.*, 9 (1941) 117.
7. B.V. Erofeev, *C.R. Acad. Sc., USSR*, 52 (1946) 511.

Chapter III

CHARACTERIZATION OF Mo-SILICALITE-2 (MoS-2)

3 CHARACTERIZATION OF Mo-SILICALITE-2 (MoS-2)

3.1 Sampling Techniques and Instrumentation

3.1.1 Chemical analyses

Chemical analyses of the solid samples were done by the EDAX technique. The sample was made into a paste by adding ethyl alcohol in drops, then spreaded over a cylindrical brass stud of diameter 0.5 cm, followed by drying under an IR lamp. The results of the above analyses were verified by atomic absorption spectroscopy of the solution prepared by dissolving the sample in minimum quantity of aqueous HF (~1 mL, 38%), followed by dilution to the required concentration using double distilled water.

3.1.2 X-Ray diffraction (XRD)

Powder X-ray diffraction data for the calcined samples were collected on a computer automated diffractometer (Rigaku; Model D-MAX III VC). The samples were dried at 383 K for 2 h and equilibrated over a saturated $CaCl_2$ solution at room temperature for 6 h prior to measurements. Nickel filtered Cu K_α radiation was used with a curved graphite crystal monochromator. Data were collected in the 2θ range of 5 to 50 degrees at a scan rate of 0.5° per minute with continuous rotation of the sample during the scan. Silicon was used as the internal standard.

3.1.3 FT-Infra red spectroscopy (FTIR)

Infra-red spectra were recorded on a Nicolet FTIR spectrometer. The catalyst (1 mg) was mixed with 300 mg of KBr (spectroscopic grade) thoroughly under an IR lamp and left undisturbed for 1 hour. Then pellets were made with the above mixture under vacuum. The spectra were recorded in the range of 1300 to 400 cm^{-1}.

3.1.4 Thermal analysis (TG/DTG)

Thermogravimetric (TG) and derivative thermogravemetric (DTG) analyses were carried out in the temperature range 300 K to 1273 K with a temperature program rate of 10 K per minute (Setaram, Model 92), in a flow of air. The sample holder (platinum crucible) was boiled with aqueous HF (38%) for 10 minutes and rinsed with deionized water prior to analysis.

3.1.5 X-Ray photoelectron spectroscopy (XPS)

X-ray photoelectron spectra were recorded (ESCA-3-MK II, VG Scientific) using Mg Kα radiation. The resolution of the instrument for $Au4f_{7/2}$ was 1.6 eV. The sample was activated under vacuum (10^{-8} Torr) for 6 h prior to experiment.

3.1.6 Sorption of probe molecules

Sorption experiments were carried out with water, n-hexane and cyclohexane as the probe molecules. The sorption capacity was measured gravimetrically in a Cahn micro-balance (Model 2000 G). The samples were activated at 673 K under vacuum (10^{-5} Torr) for 3 h before carrying out the experiments. The adsorption experiments were carried out at 298 K at a p/p_o of 0.5 with an equilibration time of 3 h.

3.1.7 UV-Visible spectroscopy (UV-VIS)

UV-Visible spectra were recorded in the range of 200 to 400 nm using a Shimadzu, (Model-ISR-260) instrument. $BaSO_4$ was used as the standard for baseline correction.

3.1.8 Cyclic voltammetry

The carbon paste electrodes of the catalyst used in cyclic voltammetric studies were prepared as follows: 100 mg zeolite was mixed with 50 mg graphite, and polystyrene solution in tetrahydrofuran (10 mg/ 3 mL) was added in drops to form a paste. The paste was then coated on a graphite disc electrode of geometrical area, 0.063 cm^2. It was then dried under an IR lamp for 30 minutes. Cyclic voltammetric experiments were carried out in a computer controlled potentiostat (EG & G Model 283) using a Pt foil counter electrode and Hg/Hg_2SO_4 reference electrode in 0.5 M H_2SO_4. The contents were deoxygenated before the measurements by purging with argon.

3.2 Characterization of Mo-silicalite-2 (MoS-2)

3.2.1 Scanning electron microscopy (SEM)

The scanning electron micrograph of the MoS-2 sample with Si/Mo ratio of 50 is shown in Fig. 3.1. Clusters of small crystallites of diameter 0.2 μm were observed. The SEM pictures of samples with different Mo contents were also similar.

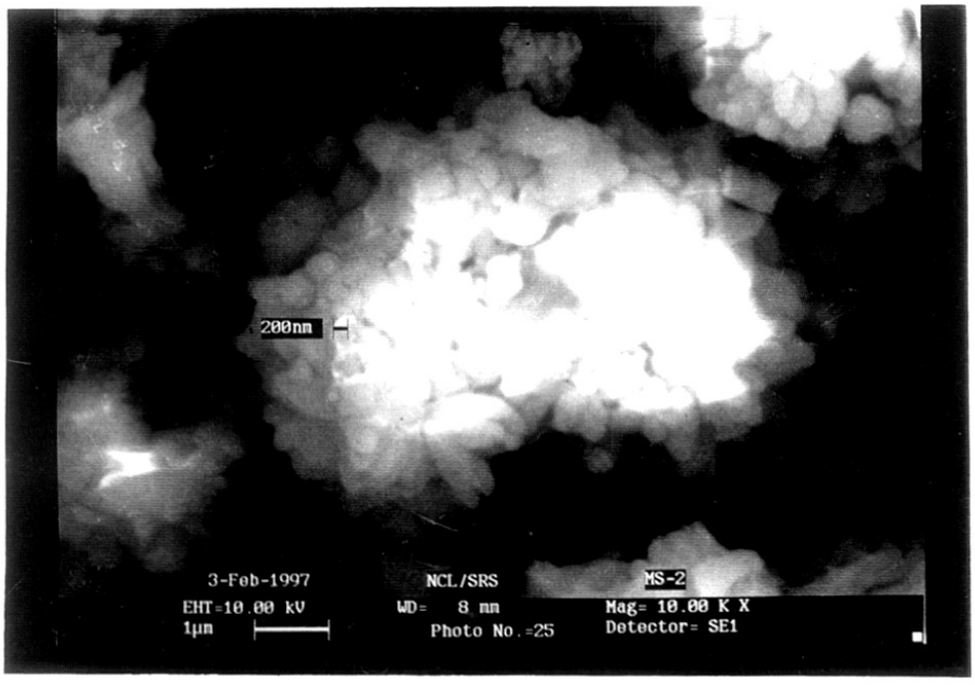

Fig. 3.1 : Scanning Electron Micrograph of MoS-2 (Si/Mo = 50)

3.2.2 *Chemical analyses*

The results of the chemical analyses of the final samples are compared with those of the corresponding synthesis gels and are presented in the Table 3.1.

TABLE 3.1

Chemical analyses of MoS-2 samples.

Sample	Si/Mo (synthesis gel)	Si/Mo (sample)
MoS-2 (35)	35.0	50.1
MoS-2 (100)	100.0	199.0
MoS-2 (200)	200.0	301.0

3.2.3 *X-Ray diffraction (XRD)*

The powder X-ray diffraction patterns of the calcined MoS-2 samples with different Si/Mo ratios were found to be similar to that of silicalite-2 and are given in Fig. 3.2. Absence of peaks at 2θ = 9.05, 24.05 degrees and a singlet peak at 2θ = 45 degrees confirms the MEL structure *[1]*. The crystallinities of the MoS-2 samples were found to be less compared to silicalite-2 (Table 3.2). The crystallinities of MoS-2 samples were found to decrease as the Mo content was increased in the initial gel. The unit cell volumes (V_{UC}) were calculated after correcting 'd' values with respect to silicon (internal standard) using a commercially available software (PDP11). The unit cell volume was found to increase with Mo content (Table 3.2).

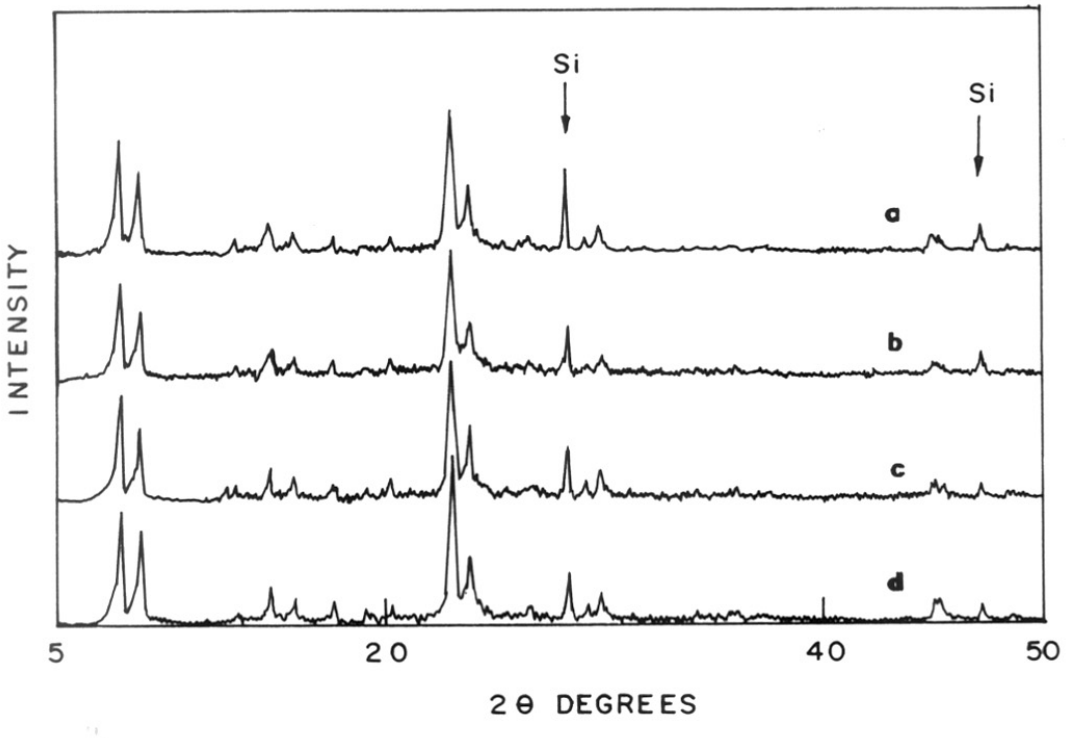

Fig. 3.2 : XRD profiles of (a) MoS-2 [50]; (b) MoS-2 [199]; (c) MoS-2 [301]; and (d) silicalite-2.

TABLE - 3.2

Physico-chemical characterization of MoS-2 samples.

Sample [a]	Si/Mo[b] (synthesis gel)	Crystallinity (%)	V_{UC} ($Å^3$)	Mo(Oh) / Mo(Td)[c]	Mo(Oh) / Mo-O-Mo[d]
MoS-2 (50)	35	72	5292.0	0.072	0.09
MoS-2 (199)	100	80	5287.9	0.069	0.11
MoS-2 (301)	200	84	5275.6	0.018	0.34
Sil-2 [e]	-	100	5269.8	-	-

[a] The values in the parantheses represents Si/Mo ratio in the final sample (output).

[b] The values represents Si/Mo ratio present in the synthesis gel (input).

[c] Ratio of intensities of band at ~360 nm (Mo_{Oh}) and ~230 nm (Mo_{Td}).

[d] Ratio of intensities of band at ~ 360 nm (Mo_{Oh}) and ~260 nm (Mo-O-Mo).

[e] Silicalite-2.

As the Mo content in the sample was increased, the V_{UC} increased suggesting the incorporation of Mo in the lattice.

3.2.4 Thermal analysis

The molybdenum present in ammonium heptamolybdate was found to sublime at around 700 K, while no weight loss due to sublimation was observed in the MoS-2 (Si/Mo = 50.1; highest Mo containing sample) sample, even up to 1273 K (Fig. 3.3). This clearly indicates that the Mo species present in the sample was thermally stable and anchored to the framework strongly even when the Mo content was high. Similar observations were also made in the case of samples with lower Mo contents.

3.2.5 FT-Infra red spectroscopy (FTIR)

The FTIR spectra of silicalite-2 and MoS-2 samples are shown in Fig. 3.4. A band at around 965 cm^{-1}, assigned to $Si\text{-}O^{\delta-}$ stretching of silanol groups present at defect sites is noticed *[2]*. The intensity of this band was more pronounced for the MoS-2 sample with low Si/Mo ratio, which indicates that the defect sites increase with increase in Mo content. Interestingly, the silicalite-2 sample also exhibited a band at ~970 cm^{-1} suggesting the presence of defect sites. However, this band shifted towards a lower wavenumber (964 cm^{-1}) in MoS-2 compared to silicalite-2 (970 cm^{-1}), probably suggesting the weakening of the Si-O bond by the electropositive Mo ions (present at the defect sites), thereby substantiating the incorporation of Mo. Moreover, the band was much broader in MoS-2 samples. An additional band, observed around 900 cm^{-1} for MoS-2 can be assigned to the symmetric stretching vibration of the terminal -Mo=O of a monomeric molybdate species *[3]*.

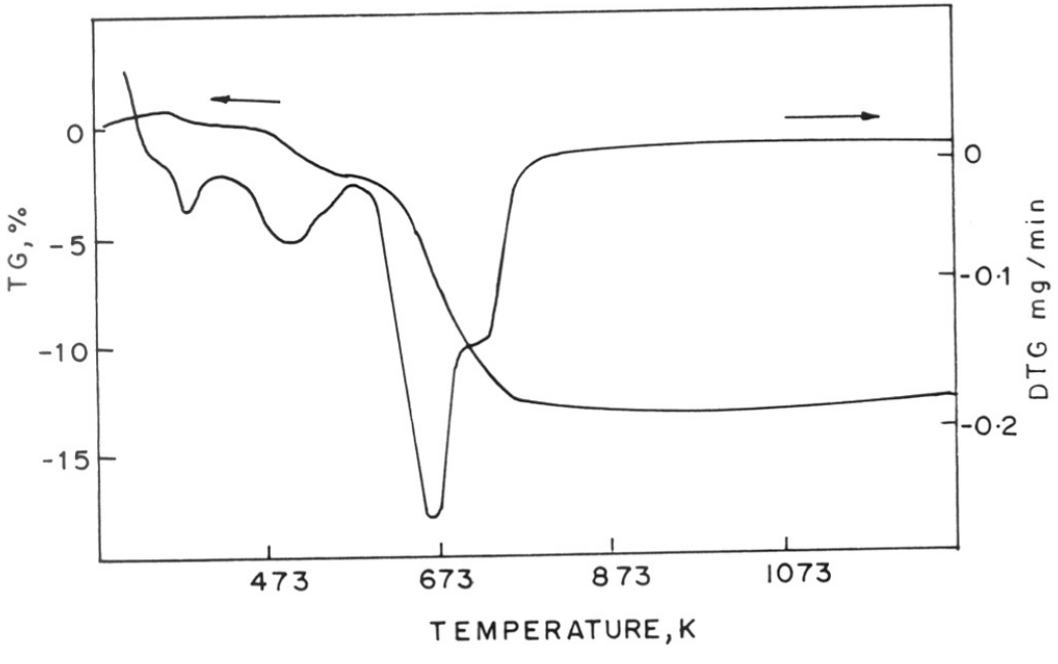

Fig. 3.3 : TG/DTG of MoS-2 [50] sample.

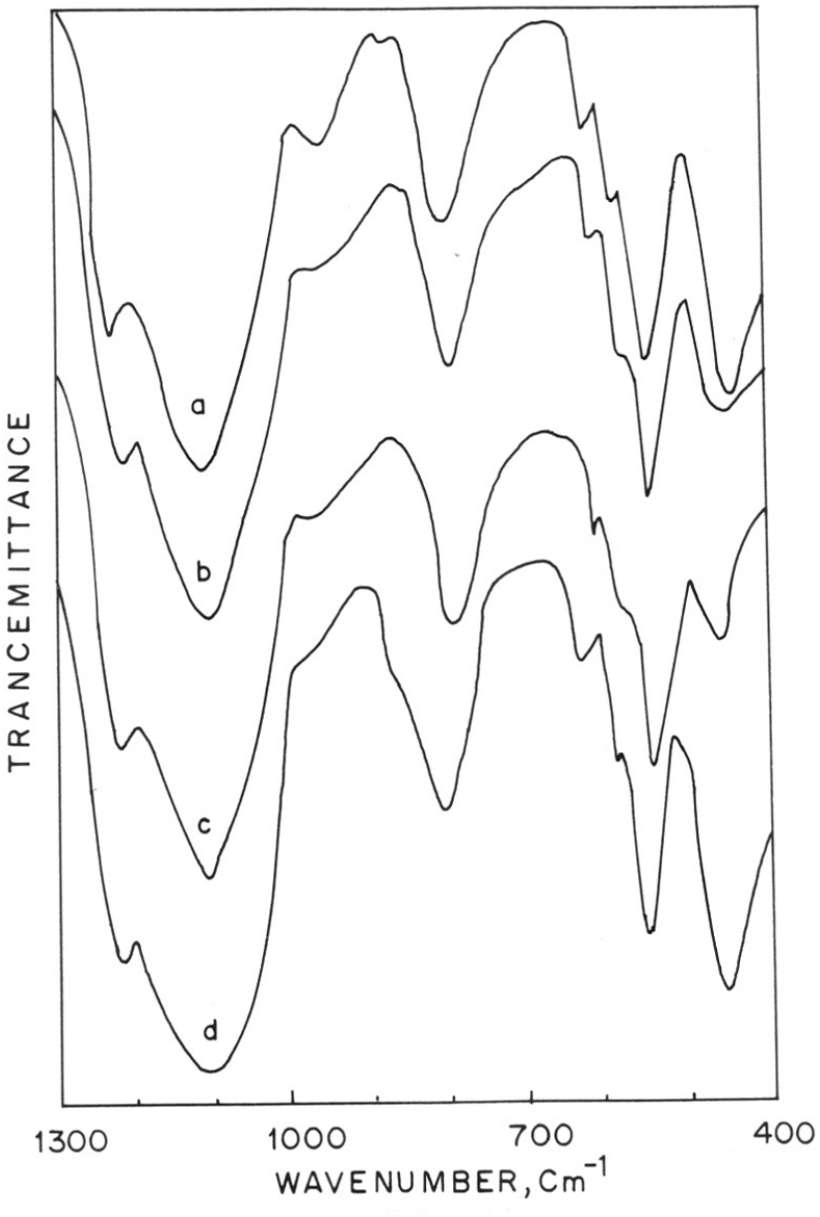

Fig. 3.4 : FTIR spectra of (a) MoS-2 [50]; (b) MoS-2 [199]; (c) MoS-2 [301]; and (d) silicalite-2.

3.2.6 *UV-Visible spectroscopy (UV-VIS)*

The UV-Vis spectra of the samples exhibited an absorption at around 230 nm indicating the presence of isolated MoO_4^{2-} in tetrahedral coordination *[5]* (Fig. 3.5). A shoulder around 260 nm can be assigned to Mo-O-Mo bridging in polyanionic species probably present at the external surface *[6]*. Another prominent absorption was observed at around 360 nm representing Mo^{6+} in octahedral coordination *[7]*. Published data on absorption bands of Mo compounds are presented in Table 3.3. The ratio of intensities of the bands at ~360nm (Mo_{Oh}) and ~230nm (Mo_{Td}) are given in Table 3.2. The decrease in the ratio of Mo_{Oh}/Mo_{Td} on increasing the Mo content indicates the formation of more tetrahedral Mo species at lower concentration of Mo. The increase in Mo-O-Mo species with Mo content (Table 3.3), suggests the deposition of excess Mo at the surface as polyanions.

3.2.6 *Cyclic voltammetry (CV)*

Cyclic voltammetric tracings of MoS-2 (Si/Mo = 50, calcined) at scan rates of 200 mV/s and 20 mV/s in 0.5 M H_2SO_4 as the electrolyte with Hg/Hg_2SO_4 as the reference electrode are shown in Fig. 3.6a and 3.6b, respectively. The electrode was dipped in the electrolyte for 1-2 hours prior to scanning. The voltammogram of MoS-2 clearly shows two peaks with $E_{1/2}$ value at -0.136 V/Hg/Hg_2SO_4 (-0.24 V/SCE) and -0.281 V/Hg/Hg_2SO_4 (0.09 V/SCE). The reversibility of the two peaks was found to be good (EP_1 = 44 mV, Ipa/Ipc =1.055, EP_2 = 72 mV, Ipa/Ipc =0.73). A comparison of the literature values for electrochemical oxidation shows that the peak at -0.281 V (0.09 V/SCE) corresponds to the $Mo^{6+/5+}$ couple *[8]*. This peak position was identical with that of the Mo source (MoO_4^{2-} ; tetrahedral). The second peak with $E_{1/2}$ = -0.136V (-0.24 V/SCE) is also probably due to the $Mo^{6+/5+}$ couple, but from Mo present at a different location (may be in octahedral

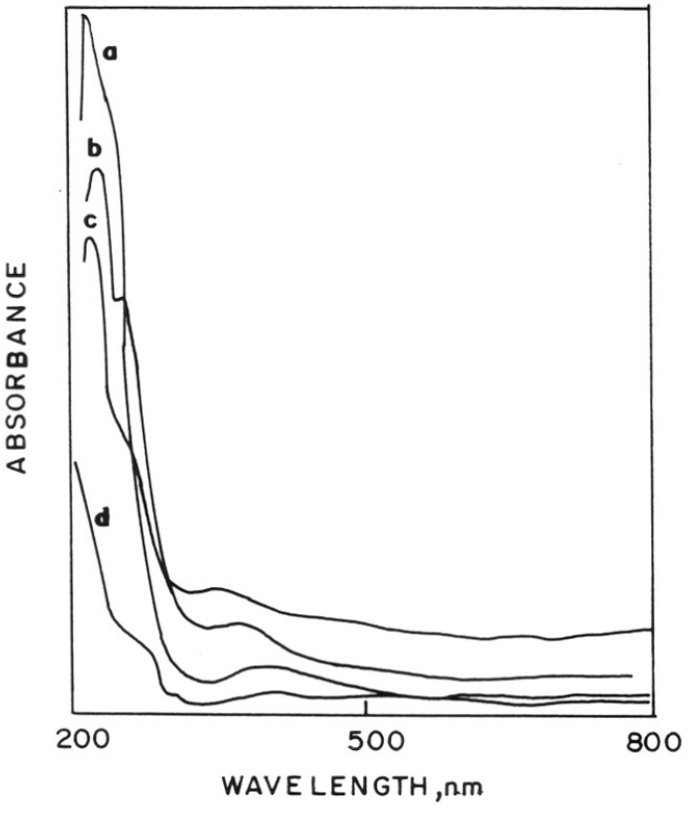

Fig. 3.5 : UV-Visible spectra of (a) MoS-2 [50]; (b) MoS-2 [199]; (c) MoS-2 [301]; and (d) silicalite-2.

TABLE - 3.3

Identification of Mo species by UV-visible and FTIR spectra of different Mo compounds.

Sample	Nature of species	FTIR	UV-Visible	Ref.
MoO_4^{2-}	Mo=O	900 cm^{-1}	--	*[3]*
Na_2MoO_4	MoO_4^{2-} (pH = 11)	--	220 nm	*[4]*
Na_2MoO_4	$Mo_7O_{24}^{2-}$ (pH = 6)	--	320 nm	*[4]*
---	Mo-O-Mo	--	260 nm	*[4]*

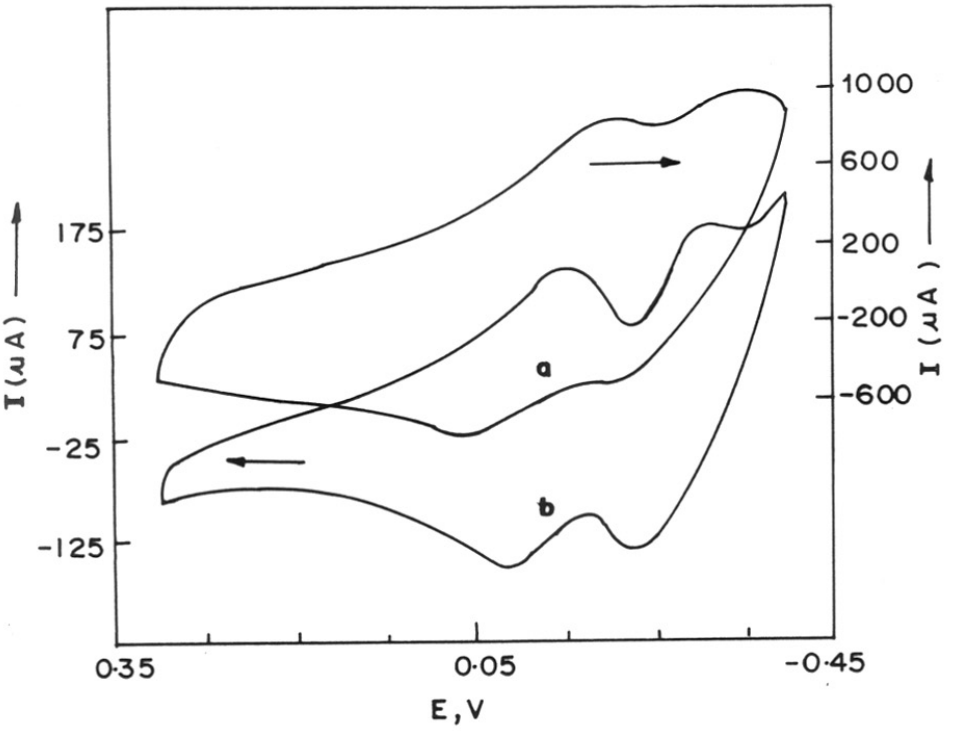

Fig. 3.6 : Cyclic voltammetric tracings of MoS-2 [50] carbon paste electrode at scan rate of (a) 200 mV/sec; (b) 20 mV/sec.

coordination). The ratios of the peak intensities of the two species (~0.05) is found to be close to that obtained from the UV-Visible spectra for Mo_{Oh} and Mo_{Td} (0.072, Table 3.2). Thus, two different types of Mo^{6+} species can be inferred to be present in MoS-2. Under identical conditions, Mo-impregnated silicalite-2 did not show the above redox features. It has been already established by earlier workers *[9,10]*, that in the case of Ti^{4+} and V^{5+} extraframework metal ions (impregnated samples) did not show any activity for cyclic voltammetry. They have also concluded that the peak current was proportional to the concentration of metal ions present in the framework of the zeolite.

3.3 Conclusions

Molybdenum containing silicalite-2 was synthesized hydrothermally under aluminium free alkaline conditions. Thermal analysis indicated the presence of a very stable Mo species in the sample. The characterization of the sample by spectral analysis has revealed the presence of Mo in both tetrahedral and octahedral coordination. Presence of different types of Mo species were also revealed by cyclicvoltammetry. The tetrahedral species of Mo is probably present in the framework in defect sites. The remaining excess Mo is grafted at the surface forming polyanionic species leading to Mo-O-Mo bridging whose coordination is ambiguous.

3.4 References

1. J. Sudhakar Reddy and Rajiv Kumar, *Zeolites,* 12 (1992) 95.
2. M.A. Camblor, A. Corma and J. Perez-Pariente, *J. Chem. Soc. Chem. Commun.*, 6 (1993) 557.
3. Helge Jeziorowski and Helmut Knozinger, *J. Phys. Chem.*, 83 (1979) 1166.
4. P. Kovacheva, N. Davidova and J.N. Vakova, *Zeolites*, 11 (1991) 54.
5. Li Wang and W. Keith Hall, *J. Catal.*, 77 (1982) 232.
6. A. Bartecki and D. Dembicka, *J. Ing. Nucl. Chem.*, 29 (1967) 2907.
7. N. Giordano, J.C.J. Bart, A. Vaghi, A. Castellan and G. Martinotti, *J. Catal.*, 36 (1975) 81.
8. A.J. Bard (Ed.,) in "*Encyclopedia of Electrochemistry of Elements*", Vol. 5, Marcel Dekker, (1976) 151.
9. S. de Castro-Martins, A. Tuel and Y. Ben Taarit, *Stud. Surf. Sci. Catal.,* 84 (1989) 501.
10. N. Venkatathri, M.P. Vinod, K. Vijayamohanan and S. Sivasanker, *J. Chem. Soc. Faraday Trans.*, 92 (1996) 473.

Chapter IV

CHARACTERIZATION OF Mo-SILICALITE-1 (MoS-1)

4 CHARACTERIZATION OF MoS-1 MOLECULAR SIEVES

4.1 Chemical Analysis

The chemical analysis of all the solid samples were carried out using both EDAX and AAS. The Mo contents in the final samples and the corresponding synthesis gels are presented in Table 4.1.

TABLE 4.1

Chemical analyses of MoS-1 samples.

Sample code	Si/Mo (synthesis gel)	Si/Mo (sample)
MoS-1 (80)	35.0	80
MoS-1 (157)	75.0	157
MoS-1 (202)	100.0	202
MoS-1 (297)	200.0	297
Mo-Impreg.	55.0	55

4.2 Scanning Electron Microscopy (SEM)

The scanning electron micro-graphs of the samples revealed that the MoS-1 particles were of uniform size with a near spheroidal shape (Fig. 4.1). The size of the crystallites was found to be in the range of 0.25 - 0.3 μm.

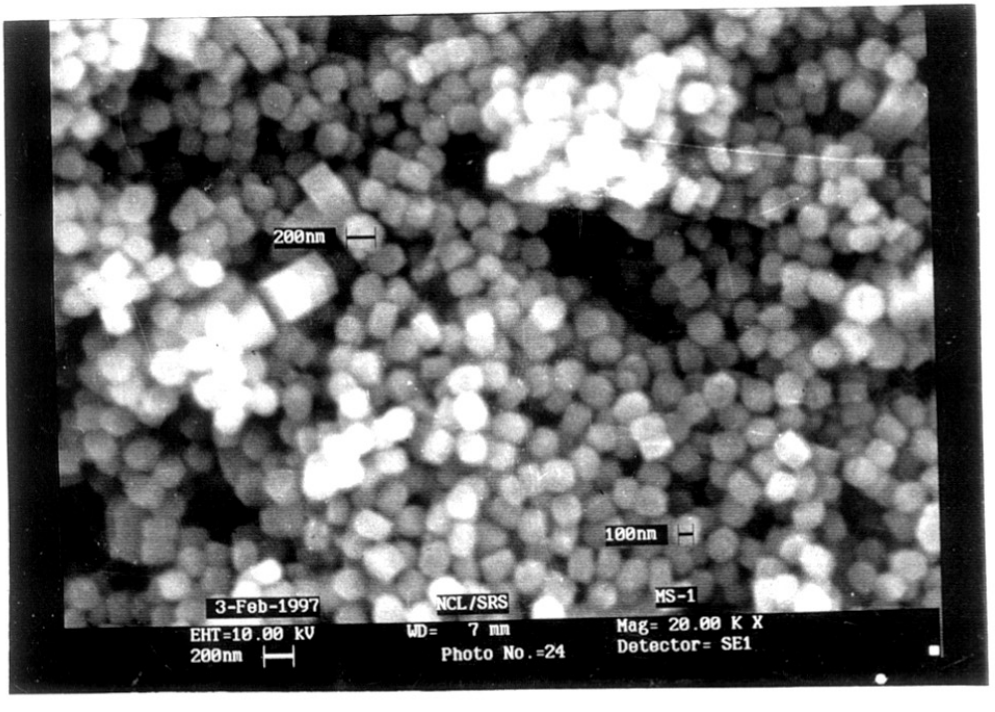

Fig. 4.1 : Scanning Electron Micrograph of MoS-1 (Si/Mo = 80).

4.3 X-Ray Diffraction (XRD)

The XRD profiles of the calcined MoS-1 samples (Fig. 4.2) matched well with that of silicalite-1 (MFI structure) *[1]*. No impurity phase of MoO_3 was observed. The peak at $2\theta = 45$ was found to be a doublet, which is a characteristic of the MFI structure. The as-synthesized form of the samples were found to possess orthorhombic symmetry (no splitting of peak at $2\theta = 24.4°$ *[2]*). Earlier workers have reported that silicalite-1 and ZSM-5 change symmetry on calcination from orthorhombic to monoclinic and this has also been observed for TS-1 samples with Ti content less than one per unit cell *[3]*. But TS-1 containing more Ti did not undergo symmetry change *[3]*. In the case of MoS-1 samples, the orthorhombic symmetry was preserved even after calcination (a singlet peak at $2\theta = 24.4°$, Fig. 4.2). The absence of symmetry change can be taken as an evidence for the incorporation of the metal in the framework. The interplanar spacings `d' (nm) were corrected with respect to silicon and used for the calculation of unit cell parameters and then further refined by least square fitting. An increase in unit cell volume (V_{uc} from 5324 to 5336 $Å^3$) with an increase in Mo content was observed. Increasing the Mo concentration further did not increase unit cell volume much. This may be due to the formation of extraframework species which does not increase the unit cell volume.

4.4 Sorption of Nitrogen

In many of the metallosilicate molecular sieves (Ti, V, Sn, etc.), a higher surface area (compared to the parent silicalite) has been reported *[4-6]*. Under alkaline conditions of synthesis, the resulting materials form smaller crystallites (confirmed by SEM) and

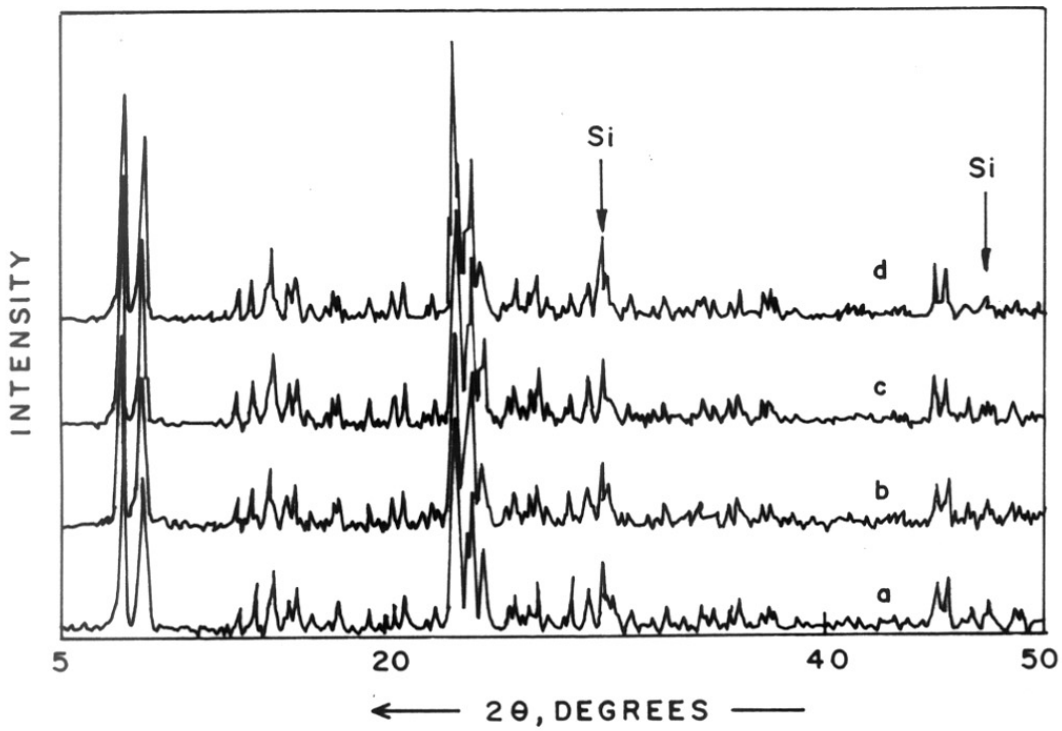

Fig. 4.2 : XRD profiles of (a) MoS-1 [80]; (b) MoS-1 [157]; (c) MoS-1 [202]; and (d) MoS-1 [297].

contain defect sites. Similar observation was also made for MoS-1 samples and the surface areas were found to be higher than that of silicalite-1 (Table 4.2). The micropore volume for the above samples were calculated by the t-plot method *[7]* and are also presented in Table 4.2. The values were comparable with silicalite-1, suggesting the absence of blockage of pores. On the other hand, a decrease in micropore volume for Mo-impregnated silicalite-1 was noted, indicating blockage of pore channels by Mo species.

4.5 Sorption of Probe Molecules

The quantities of water, n-hexane and cyclohexane sorbed by silicalite-1, MoS-1 and Mo-impregnated samples are presented in Table 4.2. Larger amounts of n-hexane and cyclohexane were adsorbed over the MoS-1 samples when compared to silicalite-1, suggesting the possible increase in pore volume. This observation also confirms the inference made from nitrogen sorption experiments, indicating a clear pore system. A steady increase in water sorption with an increase in Mo content was noticed. This is similar to the observation that ZSM-5 sorbs more water than silicalite-1 due to its greater hydrophilicity *[8]*. The enhanced water sorption of MoS-1 could also be due to the defect sites formed by the incorporation of Mo in the framework.

4.6 Extraction with Aqueous Ammonia

The calcined MoS-1 samples were extracted with aqueous ammonia (3 wt.%) at 333 K for 12 h . The above treatment has been shown to extract only loosely bound Mo

TABLE - 4.2

Physico-chemical characterization of Mo-sil and Mo-imp samples.

Sample*	S_{BET}	V_{mc}	Unit Cell	Wt.% adsorbed [a]		
	m^2/g	mL/g	Vol. ($Å^3$)	H_2O	n-C_6	Cyclo C_6
MoS-1 (80)	524	0.120	5336.9	5.99	13.20	6.53
MoS-1 (157)	525	0.191	5335.5	4.15	14.60	7.46
MoS-1 (202)	524	0.121	5332.5	4.03	14.40	7.10
MoS-1 (297)	523	0.120	5332.2	3.64	13.54	6.70
Mo-imp.(55)	373	0.081	-	4.10	12.80	3.92
Silicalite-1	384	0.116	5323.5	3.80	12.70	4.90

* values in parentheses refer to Si/Mo (output) ratios.

S_{BET} BET surface of the samples by nitrogen sorption.

V_{mc} represents micropore volume (from nitrogen sorption).

[a] gravimetric adsorption conditions: $p/p_o = 0.5$; 298 K; equilibration time = 3h.

species by the earlier workers *[9]*. The extracts of the MoS-1 samples were analyzed for Mo by AAS. No detectable amount of Mo was extracted from the MoS-1 samples suggesting that Mo species present in the samples were strongly bound. On the other hand, when the extraction was carried out on the Mo-impregnated sample, nearly 98% of the Mo was extracted, indicating that the Mo present in the impregnated sample was weakly attached to the silicalite framework.

4.7 Thermal Analysis

Thermograms of MoS-1 (80) and Mo-impregnated samples are presented in Fig. 4.3. In the case of Mo-impregnated sample, a small weight loss is observed between 1138 K and 1237 K. This weight loss could be attributed to the loss of MoO_3 from the silicalite surface. Under identical conditions of thermal treatment, no Mo loss was observed, even upto 1273 K in the case of MoS-1 (80). This further supports the fact that the Mo present in MoS-1 is strongly bound to the surface/framework and does not sublime.

4.8 X-Ray Photoelectron Spectroscopy (XPS)

The oxidation state of the Mo species present at the surface can be determined by XPS (Fig. 4.4). The C1s peak was used as the internal standard. In general, the B.E. values of Mo ions in 4+, 5+ and 6+ oxidation states (doublet due to $Mo3d_{3/2}$ and $Mo3d_{5/2}$ transitions) are not very different, the typical values being, respectively, 230.9 eV (MoO_2), 231.0 eV ($MoCl_5$) and 232.5 (MoO_3) *[10]*. The values are found to be slightly

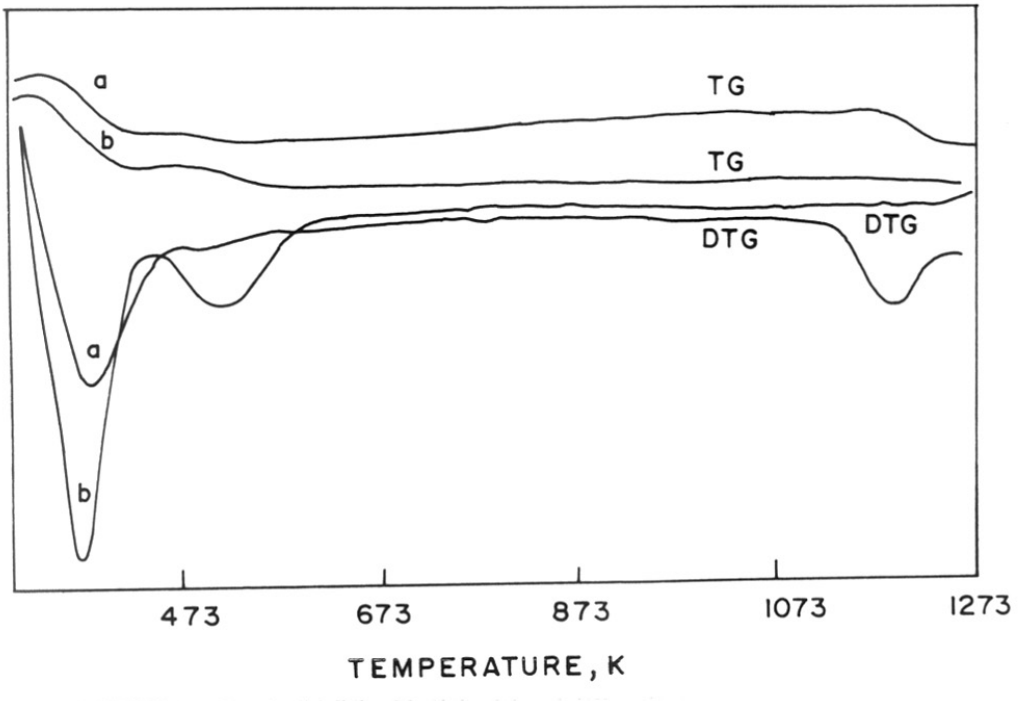

Fig. 4.3 : Thermogram (TG) of (a) Mo-impregnated silicalite-1 and (b) MoS-1 [80].

Derivative thermogram (DTG) of (a) Mo-impregnated silicalite-1 and (b) MoS-1 [80].

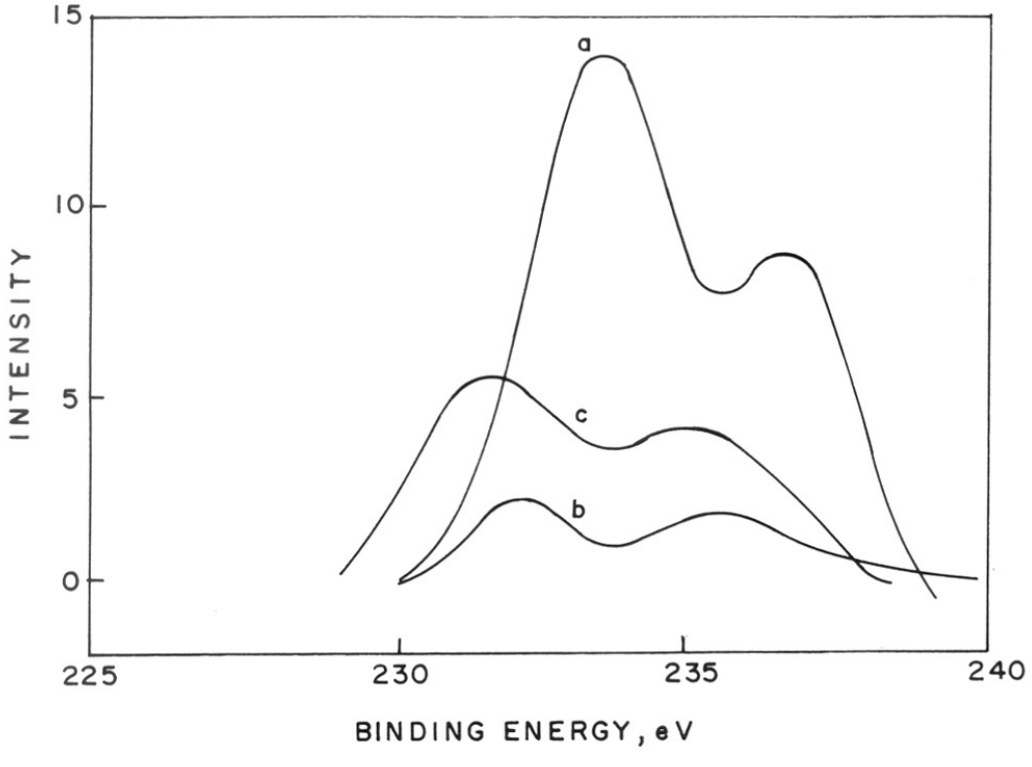

Fig. 4.4 : X-photoelectron spectra of (a) MoS-1 [80]; (b) MoS-1 [157] and (c) Mo-impregnated silicalite-1 samples.

lower for the lower oxidation states. The values obtained by us (Table 4.3) are in the range 231.7 to 233.5 eV, suggesting that the ions are mostly in the 6+ oxidation state. The results, however, do not preclude the presence of a small amount of Mo in other oxidation states such as 5+. The differences in the values observed (± 0.9 eV) are probably due more to the differences in the location of Mo ions than to differences in Mo oxidation states.

4.9 UV-Visible Spectroscopy (UV-VIS)

The spectra of molybdenum in molybdates or MoO_3 are due to charge-transfer transitions from O^{2-} to Mo^{6+}. Two broad absorption bands are observed, one at around 285 nm, due to octahedrally coordinated Mo and another absorption at around 230 nm attributable to Mo species present in tetrahedral coordination *[11]* (Fig. 4.5). The intensity of the absorption band at 230 nm increases with decreasing Mo content (Si/Mo ratio). The Mo-impregnated sample did not give any characteristic absorption under identical conditions. It was observed that as the Mo loading in the MoS-1 sample was decreased, the ratio of intensities of $Mo_{(Oh)}$ and $Mo_{(Td)}$ also decreased, indicating that more amount (relative) of Mo was in tetrahedral position (framework) in samples containing less Mo (Table 4.3).

4.10 FT-Infra Red Spectroscopy (FTIR)

The FTIR spectra for MoS-1 and silicalite samples are given in Fig. 4.6. A band at around 960 cm^{-1} was observed for all the samples including silicalite-1 (blank) sample.

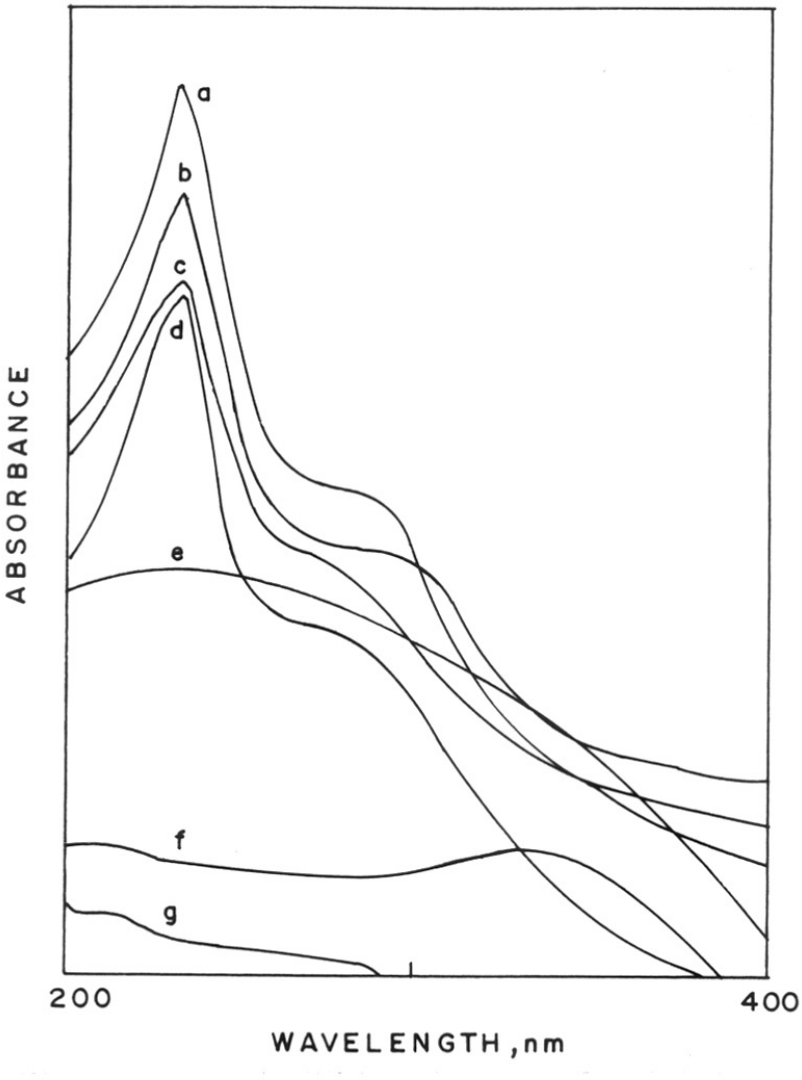

Fig. 4.5 : UV-Visible spectra of (a) MoS-1 [80]; (b) MoS-1 [157]; (c) MoS-1 [202]; (d) MoS-1 [297]; (e) Mo-impreg.; (f) MoO_3 ; and (g) silicalite-1.

TABLE - 4.3

Spectral analysis of MoS-1 and Mo-impregnated silicalite-1 samples.

Sample	B.E.		$A_{(Mo_{Oh} / Mo_{Oh+Td})}$[a]	FTIR[b]
	$Mo3d_{3/2}$	$Si2p_{1/2}$		
MoS-1 (80)	233.5	104.1	0.562	2.45
MoS-1 (157)	232.1	104.6	0.522	2.38
MoS-1 (202)	-	-	0.403	1.66
MoS-1 (297)	-	-	0.400	1.45
Mo-imp.(55)	231.7	103.6	-	-

[a] Ratio of intensities of absorption bands at 285 and 230 nm from UV-Visible spectra.

[b] Ratio of intensities of ~ 960 cm^{-1} band between MoS-1 (n) and silicalite-1 samples.

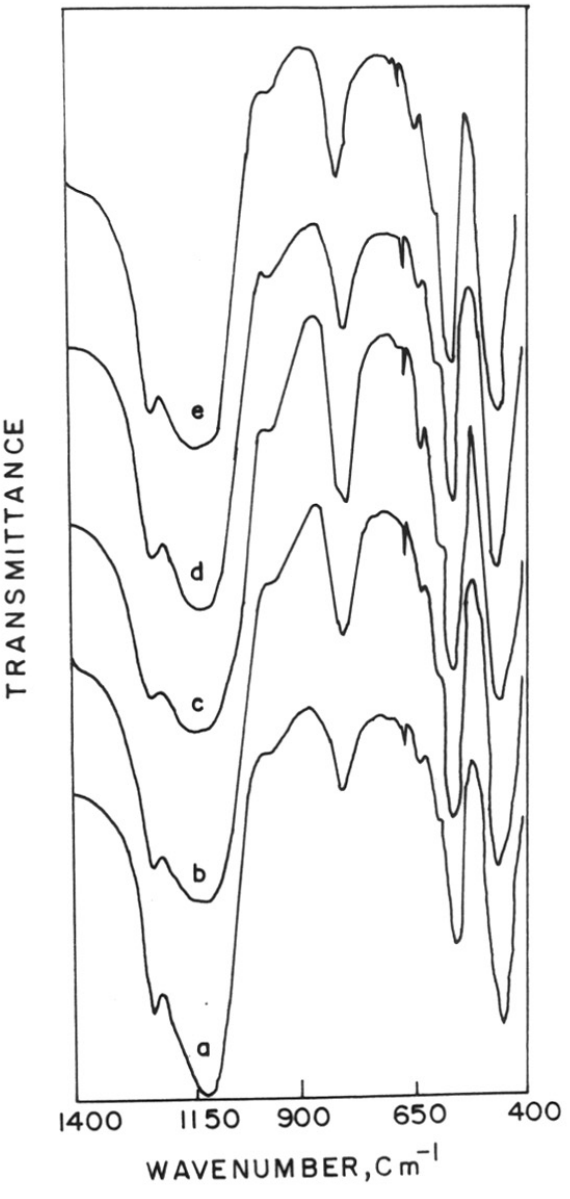

Fig. 4.6 : FTIR spectra of (a) MoS-1 [80]; (b) MoS-1 [157]; (c) MoS-1 [202]; (d) MoS-1 [297]; and (e) silicalite-1.

Earlier workers *[12]* have assigned this band to Si-O$^-$ stretching associated with defect centers containing the incorporated metal (such as Ti, V, Sn). Appearance of this band in silicalite-1 (blank) is due to the presence of defect sites as reported by Camblor *et al. [12]*. Eventhough, this band appears in all samples, the intensity of this band was more in MoS-1 samples (the ratios of the intensities of this band between MoS-1 and silicalite-1 are given in Table 4.3).

4.11 Conclusions

The expansion in unit cell volume (V_{uc}) and the preservation of orthorhombic symmetry after calcination, suggests the possible incorporation of Mo in the framework of silicalite structure. The oxidation state of Mo in our MoS-1 samples was found to be +6 (confirmed by XPS). Mo is also present in more than one coordination as revealed by UV-Visible spectral studies. When the Mo concentration was increased, more Mo-species with octahedral coordination was formed. The Mo species are linked to the Si-O-tetrahedra or grafted to the silicalite-1 structure in such a manner that they cannot be leached by dilute ammonia. The thermal stability of the samples supports the strong interaction between Mo and Si-O of the framework.

4.12 References

1. R.W. Grose and Flanigen, E.M., *U.S. Pat.* 4061,724 (1977).
2. D.G. Hay and H. Jaeger, *J. Chem. Soc. Chem. Commun.*, (1984) 1433.
3. G. Perego, G. Bellusi, C. Corno, M. Taramaosso, F. Buonomo and A. Esposito, in "Developments in Zeolite Science and Technology" (Y. Murakami *et.al.*, Eds), Elseveir, Amsterdam (1986) 129.
4. M. Taramaso, G. Perego and B. Notari, *US Pat.* 4,410,50 (1983)
5. P.R.H.P. Rao, A.A. Belhekar, S.G. Hegde, A.V. Ramaswamy and P. Ratnasamy, *J. Catal.*, 141 (1993) 595.
6. N.K. Mal, V.Ramaswamy, S. Ganapathy and A.V. Ramaswamy, *J. Chem. Commun.*(1994) 1933.
7. S. Lowell and J.E. Shields in "Powder Surface Area and Porosity", (B. Scarlett, Eds.), Chapman and Hall, (1984) 80.
8. S.P. Zhdanov, S.S. Khvoshchev and N.N. Feoktistova, in "Synthetic Zeolites Vol-II: Adsorption properties", Gordan and Breach Science Publishers, (1990) 597.
9. N. Giordano, J.C.J. Bart, A. Vaghi, A. Castellan and G. Martinotti, *J. Catal.*, 36 (1975) 81.
10. J.W. Robinson, in "Handbook of Spectroscopy", (CRC Press Inc.) , 1 (1974) 615.
11. Helge Heziorowski and Helmunt Knozinger, *J. Phys. Chem.*, 83 (1979) 1166.
12. M.A. Camblor, A. Corma and J. Perez-Pariente, *J. Chem. Soc. Chem. Commn.*, 6 (1993) 557; M. Chatterjee, D. Bhattacharya, N. Venkatathri and S. Sivasanker, *Catal. Lett.*, 35(1995)313; T. Sen, M. Chatterjee and S. Sivasanker, *J. Chem. Soc. Chem.Commun.*, (1995)207.

Chapter V

CATALYTIC PROPERTIES OF Mo-SILICALITES

5 CATALYTIC PROPERTIES OF Mo-SILICALITES

5.1 Oxidation of Thioethers to Sulfoxides

The results of MoS-1 catalyzed oxidation of thioethers with 30% H_2O_2 at 293 K in methanol are presented in Table 5.1. In a typical reaction procedure, a mixture of phenyl allyl sulfide (0.50 g, 0.0034 mol), MoS-1 (50 mg) and 30% H_2O_2 (0.69 mL, 0.0068 mol) in methanol (20 mL) was stirred at 293 K for 6 h. The catalyst was filtered off and the product was purified by flash chromatography (SiO_2, 50% ethyl acetate : pet. ether as eluant).

A variety of aromatic and aliphatic thioethers are smoothly oxidized to the corresponding sulfoxides in high yields and 100 % selectivity (GLC) with the MoS-1-H_2O_2 system (Table 5.1). Even the sterically hindered thioethers (entries 2-5 in Table 5.1) underwent conversion to the corresponding sulfoxides in good yields. Even the unsaturated ethers (entries 6 and 7 in Table 5.1) reacted efficiently with the present catalytic system and the reaction was found to be essentially chemoselective. It should be noted here that TS-1-H_2O_2 combination failed to oxidize sterically hindered thioethers, e.g. diphenyl sulfide *[1-3]*. This suggests that in MoS-1, the Mo species present at the surface sites are responsible for the above activity. It is also possible that the defect sites created during Mo incorporation enable easier access to the Mo species inside the pores (near the surface). Besides, the non-detectability of Mo in the solution suggests that homogeneous catalysis by leached out Mo species is not the major oxidation route.

When the oxidation of allyl phenyl sulfide with 30 % H_2O_2 was carried out over Mo-impregnated silicalite-1, no significant formation of sulfoxide (<5%) was observed even after

TABLE - 5.1

Sulfoxidation of various thioethers with H_2O_2 as oxidant over MoS-1 (80) catalyst.

Sl. No.	Substrate	Time, h	Conversion (%)	Selectivity (%) (towards sulfoxide)
1.	$(CH_3)_2$ S	2	96	94
2.	$(n\text{-}C_4H_9)_2$ S	3	98	93
3.	C_6H_5-S-CH_3	3	93	90
4.	$(C_6H_5)_2$S	8	80	75
5.	$(C_6H_5CH_2)_2$ S	3	90	85
6.	C_6H_5-S-$CH_2C{=}CH_2$	7	89	85
7.	C_6H_5-S-$CH_2C{\equiv}CH$	7	98	84
8.	tetrahydrothiophene	2	98	94

stirring for 24 h at 293 K. The inability of Mo-impregnated silicalite-1 to catalyze the reaction demonstrates that the Mo specie present in the framework (defect sites) of MoS-1 or strongly anchored to the external surface, are responsible for its activity. Similar observations were made by Sen *et al.* during the catalytic oxidation of alkyl aromatics *[4]*. They have reported that V-incorporated silicalite-2 was active, while V-impregnated silicalite-2 was inactive for the reaction. A plausible mechanism for the oxidation of thioethers on the Mo species present in the framework (defect sites) is shown in Fig. 5.1.

5.2 Oxidation of Ethanol over MoS-1 and MoS-2 Molecular Sieves.

5.2.1 Introduction

Acetaldehyde is an important intermediate product used in the manufacture of acetic acid and its derivatives like esters, plastics, n-butanol, 2-ethyl hexanol and other aldol products. Oxidative dehydrogenation of ethanol is one of the main routes used for the manufacture of acetaldehyde. Tatibouet *et al.* have studied the oxidation of ethanol over MoO_3 crystals *[5]*. They have proved that -M=O sites were responsible for the formation of acetaldehyde. It has been established by Iwasawa *et al.* that the Mo dimers were the active centers for the oxidation of ethanol over MoO_3/SiO_2 *[6]*. The reaction has been suggested to proceed through the formation of an ethoxide type intermediate *[7]*. Recently, based on *in situ* laser Raman studies, the formation of two types of ethoxide intermediates over -M=O and Mo-O-Mo sites were reported by Zhang *et al.[8]*. The transformation of ethanol has been used to evaluate the nature of the active sites in the MoS-1 samples.

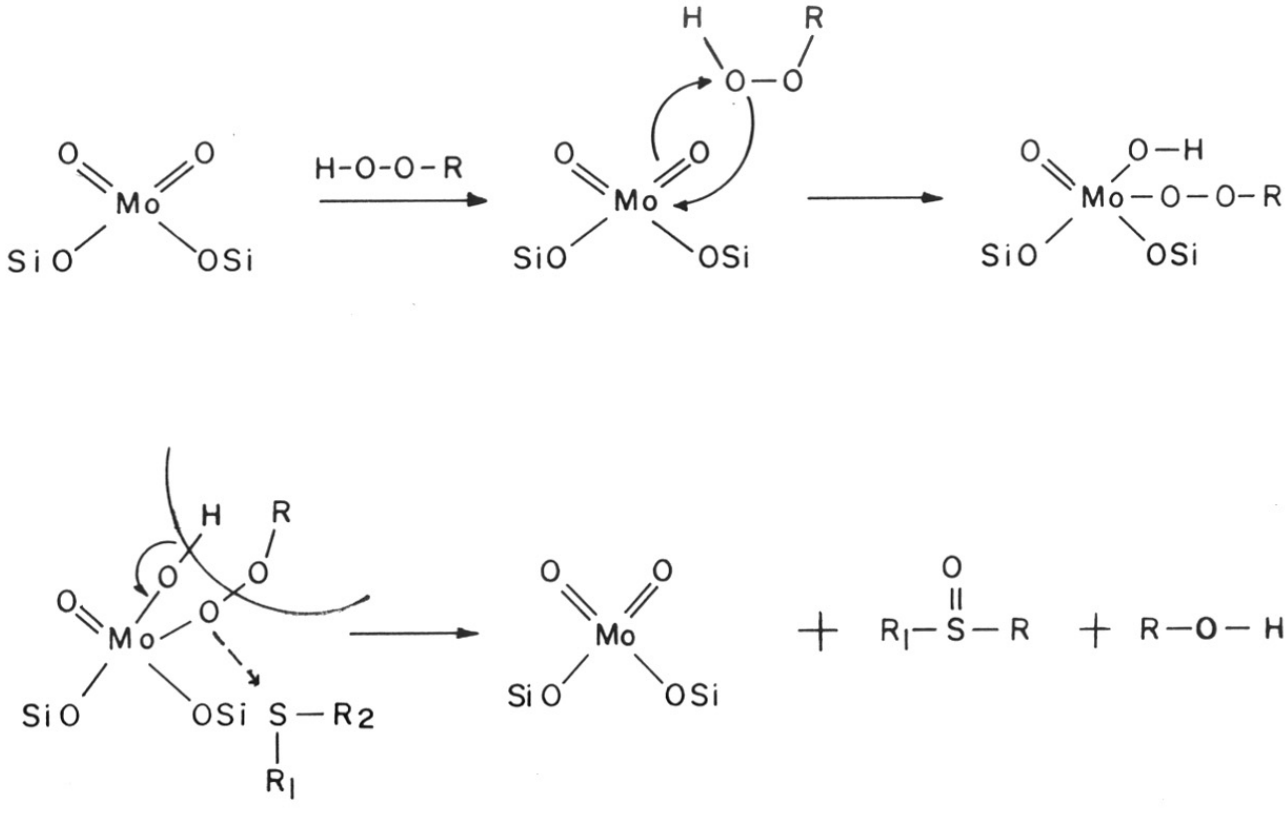

Fig. 5.1 : Mechanism for oxidation of thioethers over MoS-1 [80].

5.2.2 *Experimental*

The oxidative dehydrogenation of ethanol over MoS-1 samples were carried out in a fixed bed glass reactor (1.9 cm i.d., down flow mode), attached to a spiral condenser and a gas-liquid separator. Mass balance was carried out after analyzing both the gas and the liquid products using a HP-5880A gas chromotograph fitted with a capillary column (50m X 0.2 mm). The reactor was charged with 2.0 g of the catalyst (12-14 mesh, ASTM). Ceramic beads were used in the pre-heating zone. The experiments were carried out at different temperatures. The alcohol/oxygen ratio was maintained well below the explosion limit (1.52 vol. %). Under experimental conditions, only a negligible amount of CO_2 (0.5 - 1.2 %) was produced.

5.2.3 *Oxidation of ethanol over MoS-1*

Conversion of ethanol over MoS-1(71) at different temperatures are presented in Table 5.2. The total conversion of ethanol increased with increase in temperature. Maximum selectivity of acetaldehyde (~85%) was observed at 630 K. Any further increase in the temperature led to a gradual decrease in the selectivity of both acetaldehyde and ethylene. The loss in ethylene selectivity may be due to its subsequent polymerization and cracking.

The influence of temperature on the selectivity of acetaldehyde and ether over MoS-1 with different Si/Mo ratios is presented in Fig. 5.2. In the case of MoS-1 with a lower Mo content (Si/Mo = 137), the selectivity to acetaldehyde was found to be quite low (63.9%) and decreased with an increase in temperature. The selectivity to acetaldehyde was found to be more and nearly constant over MoS-1 (90). When the Mo content was further increased

TABLE - 5. 2

Oxidation of ethanol over MoS-1 (71) : Influence of temperature.

Temperature	Conversion	Selectivity, %				
K	%	C_2H_4	CH_3CHO	CH_3CO_2H	Ether	Others
573	19.9	10.1	67.8	3.4	13.6	5.1
600	28.9	7.9	74.8	2.0	9.4	5.9
630	32.2	4.4	85.6	-	3.0	7.0
655	35.8	2.6	69.2	-	6.1	22.1
680	40.9	0.9	59.5	-	4.0	35.6

TOS = 1h

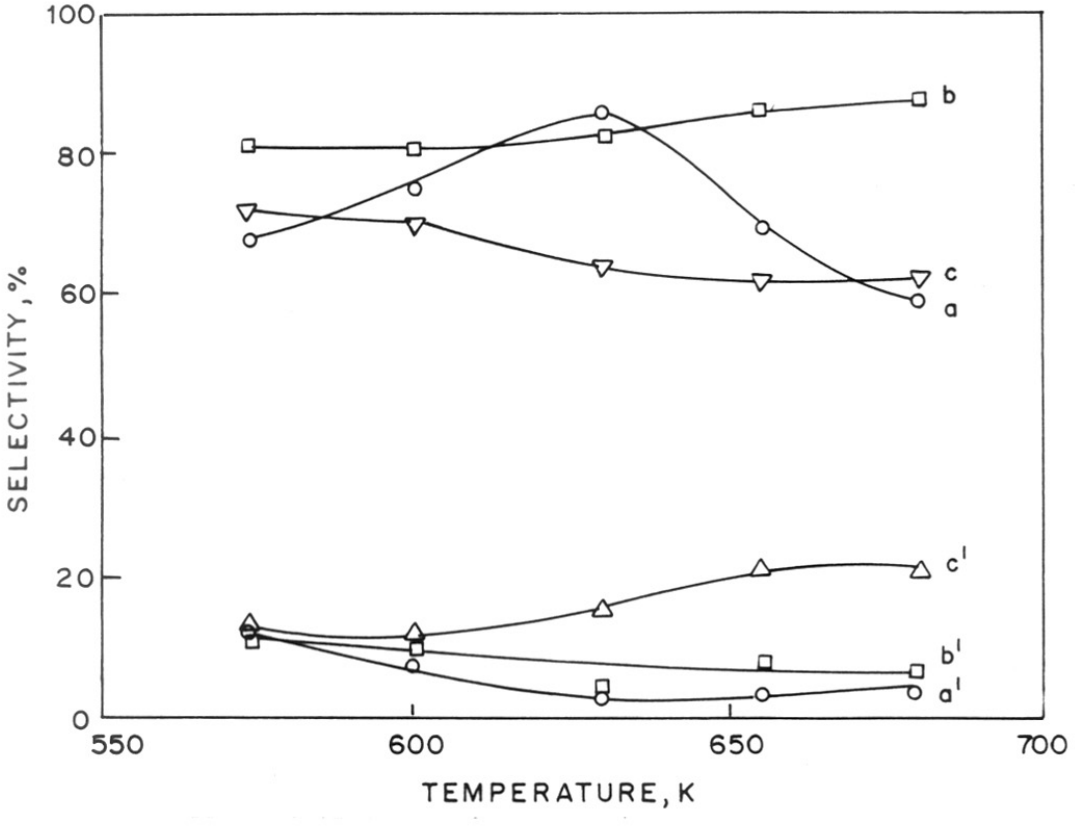

Fig. 5.2 : Oxidation of ethanol over MoS-1: Influence of temperature

- selectivity of acetaldehyde over (a) MoS-1[71]; (b) MoS-1[90]; and (c) MoS-1[137].
- selectivity of ether over (a^1) MoS-1[71]; (b^1) MoS-1[90]; and (c^1) MoS-1[137].

(Si/Mo = 71), a maximum selectivity of ~85% was observed at 630 K, which then decreased due to secondary reactions.

The results of ethanol oxidation over MoS-1 with different Si/Mo ratios are presented in Table 5.3. MoS-1 with Si/Mo ratio of 71 produced more acetaldehyde and less ether, while the selectivity of ether was found to be more than that of acetaldehyde over MoS-1 (137). As the Mo content was increased, more -Mo=O sites were available for the reaction, thereby producing more acetaldehyde. A corresponding decrease in the selectivity of ether was observed. A reverse trend was observed over MoS-1 with low Si/Mo ratio (Table 5.3).

A plot of 1/T *vs.* turn over rates (moles of product formed per mole of active site in the catalyst) is given in Fig. 5.3. From the slope, the energy of activation (E_a) values for the reaction over the three samples were calculated and are given in Table 5.3. The E_a values for the reaction over MoS-1 catalysts with different Si/Mo ratios were found to decrease with decreasing Mo content. The activity of MoS-1 with intermediate Si/Mo ratio of 90 is compared with that of MoO_3/SiO_2 samples (Table 5.4). The conversion of ethanol over MoS-1 with different Si/Mo ratio was found to match with that reported by earlier workers on MoO_3/SiO_2 catalysts *[9]* (Fig. 5.4). Even though, more amount of ether was produced over MoS-1 (90), the selectivity to acetaldehyde was better compared to MoO_3/SiO_2 (Table 5.4).

5.2.4 Oxidation of ethanol over MoS-2

Figure 5.5 shows the product distribution and conversion of ethanol at different temperatures over MoS-2 with Si/Mo = 51. With an increase in the temperature, the selectivity to acetaldehyde decreased and that to ether increased. The product distribution and

TABLE - 5. 3

Oxidation of ethanol over MoS-1 : Influence of Si/Mo ratio.

Sample	Si/Mo	MoO_3	Conv.	Selectivity, %					E_a
	(atom)	Wt.%	%	C_2H_4	CH_3CHO	CH_3CO_2H	Ether	Others	$KJmol^{-1}$
MoS-1	71	3.25	32.2	4.4	85.6	-	3.0	7.0	28.0
MoS-1	90	2.62	21.9	2.6	83.0	2.6	10.4	1.4	23.9
MoS-1	137	1.71	7.31	14.5	63.9	4.3	15.6	1.7	14.8

Conditions : Temperature - 630 K ; TOS = 1 h.

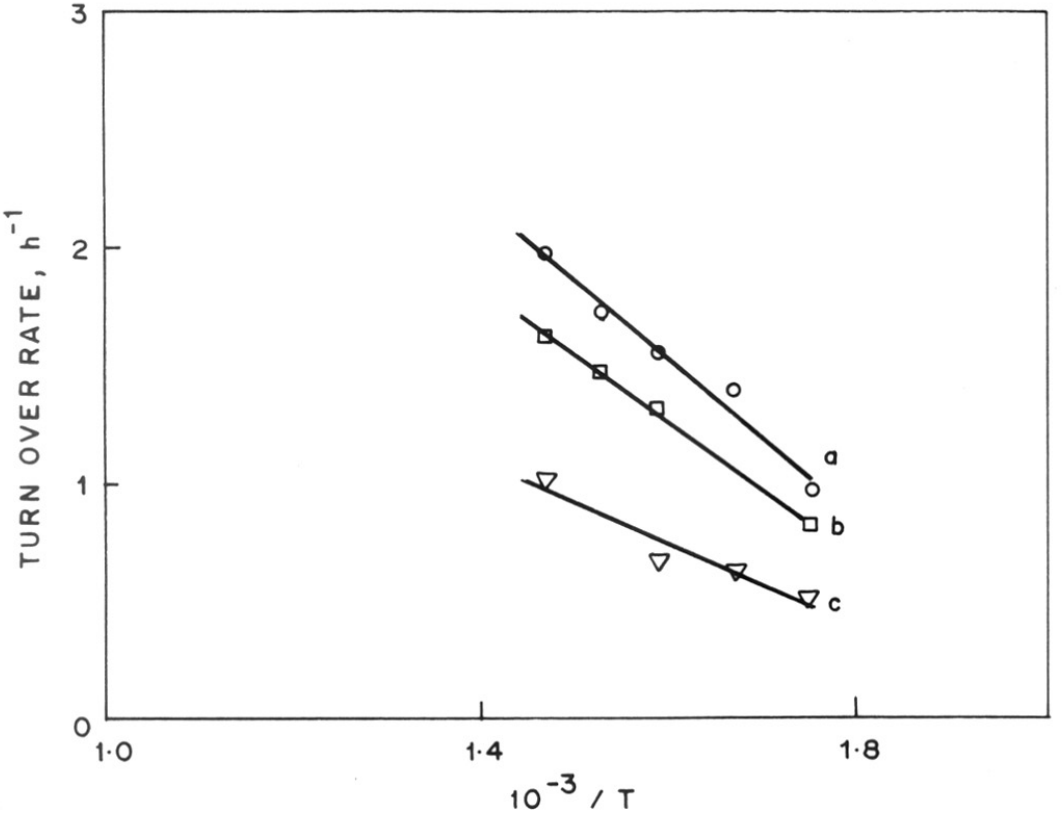

Fig. 5.3 : Plots of 1/T vs. Turn over rate (a) MoS-1[71]; (b) MoS-1[90]; and (c) MoS-1[137].

TABLE - 5.4

Oxidation of ethanol over MoS-1 and MoO_3/SiO_2 catalysts.

Sample	MoO_3	Temp.	Conv.	Selectivity, %					E_a
	Wt.%	K	%	C_2H_4	CH_3CHO	CH_3CO_2H	Ether	Others	$KJmol^{-1}$
MoO_3 /SiO_2	1	575	2.4	3	81.0	14	2	-	54
MoS-1	2.62	573	13.8	1.9	84.3	3.6	8.3	1.9	23.9
MoO_3 /SiO_2	9	563	42.7	4.0	72.0	7	4	13 #	92

* Values taken from Ref. No. 9.

Includes ethylacetate and CO_2.

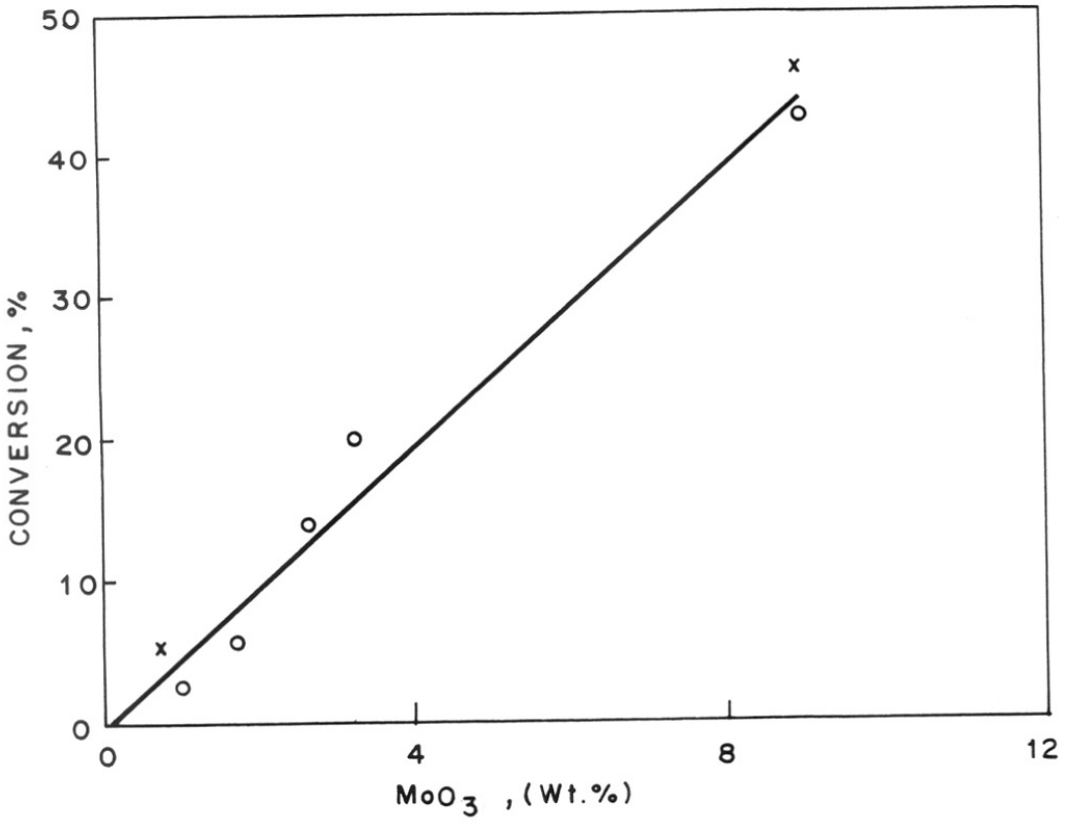

Fig. 5.4 : Conversion of ethanol over (x) MoO_3/SiO_2 and (o) MoS-1.

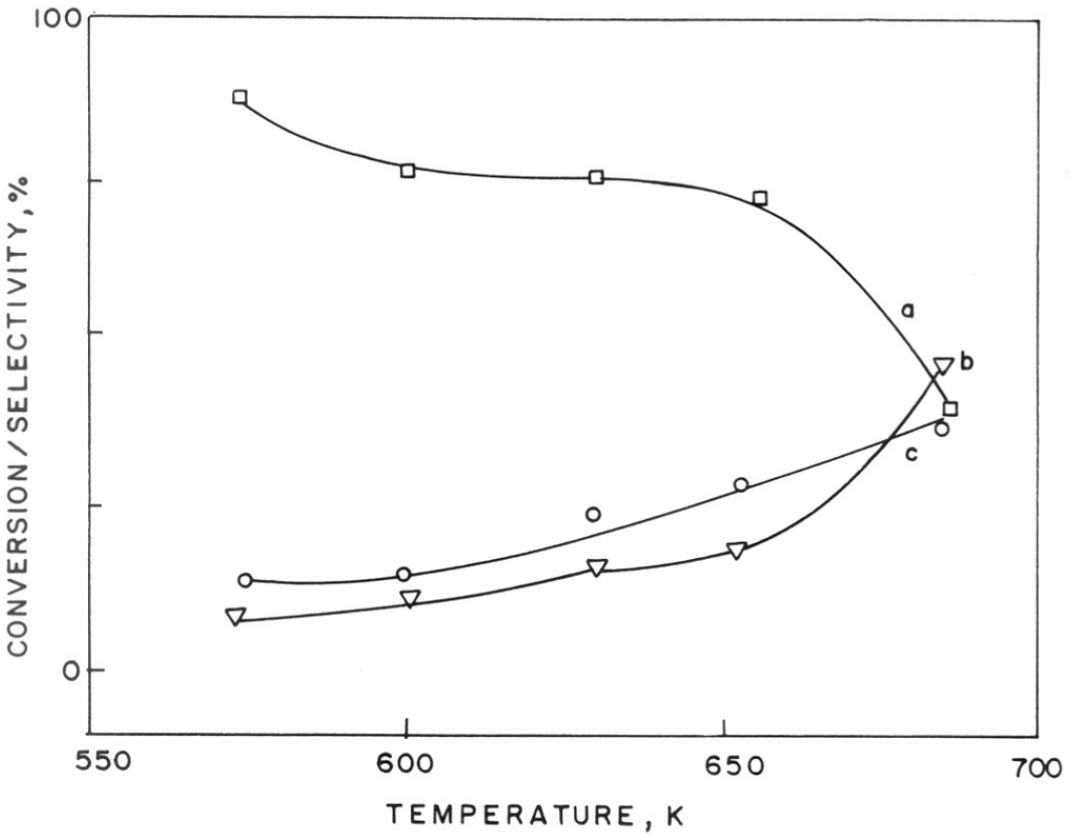

Fig. 5.5 : Oxidation of ethanol over MoS-2[50]: Influence of temperature. (c) conversion; selectivity of (a) acetaldehyde and (b) ether.

conversion over MoS-2 at different space velocities are given in Fig. 5.6. It is clear from the figure that even though there was a decrease in the conversion with an increase in the space velocity, the product distribution was nearly the same.

The turn over frequencies at different temperatures over MoS-2 were calculated, assuming that all Mo sites were accessible for the reaction and plotted against 1/T (Fig. 5.7). From the slope of the plot the activation energy was calculated to be 21 KJ.

5.2.5 A comparison of activities of MoS-1 and MoS-2 in the oxidation of ethanol

The results of oxidation of ethanol over MoS-1 and MoS-2 with Si/Mo ratio of 71 and 51, respectively, under identical experimental conditions are presented in Table 5.5. It is revealed from the table that even though the conversion was nearly the same, the selectivity to acetaldehyde was better in the case of MoS-1. The selectivity to ether was found to be twice over MoS-2 compared to MoS-1.

The time on stream data over MoS-1 and MoS-2 are given in Fig. 5.8. The conversion and acetaldehyde selectivity over MoS-2 were found to be less compared to MoS-1. MoS-2 was found to deactivate faster. The deactivation was accompanied with an increase in the selectivity of ether.

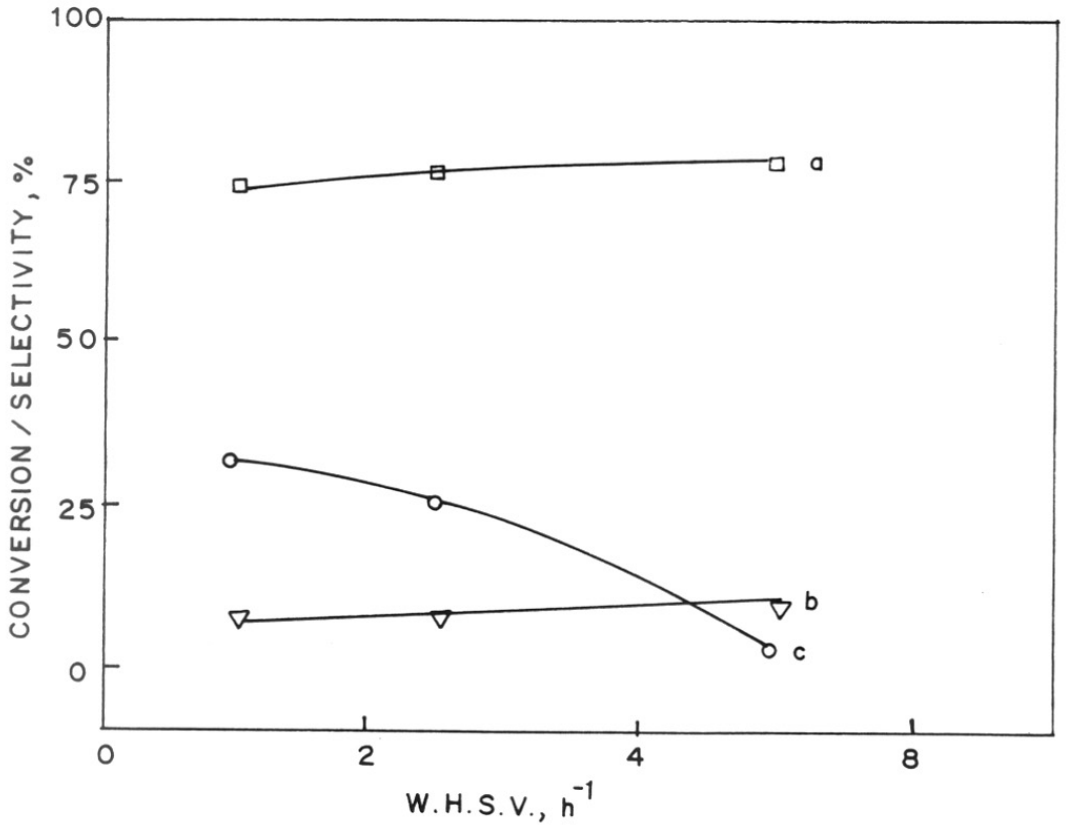

Fig. 5.6 : Oxidation of ethanol over MoS-2[50]: Influence of space velocity. (c) conversion; selectivity of (a) acetaldehyde and (b) ether.

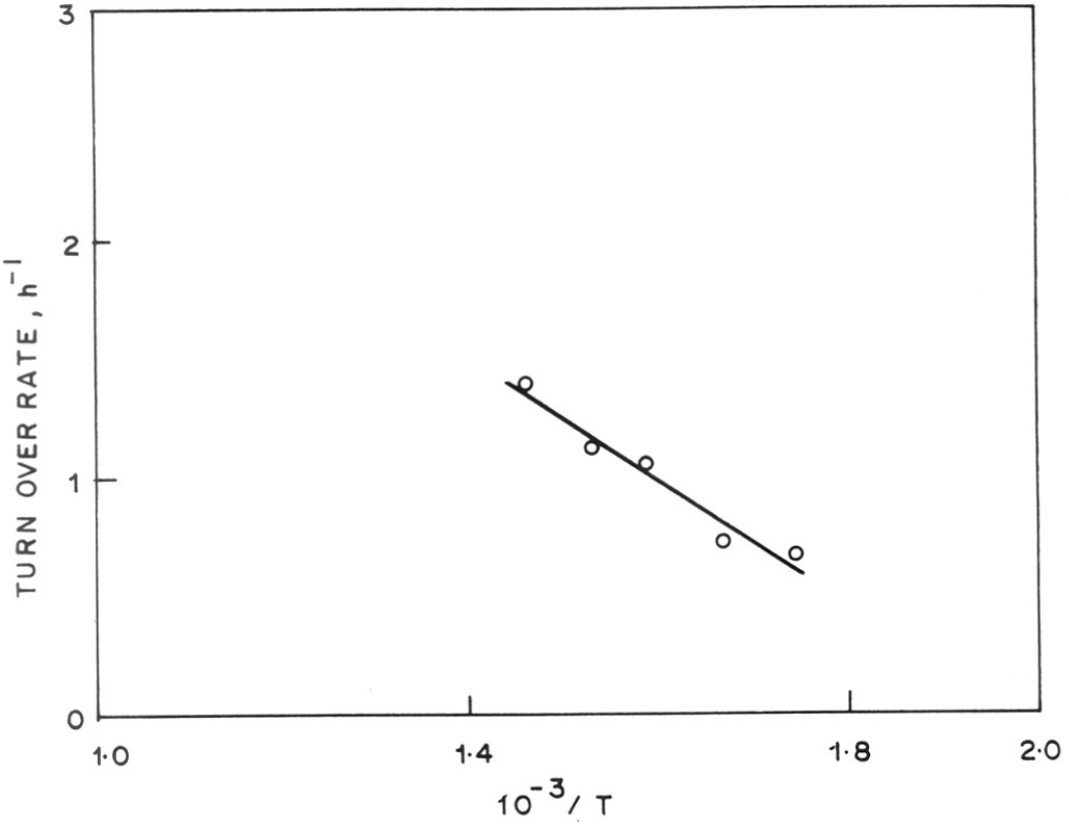

Fig. 5.7 : A plot of 1/T vs. Turn over rate.

TABLE - 5. 5

Oxidation of ethanol over MoS-1 and MoS-2.

Sample	Si/Mo	Temp.	Selectivity (%)					Cov.
	(mole)	K	C_2H_4	CH_3CHO	$(C_2H_5)_2O$	CH_3CO_2H	Others	(%)
MoS-1	71.0	630	4.4	85.6	3.0	-	7.0	32.2
MoS-2	50.1	630	15.1	75.8	6.8	0.3	2.0	30.2

TOS = 1 h; space velocity - 2.5 h^{-1}; oxygen/alcohol ratio (v/v) = 1.52.

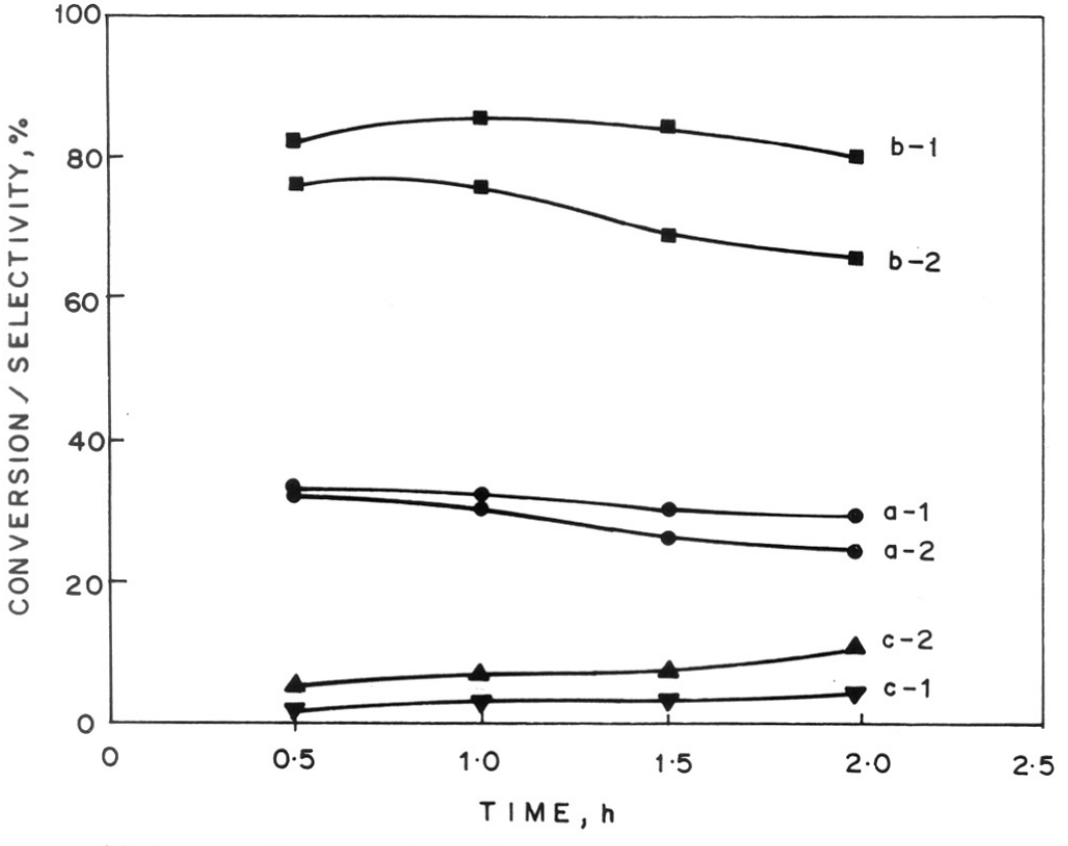

Fig. 5.8 : Oxidation of ethanol over MoS-1[71] and MoS-2[50] catalysts.

- conversion of ethanol over (a-1) MoS-1 and (a-2) MoS-2.
- Selectivity of acetaldehyde over (b-1) MoS-1 and (b-2) MoS-2.
- Selectivity of ether over (c-1) MoS-1 and (c-2) MoS-2.

5.2.6 Conclusions

The Mo-silicalites were found to be better catalysts for the oxidation of ethanol to acetaldehyde compared to supported Mo catalyst.

The selectivity of acetaldehyde was found to be better over MoS-1 compared to MoS-2, indicating the presence of distinct Mo=O sites in the former.

The MoS-2 was found to deactivate faster compared to MoS-1.

Production of ether over Mo-silicalites substantiates the presence of defect sites and the formation of acetic acid over MoO_3/SiO_2 indicates the presence of polyanions at the surface.

5.3 References

1. W. Adam, C.M. Mitchell and C.R.S. Moller, *Tetrahedron*, 50 (1994) 13121.
2. R. Balicki, L. Kaczmarek and P. Nantka-Namirski, *Liebigs Ann. Chem.*, (1992) 883.
3. R.S. Reddy, J.S. Reddy, R. Kumar and P. Kumar, *J.Chem.Soc.Chem.Commun.*,(1992) 847.
4. T.Sen, V. Ramaswamy, S. Ganapathy, P.R. Rajamohanan and S. Sivasanker, *J. Phys. Chem.*,100 (1996) 3809; T. Sen, P.R. Rajamohanan, S. Ganapathy and S. Sivasanker, *J. Catal.*, 163 (1996) 354.
5. J.M. Tatibouet , J.E. Germain, J.C. Volta, *J. Catal.*, 82 (1983) 240.
6. Y. Iwasawa, H. Tanaka, *Proc Int Congr Catal, 8th,* Berlin, 1984, IV-381.
7. W.E. Farneth, R.H. Staley, A.W. Sleigh, *J. Am. Chem. Soc.*,108 (1986) 2327.
8. W. Zhang, A.N. Desikan and S. Ted Oyama, *J. Phys. Chem.*, 99 (1995) 14468.
9. T. Ono, H. Kamisuki, H. Hisashi, H. Miyata, *J. Catal.*, 116 (1989) 303.

Chapter VI

STUDIES ON Mo and Al CONTAINING MEL/MFI MOLECULAR SIEVES

6 STUDIES ON Mo AND Al CONTAINING MEL/MFI MOLECULAR SIEVES

A. Synthesis and Characterization

6.1 Introduction

Activation of highly inert methane to higher hydrocarbons has been a challenge in the past several decades. The possibility of converting methane to higher hydrocarbons through oxidative coupling of methane (OCM) was investigated by the scientists in eighties. Although significant progress has been made in this area, it has not been found to be commercially attractive *[1]*. The direct formation of aromatics from methane has also been reported and a number of groups have been working on the above process *[2]*. More recently, Wang *et al.* have achieved the conversion methane directly to benzene under non-oxidative conditions *[3]*. Among the tested catalysts, Mo/H-ZSM-5 (MoO_3 impregnated on H-ZSM-5) was found give better results. Studies on the mechanism of the above reaction have been carried out by some authors *[4,5]*. A detailed investigation of the active site was made by Solymosi *et al.* *[6]*. In this section, the activity of Mo containing ZSM-5 (Al and Mo ions in the 'framework') on the methane aromatization reaction is reported.

6.2 Experimental

6.2.1 Chemicals used in the syntheses

The template used in the synthesis of samples with MFI structure was tetrapropylammonium hydroxide (TPAOH, Aldrich, 20% aqueous solution), and that used for MEL samples was tetrabutylammonium hydroxide (TBAOH, Aldrich, 40% aqueous solution). The silica source used was tetraethyl orthosilicate (TEOS, Aldrich). Sodium

molybdate (Na_2MoO_4, LOBA Chemie) was used as the Mo source and aluminium sulfate ($Al_2(SO_4)_3.18H_2O$, LOBA Chemie) was used as the Al source.

6.2.2 Synthesis of Al free Mo containing silicalite-1 (MoS-1)

The synthesis of Al free MoS-1 samples has already been reported (Chapter 2.3). The samples are represented as MoS-1 (n), where 'n' represents, Si/Mo (mole) ratio in the final sample.

6.2.3 Synthesis of Al and Mo containing silicalites with MFI topology (H-AMoS-1)

The synthesis of a typical sample is described below:

TEOS (29.9 g) and TPAOH (47.3 g) were mixed under vigorous stirring. After 15 min., 0.87 g of the aluminium sulfate dissolved in 10 g of deionized water was added and the stirring continued for another 15 min. Then, 0.1 g of sodium molybdate, dissolved in 15.1 g of deionized water was added and the contents were left undisturbed for 10 min. The transparent gel was then transferred into a stainless steel autoclave and treated hydrothermally at 443 K under autogeneous pressure for 24 h. The catalyst was then separated by centrifugation and dried at 383 K for 12 h. Samples with other Mo contents were prepared using the above procedure but with different amounts of sodium molybdate. The samples were calcined at 783 K for 8 h with the increase in temperature being done at a heating rate of 10 K/min. and holding for 1 h after every 100 K increase. The H-form of the sample was obtained by treating the above calcined sample with 90 % glacial acetic acid (1 g in 10 mL) at 333 K for 2 h. The contents were filtered, dried and calcined at 723 K for 6 h. The samples are represented as H-AMoS-1 (X,Y), where X represents Si/Mo (mole) ratio and Y represents Si/2Al ratio in the final sample.

6.2.4 Preparation of H-ZSM-5

TEOS (29.9 g) was mixed with TPAOH (47.3 g) under stirring. After complete hydrolysis, 1.4 g of the aluminium sulfate dissolved in 25.1 g of deionized water was added in drops and stirring was continued for 15 minutes. The contents were then transferred into a stainless steel autoclave and treated hydrothermally at 443 K for 24 h. The zeolite was then separated by filtration and dried at 383 K for 12 h. The H-form of the zeolite was obtained by exchange with 1 N ammonium acetate at 333 K for 4 h and calcining at 723 K for 6 h.

6.2.5 Preparation of Mo-impregnated H-ZSM-5 (Mo/H-ZSM-5)

The required amount of sodium molybdate (0.16 g) was dissolved in a minimum quantity of water. H-ZSM-5 (3g; obtained using the procedure adopted in Section 6.2.4) was added and mixed well. The contents were dried at 343 K under evacuation. The sample was then dried at 382 K for 12 h, calcined at 573 K for 3 h and at 773 K for 4 h. This sample is represented as Mo/H-ZSM-5.

6.2.6 Synthesis of silicalite-2 (MEL)

The synthesis of silicalite-2 has already been described in Chapter 2.2.

6.2.7 Synthesis of Al free Mo-silicalite-2 (MoS-2)

The synthesis of Al free MoS-2 has already been described in Chapter 2.

6.2.8 Synthesis of Al and Mo containing silicalite with MEL topology (H-AMoS-2)

The synthesis of a typical sample is described below:

TBAOH (28 g) was added in drops to 30 g of TEOS under vigorous stirring. After 15 minutes, 0.98 g of sodium molybdate and 0.96 g of aluminium sulfate were dissolved in 60 g of deionized water and added to the above gel with continuous stirring. The contents were transferred to stainless steel autoclave after aging for 15 minutes and treated hydrothermally at 453 K for 45 h. The crystalline material was then separated, dried at 383 K for 12 h and calcined at 783 K for 8 h. The H-form of the samples were obtained by adopting the procedure described in the *section 6.2.3*.

6.2.9 Conversion of methane to aromatics

The activation of methane over all the catalysts was carried out in a fixed bed quartz reactor (1.5 cm i.d., down flow mode), followed by a condenser and a gas-liquid separator. Due to the large gas flow rates, no liquid products was collected under experimental conditions. The analysis of the gas samples were carried out on a HP-5880A gas chromotograph fitted with a capillary column (50m X 0.2 mm). The reactor was charged with 2.0 g of the catalyst (12-14 mesh size, ASTM), without using any binder. Ceramic beads were used in the pre-heating zone. Prior to the experiments, the catalysts were activated in a flow of air (50 mL/min) for 6 h under experimental conditions and purged with nitrogen (20 mL/min.) for 2 h. The experiments were carried out at different temperatures and space velocities.

6.3 Characterization of Mo and Al Containing Molecular Sieves

6.3.1 X-ray diffraction

The XRD patterns of H-AMoS-1 samples were found to match well with H-ZSM-5 (Fig. 6.1). The crystallinity of the samples were determined by measuring the intensity of the

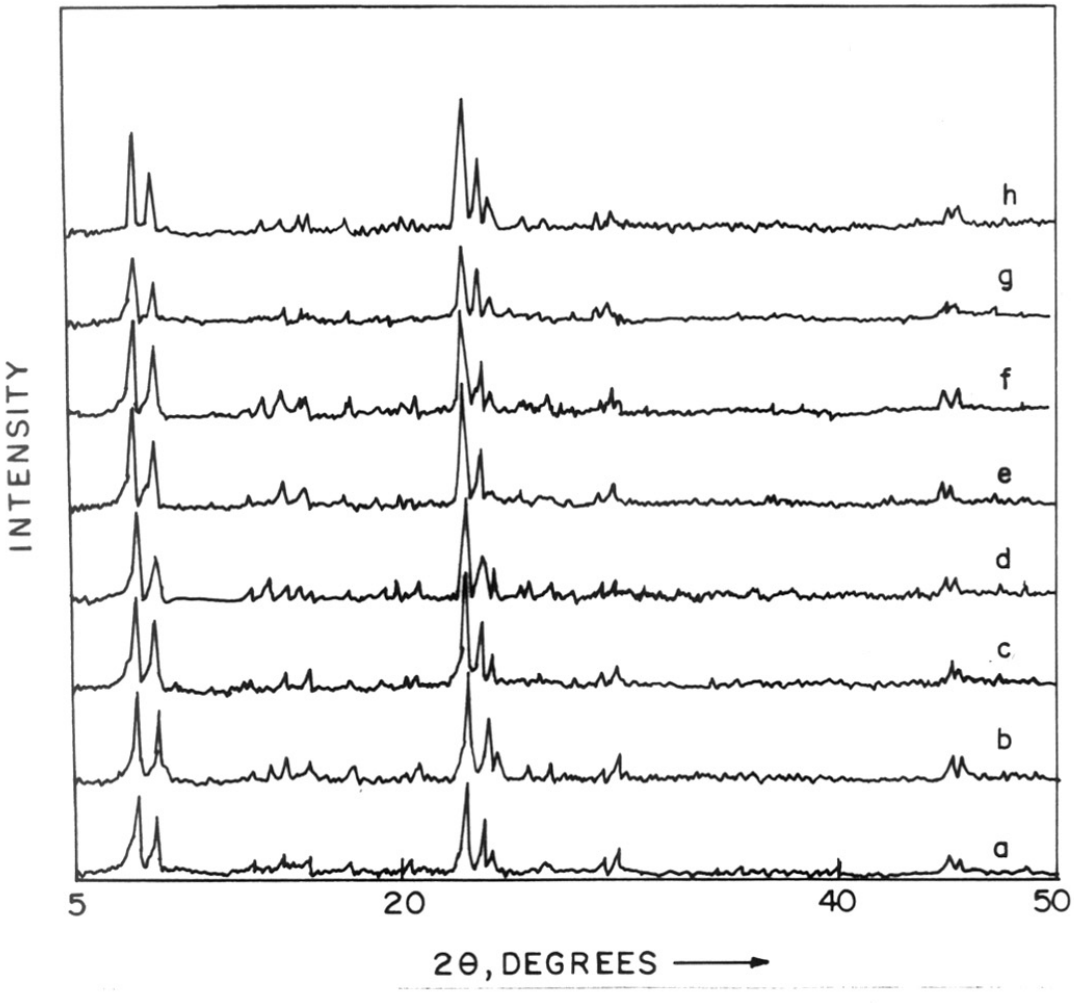

Fig. 6.1 : XRD profiles of H-AMoS-1 with [Si/Mo, Si/2Al] ratio of (a) [63, 68]; (b) [79, 210]; (c) [82, 106]; (d) [136, 134]; (e) [160, 108]; (f) MoS-1[70]; (g) Mo/HZSM-5 (h) HZSM-5.

TABLE - 6.1

Physico-chemical characterization of Mo and Al containing molecular sieves with MFI topology.

Sample	Si/Mo	Si/2Al	Crystal-linity	Crystal size	S_{BET}	pore vol.	UV-Visible spectra [a]
	(mole)	(mole)	(%)	μm	m^2/g	mL/g	Mo_{Td}/Mo_{Oh}
H-AMoS-1	63	68	77	~ 1	421.0	0.159	1.37
H-AMoS-1	79	210	89	~ 1	445.0	0.181	1.80
H-AMoS-1	82	106	86	~ 1	442.1	0.173	1.72
H-AMoS-1	136	134	92	~ 1	439.6	0.171	1.90
H-AMoS-1	160	108	93	~ 1	446.0	0.169	1.80
MoS-1	70	-	97	0.25	523.0	0.200	1.83
Mo/H-ZSM-5	72	81	-	-	369.0	0.146	-
H-ZSM-5	-	68	100	2 - 3	384.0	0.189	-

[a] Ratio of intensities of absorption at 220 nm (Mo_{Td}) and 290 nm (Mo_{Oh}) from the UV-Visible spectra.

100% peak (2θ = ~23 degree). The H-ZSM-5 (blank) was taken as the reference sample and considered as 100 % crystalline. The relative crystallinities of all the samples are presented in Table 6.1. The H-AMoS-1 samples were found to be less crystalline compared to the Al free analogue (MoS-1). But, the crystallinity of H-AMoS-1 was found to increase on decreasing the Mo content in the sample. The influence of Mo content on the crystallinity of the sample was more pronounced than that of the Al content.

The XRD profiles of Mo/Al-MEL (H-AMoS-2) samples were found to match well with silicalite-2 (MEL) (Fig. 6.2). The absence of peaks at 2θ = 9 and 24 degrees and a singlet peak at 2θ = 45° confirmed the MEL structure *[7]*. The silicalite-2 sample was taken as the standard (100% crystalline). The crystallinity of the samples were found to decrease with an increase in the Mo content (Table 6.2).

6.3.2 Nitrogen sorption

An increase in the surface area was observed for the hydrothermally prepared Mo/Al-MFI samples, while the surface area decreased in the case of Mo/H-ZSM-5 (Table 6.1). The very large increase in surface area for the MoS-1 sample could be attributed to the smaller crystallite size (0.25 μm) and probably defect sites. A small decrease in the surface area and pore volume of H-AMoS-1 samples compared to MoS-1 could be partly due to the larger crystallite size of the former (Table 6.1). A decrease in surface area and pore volume was observed as the Mo and Al contents were increased in the synthesis gel (Table 6.2).

6.3.3 UV-Visible spectroscopy

The UV-Visible spectra for the H-AMoS-1 samples are given in Fig. 6.3. The H-ZSM-5 (blank) did not show any characteristic absorption, while Mo/H-ZSM-5 showed a

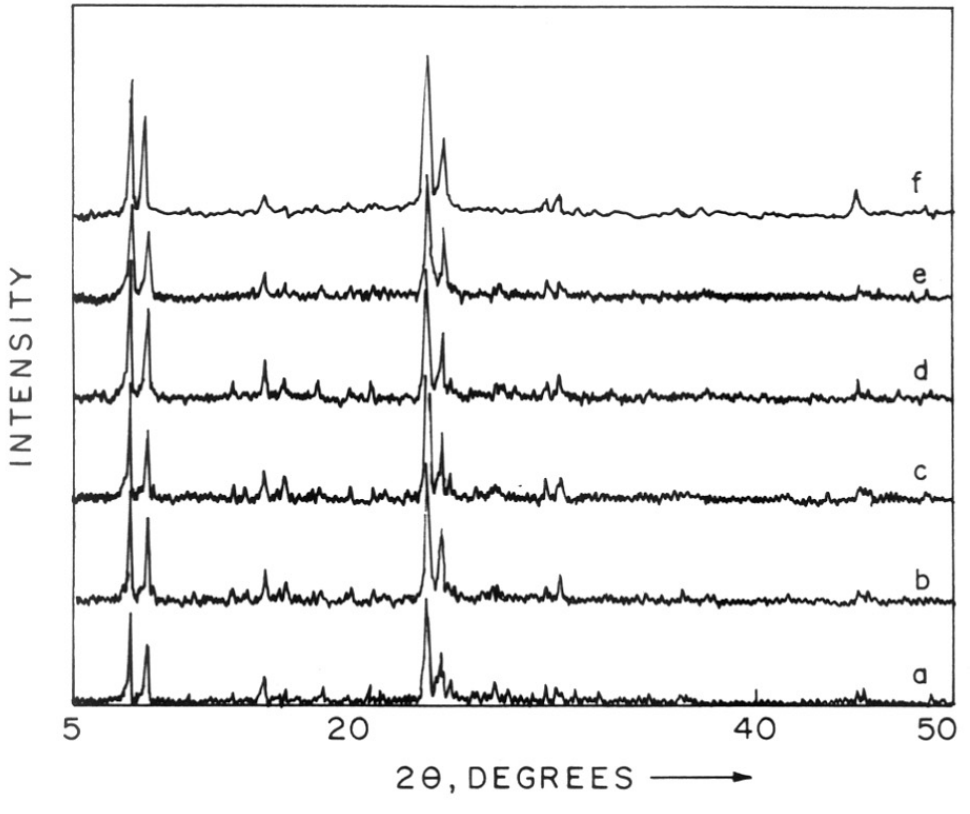

Fig. 6.2 : XRD profiles of H-AMoS-2 with [Si/Mo, Si/2Al] ratio of (a) [31.5, 86]; (b) [30.8, 149]; (c) [41, 212]; (d) [72, 81]; (e) [103, 79]; and (f) Silicalite-2.

TABLE - 6.2

Physico-chemical characterization of Mo and Al containing molecular sieves with MEL topology.

Sample	Si/Mo	Si/2Al	Cryst.	S_{BET}	pore vol.	UV-Visible spectra [a]
	(mole)	(mole)	(%)	m^2/g	mL/g	Mo_{Td}/Mo_{Oh}
H-AMoS-2	31.5	86	72	284.3	0.1025	1.25
H-AMoS-2	30.8	147	88	331.7	0.1232	1.48
H-AMoS-2	41.0	212	92	333.1	0.1210	2.26
H-AMoS-2	72	81	91	327.0	0.1192	1.47
Silicalite-2	-	-	100	342.0	0.1200	-

[a] Ratio of intensities of absorption at 220 nm (Mo_{Td}) and 300 nm (Mo_{Oh}) from the UV-Visible spectra.

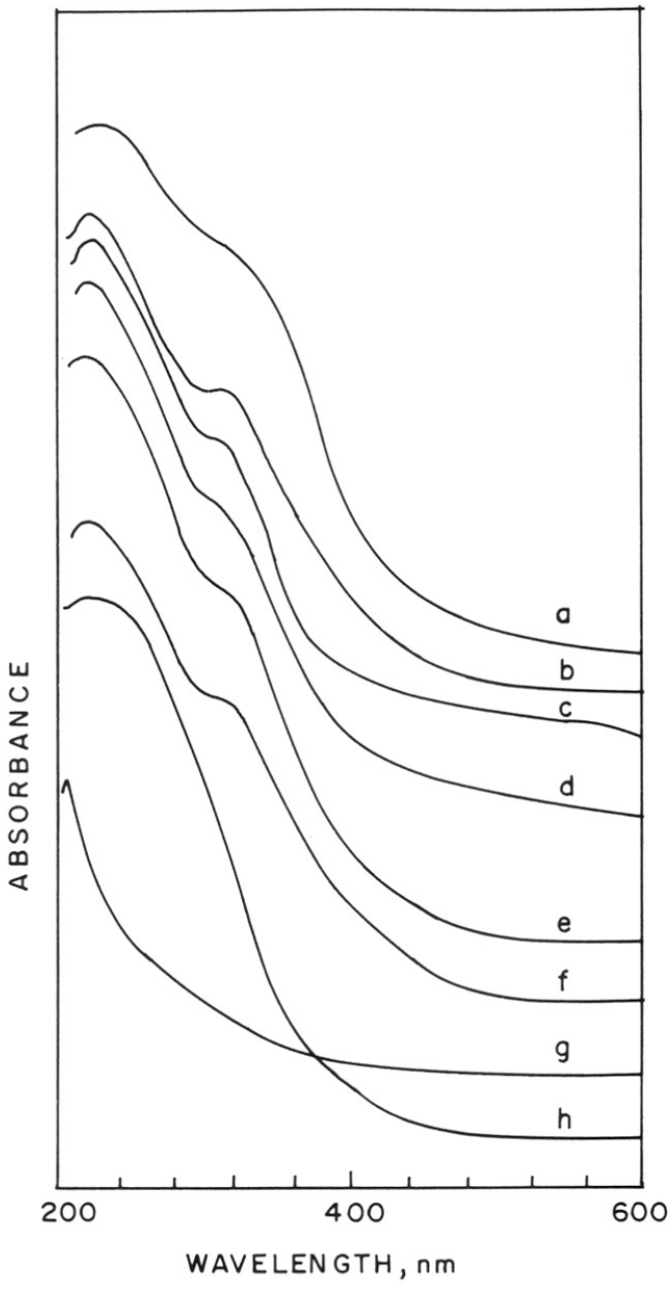

Fig. 6.3 : UV-Visible spectra of H-AMoS-1 with [Si/Mo, Si/2Al] ratio of (a) [63, 68]; (b) [79, 210]; (c) [82, 106]; (d) [136, 134]; (e) [160, 108]; (f) MoS-1[70]; (g) HZSM-5 (h) Mo/HZSM-5.

broad band. The H-AMoS-1 samples gave two distinct absorptions at around 220 nm and 290 nm. As reported by earlier workers *[8]*, the former absorption (220 nm) was attributed to Mo species present in tetrahedral coordination and the later (290 nm) was attributed to the Mo species present in octahedral coordination. The ratio of intensities of absorption of the bands corresponding to tetrahedral and octahedral species of Mo are presented in Table 6.1.

The UV-Visible spectra of H-AMoS-2 samples are presented in Fig. 6.4. The spectra were found to be identical with that of H-AMoS-1, and the ratios of intensities of 220 nm and 290 nm are presented in Table 6.2. A gradual decrease in the ratio of Mo_{Td}/Mo_{Oh} with the increase in the Mo content suggests an increase in octahedral species of Mo.

6.3.4 Conclusions

The H-AMoS-1 and H-AMoS-2 samples were found to be crystalline (confirmed by XRD) with a clear pore system (confirmed by nitrogen sorption experiments). A direct correlation was observed between the surface area and particle size. Two different types of Mo species with different coordinations were found to exist in the Mo-silicalite samples (confirmed by UV-Visible spectral analysis). A part of the Mo is probably present in the framework or as molybdate species in tetrahedral coordination, while another part is grafted to the silicalite structure at the surface.

B. Conversion of Methane over Mo and Al Containing Molecular Sieves

6.4 Activation of Methane over Mo/Al-MFI Molecular Sieves

The reaction was carried out at 958 K and the results are presented in Table 6.3. The time on stream data for the samples with different Mo contents is shown in Fig. 6.5. It

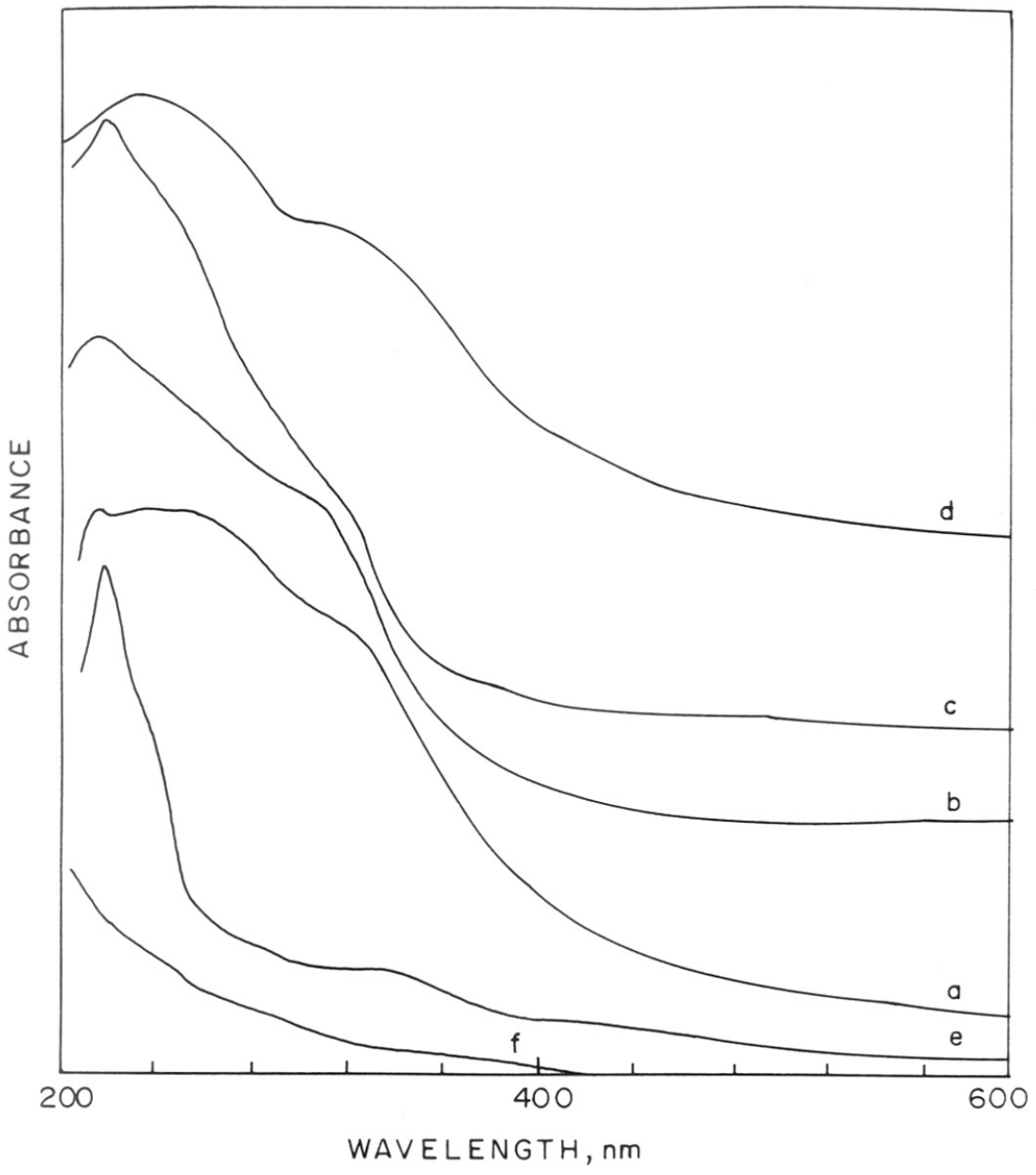

Fig. 6.4 : UV-Visible spectra of H-AMoS-2 with [Si/Mo, Si/2Al] ratio of (a) [31.5, 86]; (b) [30.8, 149]; (c) [41, 212]; (d) [72, 81]; (e) [103, 79]; and (f) Silicalite-2.

TABLE - 6.3

Conversion of methane to aromatics over Mo and Al containig zeolites with MFI topology.*

Sample (x,y) [a]	Conversion (%)	Benzene (%)	Ethylene (%)
H-AMoS-1 (63,68)	1.8	60	2.0
H-AMoS-1 (79,210)	4.2	61	17.0
H-AMoS-1 (82,106)	7.1	92	1.9
H-AMoS-1 (136,134)	3.5	52	7.2
H-AMoS-1 (160,108)	0.7	71	6.5
MoS-1 (70)	2.5	40	52
Mo/H-ZSM-5	0.4	25	33
H-ZSM-5	0.5	10.3	-

* Conditions : Temperature - 958 K, GHSV = 138.5 h^{-1} g $cat.^{-1}$, TOS = 1.5 h^{-1}.

[a] 'x' represents Si/Mo ratio and 'y' represents Si/2Al ratio.

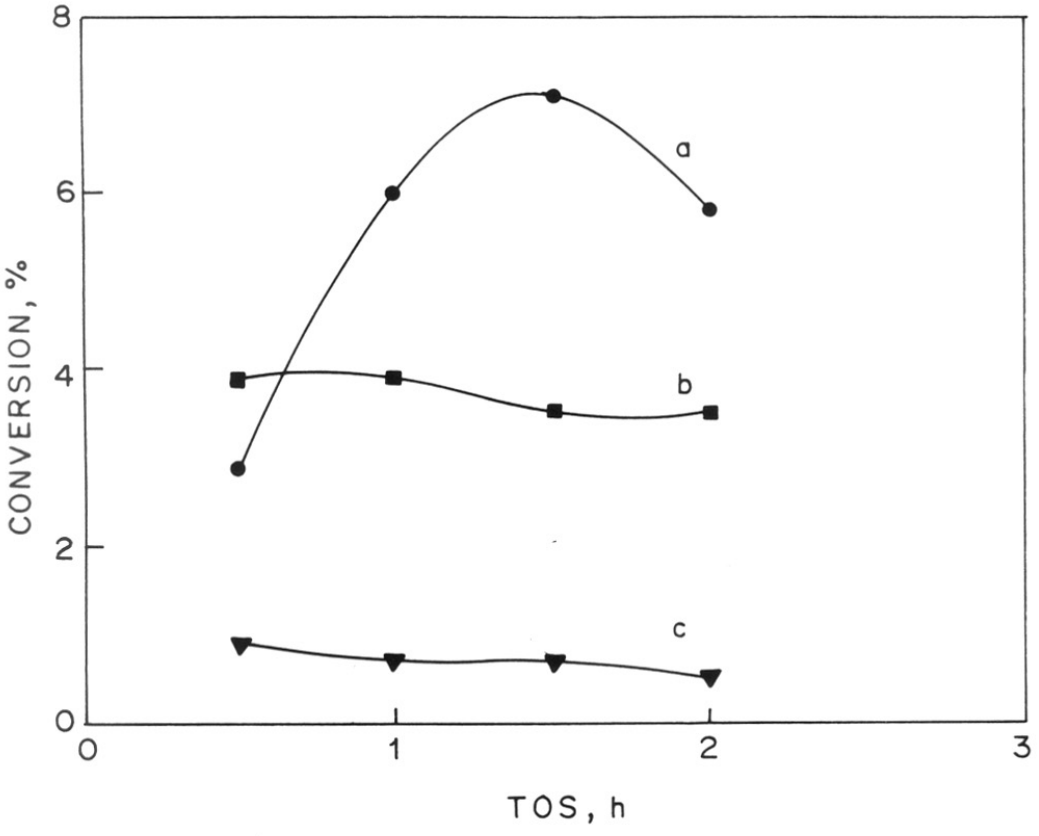

Fig. 6.5 : Conversion of methane to benzene over H-AMoS-1: Influence of Mo content. [Si/Mo, Si/2Al] ratios of samples (a) [82, 106]; (b) [136, 134]; and (c) [160, 108].

appears from the figure that when the Mo content was decreased, the conversion was suppressed. A maximum conversion of 7.1 % was observed over H-AMoS-1 with Si/Mo = 82 and Si/2Al = 106. The benzene selectivity over the same catalysts are shown in Fig. 6.6. The H-AMoS-1 (82,106) had a better selectivity for benzene (92 %). An increase in Mo content lead to the suppression in the activity and selectivity of the catalyst (H-AMoS-1 (63,68) Table 6.3).

The effect of Al content on the conversion of methane is given in Fig. 6.7. It is clear from the figure that the conversion is maximum at an optimum content of Al. The selectivity of benzene over H-AMoS-1 with different Al contents is given in Fig. 6.8. The sample with higher Al content was found to deactivate faster with a rapid decrease in the selectivity of benzene. The sample with a lower Al content gave a better conversion, but the selectivity of benzene was found to be less (Table 6.3). Hence, in order to get a better selectivity of benzene with good conversion, an optimum amount of Al (Si/2Al = ~100) appears necessary.

The influence of gas hourly space velocity (GHSV, $h^{-1}g\ cat^{-1}$) on the reaction over H-AMoS-1(82,53) is given in Fig. 6.9. At lower space velocities, formation of the thermodynamically favored product (benzene) was more. At higher space velocities, the selectivity of the kinetically controlled product (ethylene) was more, while that of benzene was less. This clearly indicates that the primary product during the course of the reaction is ethylene which then aromatizes to form benzene.

The role of acid sites in the aromatization reaction to form benzene is revealed by the experiments carried out over Al free Mo-silicalites. The time on stream data for the reaction

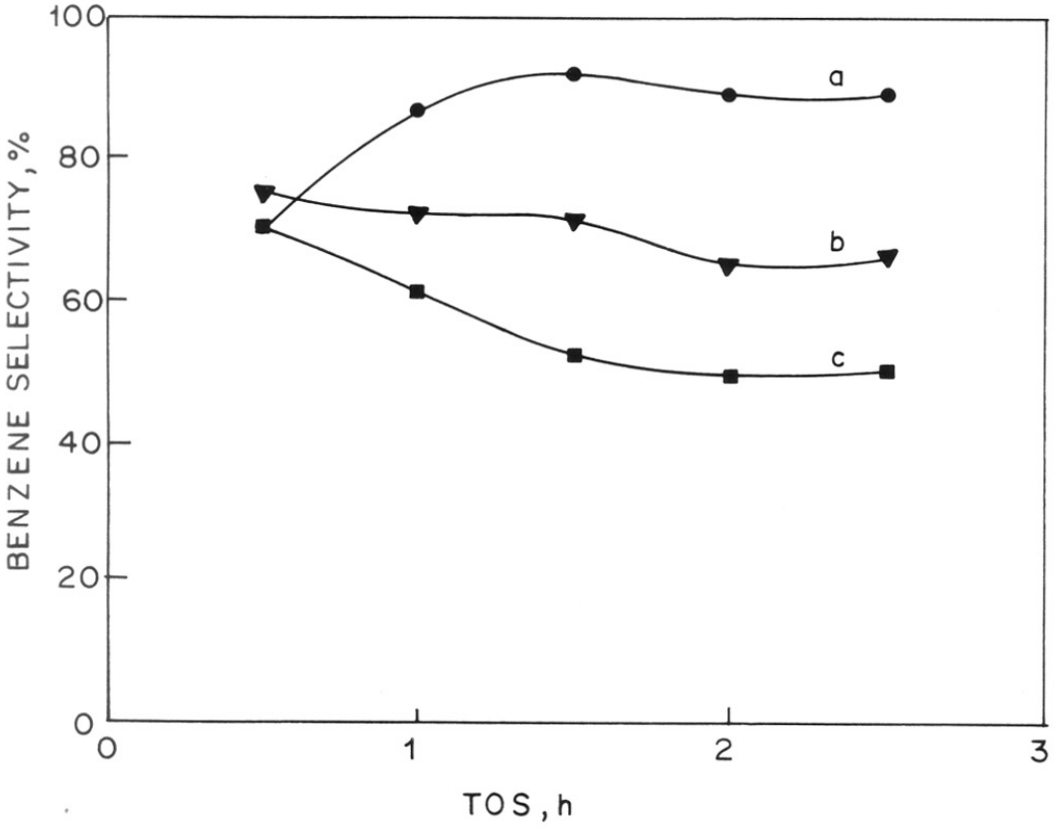

Fig. 6.6 : Selectivity of benzene over H-AMoS-1 with different Mo content. [Si/Mo, Si/2Al] ratios of samples
(a) [82, 106]; (b) [136, 134]; and (c) [160, 108].

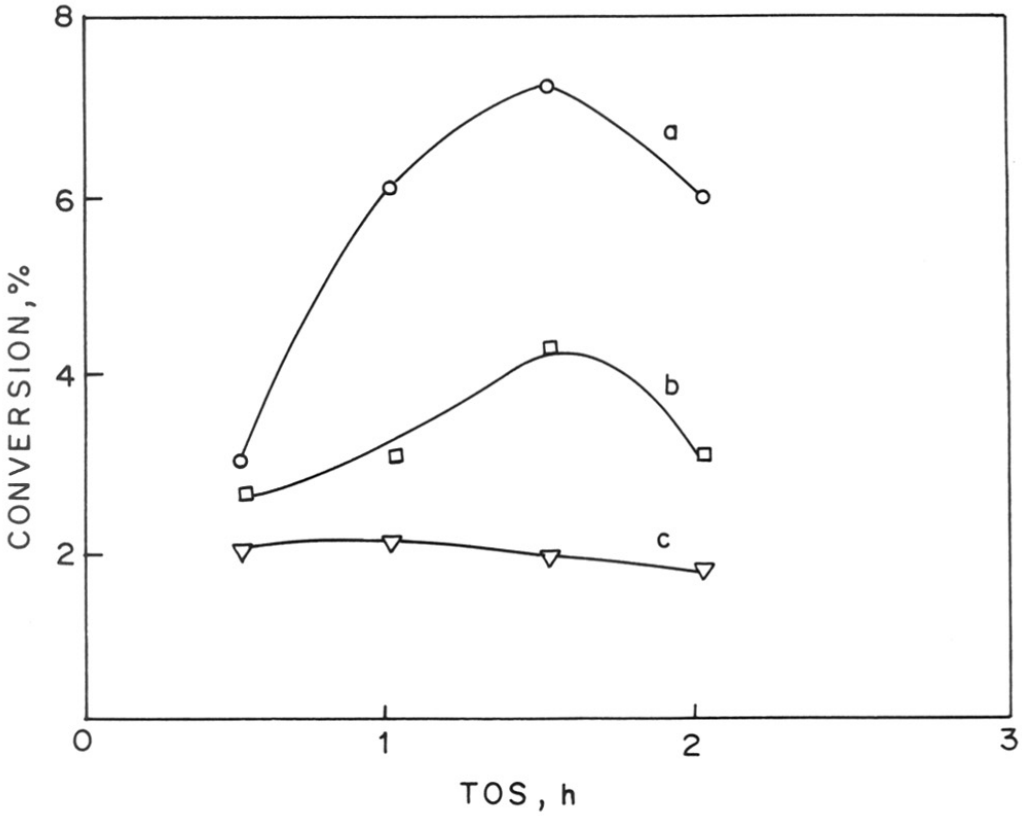

Fig. 6.7 : Conversion of methane to benzene over H-AMoS-1: Influence of Al content. [Si/Mo, Si/2Al] ratios of samples (a) [82, 106]; (b) [79, 210]; and (c) [63, 68].

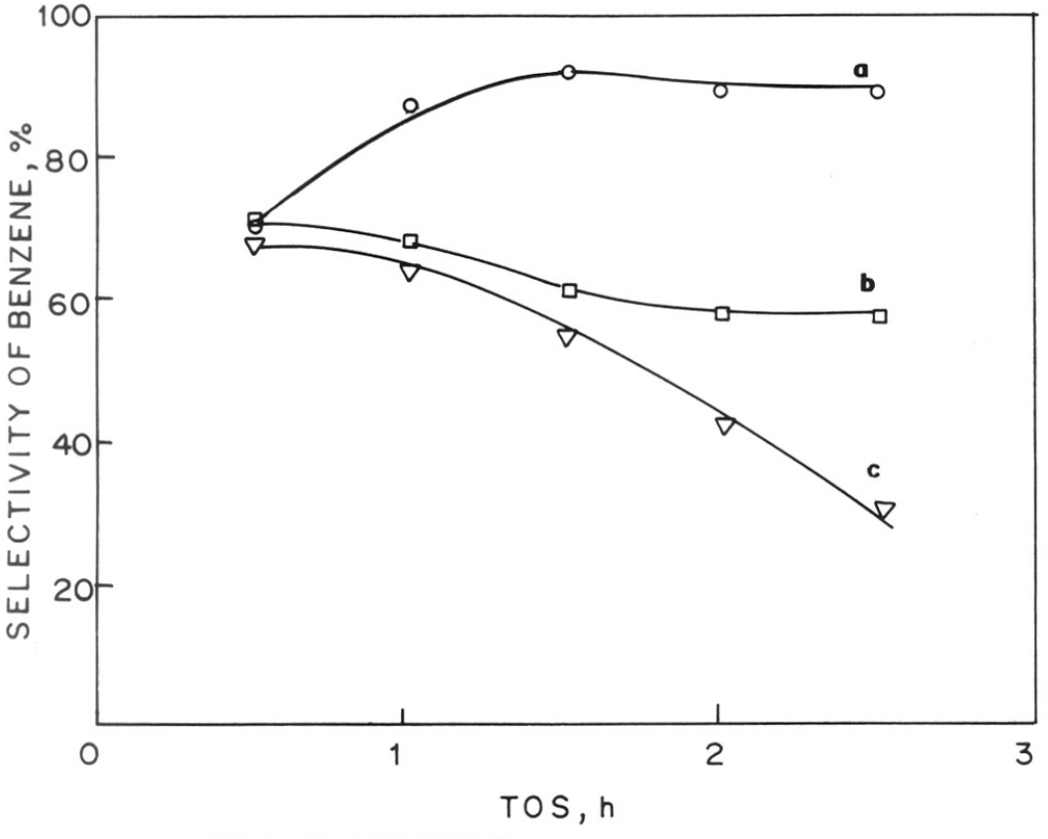

Fig. 6.8 : Selectivity of benzene over H-AMoS-1 with different Al content. [Si/Mo, Si/2Al] ratios of samples
(a) [82, 106]; (b) [79, 210]; and (c) [63, 68].

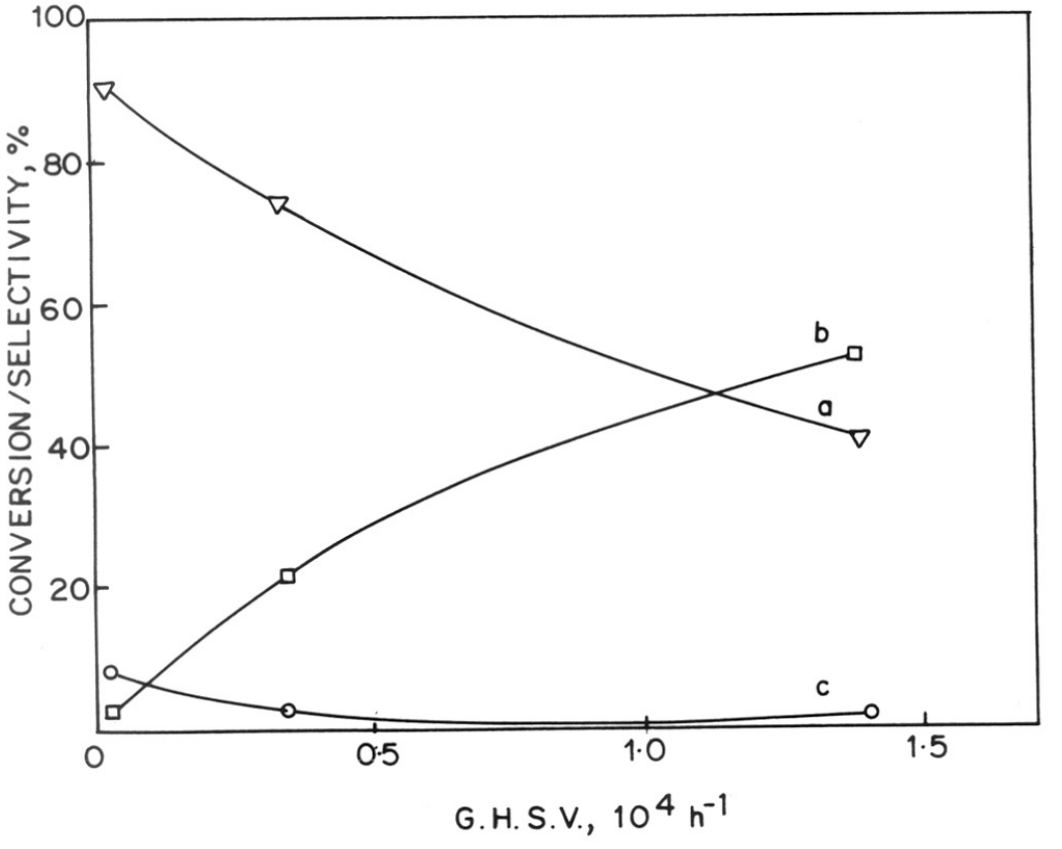

Fig. 6.9 : Conversion of methane to benzene over H-AMoS-1[82, 106]. Influence of space velocity at 958 K.
(c) conversion and selectivity of (a) benzene and (b) ethylene.

carried out over MoS-1 (Si/Mo = 70) is given in Fig. 6.10. The conversion of methane was found to decrease gradually with time, but, an increase in benzene selectivity was observed initially, which was suppressed after 1 h. On the other hand, a corresponding increase in the selectivity of ethylene was observed. Even though acid sites are absent in this case, the formation of benzene could be attributed to the defect sites (-Mo-OH) which are also mildly acidic. The Mo impregnated Mo/H-ZSM-5 when tested under identical conditions gave a very low conversion (0.4 %) with a low selectivity to benzene (25%). Finally, the blank catalyst (H-ZSM-5) was also tested and was found to be poorly active under the experimental conditions (conversion = 0.5 %; benzene selectivity = 10.3 %).

6.5 Activation of Methane over Mo/Al-MEL Molecular Sieves

The results of the conversion of methane to benzene over Mo/Al-MEL samples with different Mo and Al contents are presented in Table 6.4. The selectivity of benzene and ethylene was found to be complementary to each other. The effect of Mo content on the reaction is given in Fig. 6.11. The Si/2Al ratio was nearly the same in the range 79 - 86. The conversion was found to be maximum at an intermediate Mo content. The selectivity to benzene was found to be maximum over the sample with an intermediate Mo content while the selectivity to ethylene was the least.

The influence of Al content on the reaction was studied over H-AMoS-2 samples with different Si/2Al ratios and the results are plotted in Fig. 6.12. The conversion of methane was found to be nearly constant, while the selectivity to benzene was found to decrease drastically with a decrease in the Al content. On the other hand, the selectivity of ethylene and other cracked products were found to increase.

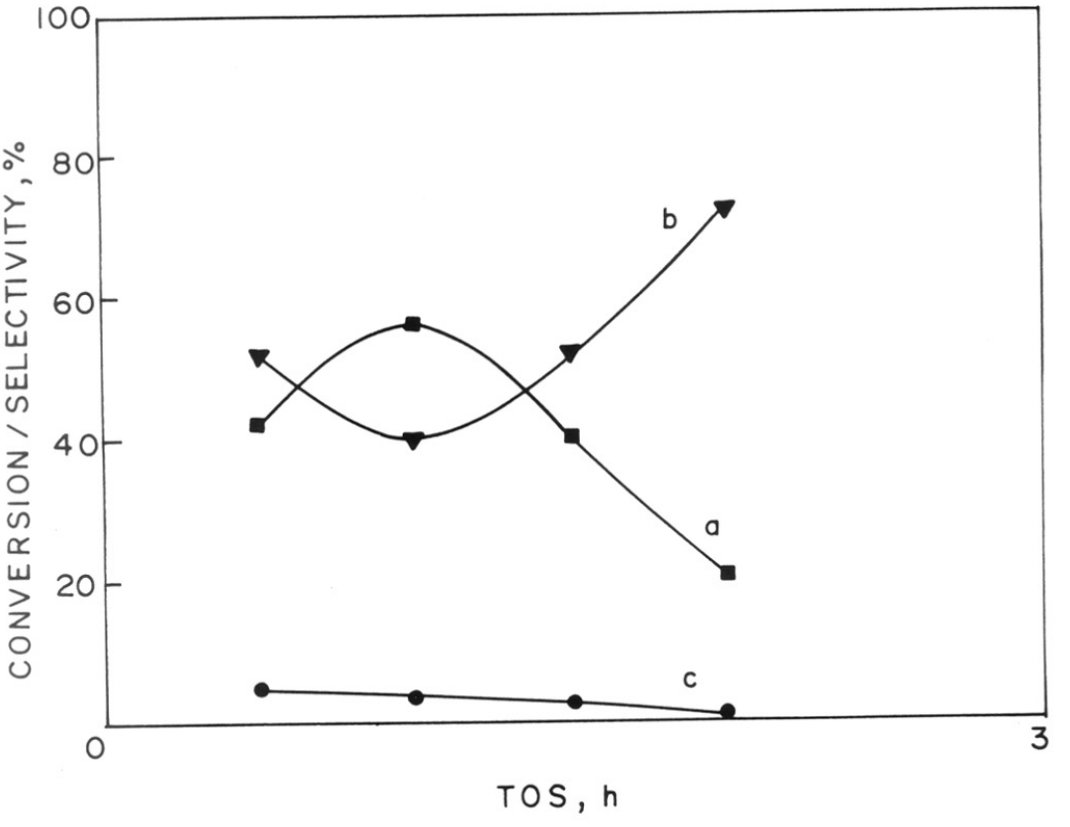

Fig. 6.10 : Conversion of methane to benzene over MoS-1[70].
Temperature - 958 K; GHSV- 138.5 h^{-1}.
(c) conversion and selectivity of (a) benzene and (b) ethylene.

TABLE - 6.4

Conversion of methane to aromatics over Mo and Al containig zeolites with MEL topology.*

Sl.No	Sample (x,y) [a]	Conversion (%)	Benzene (%)	Ethylene (%)
1.	H-AMoS-2 (31.2, 86)	2.3	89	3.0
2.	H-AMoS-2 (30, 147)	2.5	73	8.3
3.	H-AMoS-2 (41, 212)	2.9	68	9.7
4.	H-AMoS-2 (72, 81)	4.5	95	1.1
5.	H-AMoS-2 (103,79)	3.1	71	6.5

* Conditions : Temperature - 958 K, GHSV = 138.5 h^{-1} g $cat.^{-1}$, TOS = 1.5 h^{-1}.

[a] 'x' represents Si/Mo ratio and 'y' represents Si/2Al ratio.

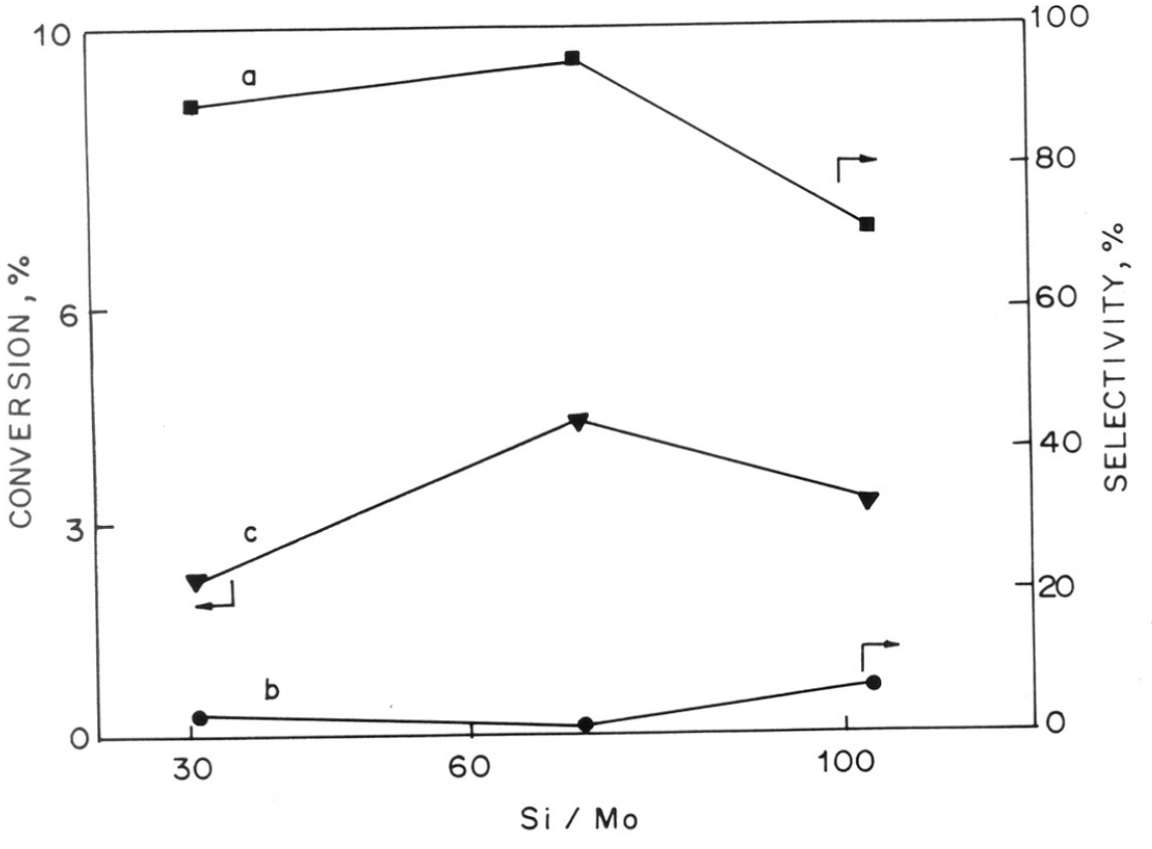

Fig. 6.11 : Conversion of methane to benzene over H-AMoS-2.
Influence of Mo content at 958 K; GHSV- 138.5 h^{-1}.
(c) conversion and selectivity of (a) benzene and (b) ethylene.

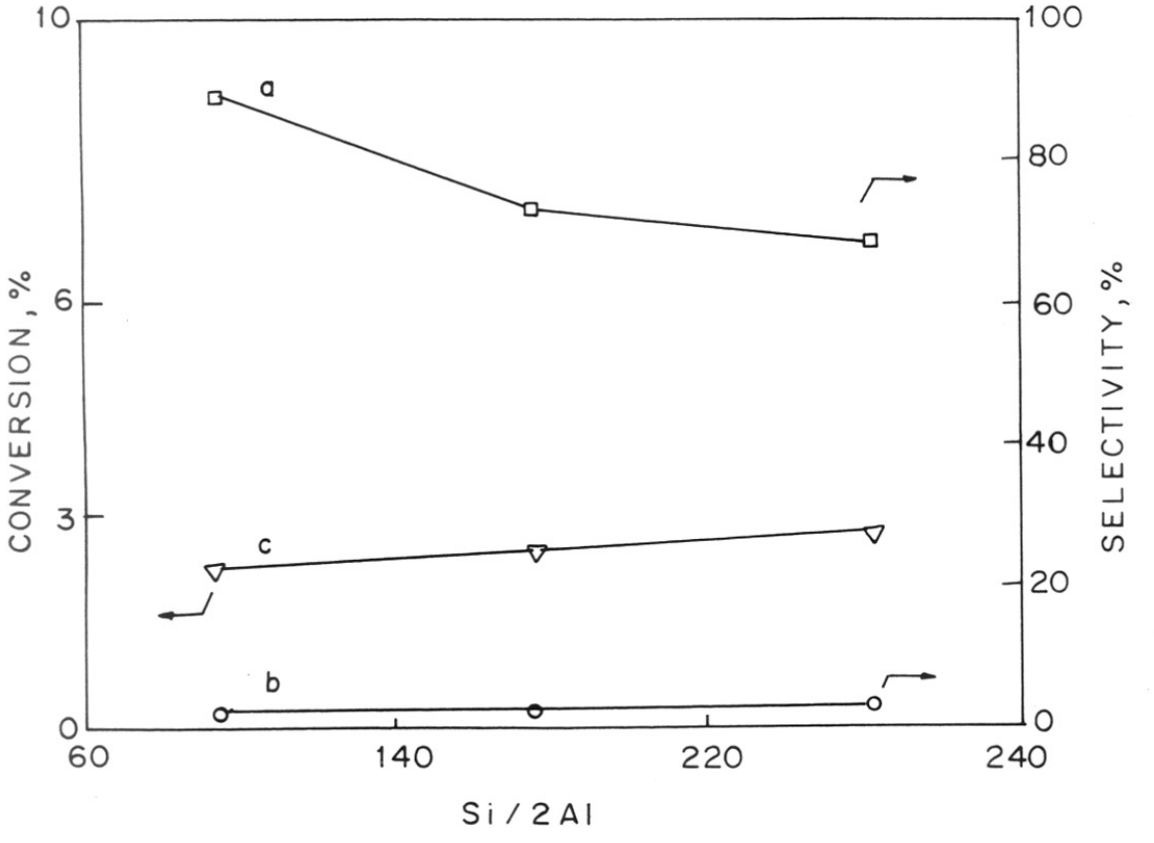

Fig. 6.12 : Conversion of methane to benzene over H-AMoS-2.
Influence of Al content at 958 K; GHSV- 138.5 h^{-1}.
(c) conversion and selectivity of (a) benzene and (b) ethylene.

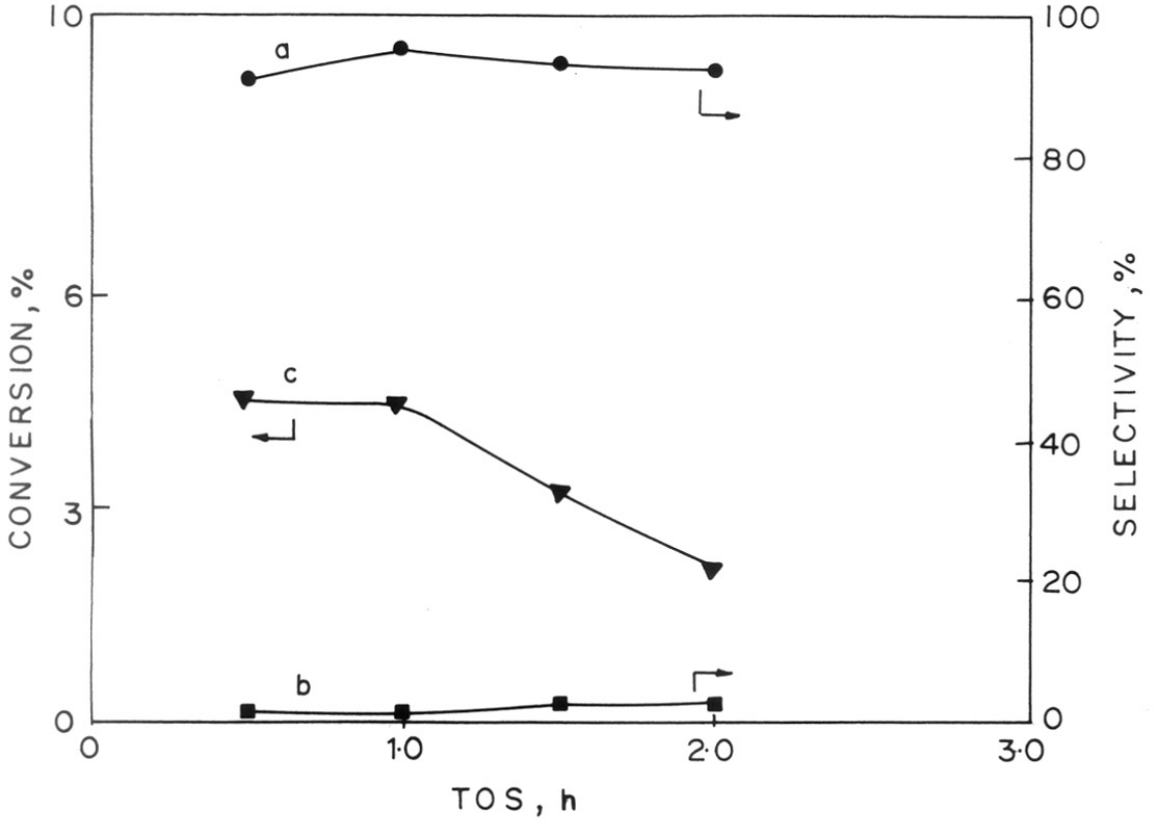

Fig. 6.13 : Conversion of methane to benzene over H-AMoS-2 [71, 81]. at 958 K and GHSV = 138.5 h^{-1}.
(c) conversion and selectivity of (a) benzene and (b) ethylene.

Based on the above studies, the H-AMoS-2 sample with Si/Mo = 72 and Si/2Al = 81 was found to give maximum conversion of 4.5 % with 95 % selectivity of benzene. The results of time on stream studies over the above catalyst are presented in Fig. 6.13. The selectivity to benzene was found to be nearly constant and that to ethylene was found to increase marginally due to deactivation. The conversion was found to decrease drastically after a TOS of 1 h.

In general, the H-AMoS-2 samples were found to be less active in the conversion of methane to benzene, compared to H-AMoS-1. But the selectivity to benzene was found to be better in the case of the former. The lower activity of the H-AMoS-2 catalysts may probably be due to the lower surface area of the samples due to the agglomeration of small crystallites (of dimensions of ~0.2 μm) into large clusters. Other reasons such as intrinsic structural differences and pore size differences may also be responsible.

6.6 Conclusions

The Mo and Al containing silicalites with MFI and MEL structures were found to be active in the conversion of methane to benzene. Their activity was found to be more compared to the Mo-impregnated analogues. The Mo/Al-MFI (H-AMoS-1) samples were found to be more active than the Mo/Al-MEL (H-AMoS-2) samples. An optimum amount of Mo content was necessary (to get good benzene yields), below which the activity was found to be poor and beyond which the selectivity to benzene was less. An optimum amount of Al content was also found to be essential.

A maximum conversion of ~7.1 % with ~92 % selectivity to benzene was obtained over Mo/Al-MFI (Si/Mo = ~80, Si/2Al = ~100). Mo/Al-MEL gave a maximum conversion of ~4.5 % with ~95 % selectivity of benzene (Si/Mo = ~70, Si/2Al = ~80).

6.7 References

1. J.H. Lunsford, *Stud. Surf. Sci. Catal.*, 75 (1993) 103.
2. S.A. Shepelev and K.G. Ione, *React. Kinet. Catal. Lett.*, 23 (1983) 323; J.R. Anderson and P. Tsai, *Appl. Catal.*, 19 (1985) 141; S.S. Shepelev and K.G. Ione, *J. Catal.*, 117 (1989) 362.
3. L. Wang, J. Huang, L.Tao, Y. Xu, M. Xie and G. Xu, *Catal. Lett.*, 21 (1993) 35.
4. L. Chen, L. Lin, Z. Xu, X. Li and T. Zhanag, *J. Catal.*, 157 (1995) 190.
5. D. Wang, J.H. Lunsford and M.P. Rosynek, *Topics in Catalysis*, 3 (1996) 289; Y. Xu, S. Lin, L. Wang, M. Xie and X. Guo, *Catal. Lett.*, 30 (1995) 138.
6. F. Solymosi, A. Erdohelyi and A. Szoke, *Catal. Lett.*, 32 (1995) 43.
7. J.S. Reddy and R. Kumar, *Zeolites*, 12 (1992) 95.
8. H. Jeziorowski and H. Knozinger, *J. Phys. Chem.*, 83 (1979) 1166.
9. Y. Xu, S. Lin, L. Wang, M. Xie and X. Guo, *Catal. Lett.*, 30 (1995) 135.
10. F. Solymosi, J. Cserenyi, A. Szoke, T. Bansaagi and A. Oszko, *J. Catal.*, 165 (1997) 150.
11. S.T. Wong, Y. Xu, W.Lin, L. Wang, and X. Guo, *Appl. Catal.*, 136 (1996) 7.

Chapter VII

SUMMARY AND CONCLUSIONS

7 SUMMARY AND CONCLUSIONS

Zeolites are crystalline, microporous, aluminosilicates with a 3-dimensional framework made up of SiO_4^{4-} and AlO_4^{5-} tetrahedra. Replacements of Al ions by transition metals alter the catalytic properties of the resulting metallosilicates. The most important metallosilicate to be used commercially is the titaniumsilicate, TS-1. The characterization and catalytic activity of supported Mo on alumina (oxide form) are well documented in the literature. Various methods such as wet impregnation, coprecipitation, equilibrium adsorption methods have been adopted by different groups in order to fix the Mo at the surface of the support. Eventhough, appreciable work has been carried out on supported Mo catalysts, the literature on the incorporation of Mo in the zeolite framework is scarce. This thesis is a study of the incorporation of Mo in medium pore zeolites of the MFI and MEL types, their characterization and catalytic properties.

Molybdenum containing silicalite-2 (MoS-2) was synthesized hydrothermally under aluminium free alkaline conditions. The influences of various synthesis parameters like temperature, Mo content, water concentration, organic template concentration, aging time and pH of the synthesis gel on the crystallization of Mo containing molecular sieves with MFI and MEL structures have been investigated (Chapter II). The results showed that highly crystalline Mo-silicalite-2 (MoS-2) can be synthesized using a gel of composition: $SiO_2/MoO_3 = 100$, $TBAOH/SiO_2 = 0.3$, $H_2O/SiO_2 = 23$. The aging time has a significant impact on the crystallization of MoS-2. A longer aging time leads to an amorphous silica-molybdenum oxide mixture. The most crystalline samples were obtained when the organic base content was in the narrow range of $TBAOH/SiO_2 = 0.3 - 0.4$. Mo-silicalite-1 (MoS-1)

could be synthesized in a broad range of SiO_2/MoO_3 and $TPAOH/SiO_2$ ratios. Unlike MoS-2, the aging time did not affect the crystallinity of the sample. Based on the studies, the gel compositions most suited for the synthesis of MoS-1 were: SiO_2/MoO_3 = 35-200; $TPAOH/SiO_2 = 0.326$; $H_2O/SiO_2 = 24.3$.

The characterization of MoS-2 (Chapter III) revealed the presence of a thermally stable Mo species in the sample. Spectral analysis has revealed the presence of Mo in both tetrahedral and octahedral coordination. Presence of different types of Mo species were also revealed by cyclicvoltammetry. The tetrahedral species of Mo is probably present in the framework at defect sites. Another species of Mo is grafted to the surface as polyanionic species with Mo-O-Mo bridges.

The preservation of orthorhombic symmetry in the case of Mo-silicalite-1 even after calcination (Chapter IV) suggests the possible incorporation of Mo in the framework of silicalite-1 structure. The oxidation state of Mo in the MoS-1 samples was found to be +6 (confirmed by XPS). Mo was also present in more than one coordination, as revealed by UV-Visible studies. When the Mo concentration was increased, more Mo-species with octahedral coordination was formed. The Mo species are linked to the Si-O- tetrahedra or grafted to the silicalite-1 structure in such a manner that they cannot be leached by dilute ammonia. The thermal stability of the samples supports the strong interaction between Mo and Si-O of the framework.

The Mo-silicalites were found to be better catalysts for the oxidation of ethanol to acetaldehyde than supported Mo (Chapter V). The selectivity to acetaldehyde was found to

be more over MoS-1 compared to MoS-2, indicating the presence of distinct Mo=O sites in the former. MoS-2 was found to deactivate faster compared to MoS-1. Production of ether over Mo-silicalites was probably due to the weakly acidic silanol groups at the defect sites and the formation of acetic acid over MoO_3/SiO_2 has suggested the presence of polyanions at the surface.

The Mo and Al containing with MFI and MEL structures were found to be active in the conversion of methane to benzene (Chapter VI). Their activities were larger than those of the Mo-impregnated analogues. The Mo/Al-MFI (H-AMoS-1) was found to be more active than Mo/Al-MEL (H-AMoS-2). An optimum amount of Mo content was necessary to get good conversion, below which the activity was found to be poor and beyond which the selectivity to benzene was less. An optimum amount of Al content was also found to be essential for high benzene yields.

LIST OF PUBLICATIONS AND PATENTS

List of Publications

1. Synthesis and characterization of Mo-containing MFI type silicalite.
   P.S. Raghavan, R. Ravishankar and A.V. Ramaswamy*.
   Catalysis: Modern trends, (Eds.N.M.Gupta & D.K.Chakrabarty), Narosa Publishing House, New Delhi, (1995) 168.

2. Selective catalytic oxidation of thioethers to sulfoxides over Mo-silicalite-1 (MoS-1) molecular sieves.
   P.S. Raghavan, V. Ramaswamy, T.T. Upadya, A. Sudalai, A.V. Ramaswamy and S. Sivasanker*.
   Journal of Molecular Catalysis, 122 (1997) 75.

3. Vapour phase alkylation of benzene with 1-heptene over mordenites.
   P.S. Raghavan and S. Sivasanker*.
   Proceedings of 13th National Symposium on Catalysis, IIP, Dehradun, India, 1997.

4. Synthesis and Characterization of Mo containing Silicalite-2 (MoS-2) molecular sieve.
   P.S. Raghavan*, S. Kannan and A.A. Belhekar.
   Indian Journal of Chemistry, 36A (1997) 905.

5. Skeletal isomerization of 1-hexene over Molybdenum silicalite-1 (MoS-1) molecular sieve.
   P.S. Raghavan
   Indian Journal of Chemistry, sec.A, 1997 (Communicated).

6. Oxidative dehydrogenation of ethanol over Mo-Silicalite-1 (MoS-1) molecular sieves.
   P.S. Raghavan
   Applied Catalysis, 1997 (Communicated).

7. Can Mo-silicalite-1 be an efficient catalyst for the isomerization of 1-butene to isobutene?
   P.S. Raghavan* and S.P. Mirajkar
   Indian Journal Chemical Technology, 5 (1998) 59.

8. Production of benzene from methane under non oxidative conditions over Mo containing zeolites with MFI topology.

   P.S. Raghavan and S. Sivasanker*.

   Proceedings of 14th National Workshop on Catalysis, RRL, Trivandrum, 1997.

9. Fine chemicals: Present and Future.

   P.S. Raghavan* and K.R. Srinivasan.

   Chemical Business, (Fine Chemicals Asia '96 Conference Special Issue), 9 (1996) XVII.

10. Mo-Silicalite-2: Characterization and catalytic properties.

    P.S. Raghavan* and M.P. Vinod.

    Journal of Molecular Catalysis, 1998 (accepted, in press).

Patents Filed

1. A process for the preparation of novel microporous crystalline molybdenum silicalite molecular sieves.

   P.S. Raghavan, R. Ravishankar and A.V. Ramaswamy.

   *Indian Patent No.*DEL/1719/94.